DISCLAIMER

This report was prepared as an account of work sponsored by an agency of the United States Government. Neither the United States Government nor any agency thereof, nor any of their employees, makes any warranty, express or implied, or assumes any legal liability or responsibility for the accuracy, completeness, or usefulness of any information, apparatus, product, or process disclosed, or represents that its use would not infringe privately owned rights. Reference herein to any specific commercial product, process, or service by trade name, trademark, manufacturer, or otherwise does not necessarily constitute or imply its endorsement, recommendation, or favoring by the United States Government or any agency thereof. The views and opinions of authors expressed herein do not necessarily state or reflect those of the United States Government or any agency thereof. Reference herein to any social initiative (including but not limited to Diversity, Equity, and Inclusion (DEI); Community Benefits Plans (CBP); Justice 40; etc.) is made by the Author independent of any current requirement by the United States Government and does not constitute or imply endorsement, recommendation, or support by the United States Government or any agency thereof.

ANL/NEAMS-25/2

Multiphysics Modeling of Microreactors with NEAMS codes, and Validation Based on KRUSTY Reactivity Insertion

Chemical and Fuel Cycle Technologies Division

Nuclear Science and Engineering Division

About Argonne National Laboratory
Argonne is a U.S. Department of Energy laboratory managed by UChicago Argonne, LLC under contract DE-AC02-06CH11357. The Laboratory's main facility is outside Chicago, at 9700 South Cass Avenue, Lemont, Illinois 60439. For information about Argonne and its pioneering science and technology programs, see www.anl.gov.

DOCUMENT AVAILABILITY

Online Access: U.S. Department of Energy (DOE) reports produced after 1991 and a growing number of pre-1991 documents are available free at OSTI.GOV (http://www.osti.gov/), a service of the US Dept. of Energy's Office of Scientific and Technical Information.

Reports not in digital format may be purchased by the public from the National Technical Information Service (NTIS):

U.S. Department of Commerce
National Technical Information Service
5301 Shawnee Road
Alexandria, VA 22312
www.ntis.gov
Phone: 800-553-NTIS (6847) or 703-605-6000
Fax: 703-605-6900
Email: **orders@ntis.gov**

Reports not in digital format are available to DOE and DOE contractors from the Office of Scientific and Technical Information (OSTI):

U.S. Department of Energy
Office of Scientific and Technical Information
P.O. Box 62
Oak Ridge, TN 37831-0062
www.osti.gov
Phone: 865-576-8401
Fax: 865-576-5728
Email: **reports@osti.gov**

Disclaimer
This report was prepared as an account of work sponsored by an agency of the United States Government. Neither the United States Government nor any agency thereof, nor UChicago Argonne, LLC, nor any of their employees or officers, makes any warranty, express or implied, or assumes any legal liability or responsibility for the accuracy, completeness, or usefulness of any information, apparatus, product, or process disclosed, or represents that its use would not infringe privately owned rights. Reference herein to any specific commercial product, process, or service by trade name, trademark, manufacturer, or otherwise, does not necessarily constitute or imply its endorsement, recommendation, or favoring by the United States Government or any agency thereof. The views and opinions of document authors expressed herein do not necessarily state or reflect those of the United States Government or any agency thereof, Argonne National Laboratory, or UChicago Argonne, LLC.

ANL/NEAMS-25/2

Multiphysics Modeling of Microreactors with NEAMS codes, and Validation Based on KRUSTY Reactivity Insertion

by
Yinbin Miao, Soon Kyu Lee, Kevin Sawatzky, Kun Mo

Chemical and Fuel Cycle Technologies Division
Argonne National Laboratory

Ahmed Abdelhameed, Yan Cao, Yiqi Yu, Nicolas Stauff

Nuclear Science and Engineering Division
Argonne National Laboratory

SEPTEMBER 2025

Table of Contents

Table of Figures

Table of Figures

Executive Abstract

The NEAMS Multiphysics Applications team continues to assess code usability and functionality for microreactor design and safety analyses, while demonstrating that NEAMS tools capture both steady-state and transient behavior across distinct microreactor concepts. In FY2025, the team advanced full-core, high-fidelity, multiphysics models that solve more complex problems and strengthen verification/validation for several microreactor systems: heat-pipe microreactor (HPMR), gas-cooled microreactor (GCMR), and the KRUSTY experiment. These models employ the MOOSE MultiApp/Transfers architecture with Griffin for neutronics, BISON for heat conduction/thermomechanics, Sockeye for heat pipes, SAM/THM for coolant channels and loops, and SWIFT for hydride behavior, with meshes generated via the MOOSE Reactor Module. The graphite models available in the Grizzly code were also investigated for future analyses.

For the HPMR, a Na-HPMR variant was constructed to align with recently validated heat-pipe experiments and Sockeye's LCVF capability, enabling mechanistic heat-pipe transients and startup modeling. The Na-HPMR will serve as the primary model for HPMR investigations in upcoming tasks. The load-following and single heat-pipe failure scenarios (Griffin/BISON/Sockeye), which were previously modeled for the K-HPMR, were replicated for the Na-HPMR, showing strong negative temperature feedback and highly localized thermal effects, respectively, while the startup case captured vapor-front progression and heat-removal activation. Solid mechanics was added to the previously built K-HPMR full-core model in BISON, showing minimal impact on steady-state reactivity yet enabling stress-field predictions that prepare the path for full-core TRISO performance analyses.

For the GCMR, automated steady-state and four transient scenarios were executed using Griffin/BISON/SAM/SWIFT. Results confirm robust inherent safety: power collapses promptly in loss-of-cooling events, the inlet-temperature drop settles to a new equilibrium, and a single-channel blockage yields only a ~30 K local fuel-temperature rise with <0.4% power decrease. SWIFT-predicted hydrogen redistribution affects reactivity during both steady-state and transient conditions, underscoring its importance. A Brayton-cycle balance of plant (BOP) model in SAM/THM demonstrated stable startup behavior, and xenon-driven reactivity during load following was analyzed. To improve TRISO-compact temperature fidelity, a fast multiscale Heat Source Decomposition (HSD) treatment was implemented. Against heterogeneous benchmarks, HSD reduces underprediction of kernel temperatures and lowers predicted peak powers in reactivity-insertion transients compared to previous homogenized models.

KRUSTY warm-critical validation progressed from FY2024 baselines: the 15₵ insertion shows excellent agreement in peak power (~2% high) and temperature trends, and the 30₵ case was automated via a feedback controller that maintained power near 3 kW for ~150 s with close agreement to data. The successful modeling of the warm critical tests has laid a strong foundation for simulating more complex nuclear system tests in the years ahead.

Throughout FY2025, developer feedback was provided (e.g., MOOSE batch mesh generation, distributed pre-split meshes, Griffin sweeper on displaced meshes), several new models were contributed to the Virtual Test Bed, and an OECD-NEA WPRS multiphysics benchmark based on the HPMR was initiated to enable broader cross-comparison and best-practice development with the nuclear community at large.

Acknowledgement

This work was supported by the Department of Energy – Nuclear Energy Advanced Modeling and Simulation Program (NEAMS) under the Multiphysics Applications Technical Area.

The team would like to express appreciation to Emily Shemon, Cody Permann, and Christopher Matthews for their reviews and support throughout this project.

Invaluable support was provided by the Sockeye developers (Joshua Hansel, Elia Merzari, and Lise Charlot), Griffin developers (Changho Lee, Javier Ortensi, Yaqi Wang, Hansol Park, Josh Hanophy, Zachary Prince, Vincent M. Laboure), Reactor module and MeshGenerator system developers (Emily Shemon, Shikhar Kumar, Aaron Oaks), BISON developers (Wen Jiang, Stephen Novascone, Jacob Hirschhorn), and SWIFT developer (Christopher Matthews), MOOSE framework developers (Logan Harbour, Guillaume Giudicelli, Alexander Lindsay).

The NRIC VTB model reviews from Guillaume Giudicelli were instrumental in providing directions for improvements of submitted models.

The FY2025 achievements described in the report stem from years of work developing high-fidelity multiphysics models for microreactors. The team gratefully acknowledges prior contributors to this project: Lander Ibarra, Adam Kraus, Daniel Nunez, and Stefano Terlizzi.

This research made use of Idaho National Laboratory computing resources which are supported by the Office of Nuclear Energy of the U.S. Department of Energy and the Nuclear Science User Facilities under Contract No. DE-AC07-05ID14517.

1 Introduction

Nuclear energy plays an indispensable role in ensuring a secure and resilient U.S. energy portfolio. Its impact is poised to grow significantly in the near future, driven by surging energy demand resulting from rapid technological advancements. To meet this rising demand, the timely development and deployment of advanced reactor technologies is essential, which is aligned with the missions of the U.S. Department of Energy (DOE) Office of Nuclear Energy (NE).

To accelerate the advancement of these technologies, the DOE-NE Office's Nuclear Energy Advanced Modeling and Simulation (NEAMS) program is actively developing advanced modeling tools to support core design and safety analyses for next-generation reactors. Among these, nuclear microreactors stand out for their compactness, mobility, and high efficiency. Realizing these attributes requires the integration of innovative design features such as liquid metal heat pipes, metal hydride moderators, and control drums.

Moreover, the unique deployment scenarios of microreactors demand adaptability to flexible operating conditions. This complexity presents challenges for vendors relying on traditional or commercial modeling tools, thereby creating a compelling need for the advanced capabilities being developed within the NEAMS program.

NEAMS is committed to delivering high-fidelity, multiphysics modeling solutions to support the design and licensing of a wide range of advanced reactor concepts, including those pursued by U.S. microreactor developers. Within this initiative, the Multiphysics Applications team evaluates code usability and functionality for microreactor design and analysis, while also demonstrating the tools' ability to accurately capture both steady-state and transient behaviors across diverse microreactor configurations.

This project builds on years of expertise acquired by different teams and programs [1-4]. In previous work completed in FY2024 [4], detailed high-fidelity multiphysics models of complex transient scenarios, such as inadvertent control drum rotation, were completed for the full-core heat pipe microreactor (HPMR); while the full-core steady-state high-fidelity Multiphysics simulation was performed for the newly designed gas-cooled microreactor (GCMR) concept along with some preliminary transient simulations. In addition, a preliminary full-core multiphysics model was developed for the warm critical reactivity insertion tests performed on the Kilopower Reactor Using Stirling Technology (KRUSTY) reactor.

The report covers the FY2025 assessment and application of NEAMS multiphysics tools to microreactor design and safety analysis, detailing the modeling workflow, multiphysics coupling, and validation activities. It documents a MOOSE-based multiphysics toolchain integrated via the MultiApp/Transfers system. These methods are described in Section 2.

These capabilities are applied to two full-core concepts: HPMR and GCMR, which are discussed in details in Sections 3 and 4, respectively. Code validation efforts based on the KRUSTY warm critical reactivity insertion tests are covered in Section 5. A summary is included in Section 6 along with perspectives.

2 Methodology and Assessment

This section summarizes the NEAMS capabilities applied in this project, with a focus on new and existing modules assessed in FY2025 (see Table 2-1). The microreactor multiphysics modeling toolchain comprises: Griffin [5] for neutronics; BISON [6] for solid heat conduction and solid mechanics; Grizzly [7] for graphite solid-mechanics models; Sockeye [8] for heat-pipe modeling; SAM/THM for 1D coolant-channel flow; and SWIFT for hydrogen redistribution. All codes are built within the MOOSE framework, enabling multiphysics coupling via the MultiApp system. Meshes are generated using the MOOSE Reactor Module [9] and related MeshGenerator objects. This section presents assessment highlights, including development requests and user feedback conveyed to the respective code teams.

One of the main outcomes of this project is the user experience gained by the team and our testing of new capabilities which leads to feedback to developers. Those are discussed further in Section 6.

Table 2-1 Summary of codes and module assessed in FY2025

Code/Module	Features Used/Assessed	Related Section(s)
MOOSE Reactor Module	Batch mesh generation action Quadratic elements	3.1
Griffin	DFEM-SN and CMFD for acceleration with displaced mesh Point kinetics Poison tracking MC^2-3 cross-section used in Griffin	3.2.2, 4.5, 4.6, 3.3.4, 5.1.1
BISON	Solid Mechanics, graphite models	3.4
Sockeye	Liquid-conduction vapor-flow (LCWF) model	3.2
SWIFT	Hydrogen redistribution	4.3
SAM/THM	Coolant channel model and Brayton-loop model	4.1, 4.4
Grizzly	graphite models	3.4
MultiApps/Transfers	Distributed mesh approach along with mesh pre-splitting	3.3, 3.4, 4.2, 5.2

2.1 *Mesh*

2.1.1 Moose Reactor Module

The MOOSE Reactor Module [9] is a specialized module of the Multiphysics Object-Oriented Simulation Environment (MOOSE) [10] designed to streamline the creation of finite element meshes for nuclear reactor core geometries. It empowers analysts to rapidly construct detailed meshes for reactor pins, assemblies, and full cores using built-in mesh generation tools tailored to both Cartesian and hexagonal configurations. With capabilities like automatic subdomain volume preservation, control drum modeling, and component tagging for post-processing, the module eliminates the need for external meshing software and integrates seamlessly with MOOSE-based physics applications. This open-source tool has been successfully applied to a wide range of reactor types, including fast reactors, microreactors, and high-temperature gas-cooled reactors.

With full core meshes for the three microreactors established in previous FYs, FY2025 meshing efforts focused on testing new MOOSE features by extending existing input files. A notable upgrade is the batch mesh generation Action, which streamlines meshing of repeated components. This was developed in response to FY2024 suggestions from the microreactor application driver team, to reduce the HPMR mesh input by roughly half and improve maintainability. In addition, the Reactor Module now fully supports quadratic elements. Quadratic element meshes were tested for the GCMR model in FY2025 and demonstrated improved energy balance in heat conduction simulations.

2.2 Neutronics

2.2.1 Griffin

Griffin is a reactor physics code jointly developed by Idaho National Laboratory and Argonne National Laboratory [5]. It is based on the MOOSE framework and suited for multiphysics applications of advanced reactor designs. Griffin solves the fundamental neutron transport equation using finite element methods for spatial discretization, multigroup approximations for energy discretization, and deploying a variety of methods such as discrete ordinates method, spherical harmonics expansion method and diffusion method to discrete neutron streaming directions. Griffin also supports point kinetics simulations for rapid analysis of transient behaviors. In addition, it provides a wide range of reactor physics capabilities, from cross-section preparation to radionuclide depletion. Within the Microreactor Application Driver, Griffin served as the primary tool for solving the neutronics. Specifically, the Discontinuous Finite Element Method (DFEM) with the discrete ordinates (SN) approach, coupled with the Coarse Mesh Finite Difference (CMFD) accelerator, was employed to solve the neutronics. The point kinetics solver in Griffin was also examined for lower-fidelity transient modeling.

In FY2025, Griffin served as the main application, governing neutronics and orchestrating coupling with other physics in all the three microreactor models. For most simulations, the high fidelity DFEM–SN transport solver with CMFD acceleration was employed; for cases requiring a reduced order treatment, Griffin's point kinetics (PKE) solver was used. To capture fission product effects, the poison tracking feature in Griffin was incorporated into the related microreactor models. Previously available only for the PKE and diffusion solvers, poison tracking was extended—through coordination with the Griffin developers—to the high-fidelity transport solvers and demonstrated in this work. Cross section generation workflows used with Griffin are summarized in the following two subsections.

2.2.2 Serpent

Serpent is a Monte Carlo which solves the neutron and photon transport in three-dimensional, continuous- energy and angular space [11]. The code is developed at VTT Technical Research Center of Finland and is widely used to model a variety of nuclear reactors. In the Microreactor Application Driver, Serpent models were created to generate multi-group cross sections that was used in Griffin neutronic model. Serpent calculations also provide reference solutions for evaluating Griffin models when solving steady state problems.

2.2.1 MC^2-3

It was found and reported in FY2024 [12] that Monte Carlo–generated cross sections can introduce significant biases in core criticality calculations for fast-spectrum, small, leaky cores like KRUSTY, particularly when anisotropic scattering is prominent. The ANL lattice physics code MC^2-3 [13] offers improved high-order anisotropic cross sections in the reflector region but lacks accurate fuel Doppler reactivity feedback. As a workaround, a hybrid cross section set—using MC^2-3 for the reflector and Serpent-2 for all other regions—was adopted for KRUSTY. However, due to limitations in the current MC^2-3 version, cross sections were generated using the ENDF/B-VII.0 library rather than the more recent ENDF/B-VIII.0. This approach is identical to the KRUSTY cross-section approach reported in FY2024.

2.3 Heat Conduction and Thermomechanics

2.3.1 BISON

BISON [6] is a cutting-edge nuclear fuel performance code, developed within the MOOSE framework. Designed with versatility, BISON is capable of modeling a wide variety of fuel forms, such as light water reactor fuel rods, TRISO particle fuel, and metallic rod and plate fuel.

During FY2025, BISON continued to be used and evaluated for full core, macroscopic modeling of HPMR, GCMR, and KRUSTY. A major update was the implementation of solid mechanics in the full core HPMR model: BISON, originally applied only to heat conduction, was extended to a fully coupled heat conduction and solid mechanics solve, enabling evaluation of thermal expansion effects on HPMR steady state and transient behavior. Importantly, although TRISO fuel performance was not a primary focus in FY2025, the successful development of the full core HPMR model with solid mechanics paves the way for full core TRISO fuel performance analyses targeted for FY2026.

For simplicity, the TRISO compacts in both HPMR and GCMR were modeled as a homogenized medium in the corresponding multiphysics simulations. In reality, a TRISO compact is heterogeneous, consisting of a graphite matrix and TRISO particles with multiple concentric layers that possess dissimilar thermophysical properties. As a result, homogenization may not adequately capture peak kernel temperatures. Accordingly, in FY2025, Heat Source Decomposition (HSD) was implemented to evaluate heterogeneity effects in TRISO compacts. HSD results were compared with the homogenized treatment to identify scenarios in which explicit heterogeneity is required.

2.3.2 Grizzly

Grizzly [7] is a structural materials simulation code. Built on the MOOSE framework, Grizzly is designed to model aging and degradation mechanisms in nuclear reactor components, with a particular focus on reactor pressure vessels and reinforced concrete structures. It solves coupled systems of partial differential equations to simulate complex, multiphysics phenomena across multiple length scales, enabling predictive assessments of material integrity under long-term operational conditions. Originally tailored for light water reactors, Grizzly's capabilities have expanded to support advanced reactor designs, making it a versatile tool for evaluating structural reliability and informing relicensing decisions.

The Grizzly code was not tested as part of the Multiphysics model in FY2025. Instead, a systematic comparison of the graphite models in Grizzly and BISON was conducted to inform the future strategy for modeling the thermophysical and mechanical behavior of graphite in microreactors. BISON currently provides the essential thermophysical and mechanical models for at least one nuclear-grade structural graphite, making it sufficient for baseline analyses; Grizzly offers a broader set of models across multiple graphite grades, making it better suited for advanced studies requiring grade-specific behavior. Both codes will be exercised in FY2026 to systematically assess graphite behavior in microreactors.

2.4 Heat Removal and Power Conversion

2.4.1 Sockeye

Sockeye [8] is a heat pipe modeling code to simulate and analyze thermal performance in microreactor systems. Built on the MOOSE framework, Sockeye focuses on high-temperature, liquid-metal heat pipes with annular screen or porous wick structures, offering robust capabilities for both steady-state and transient conditions. It features effective conduction model, liquid-conduction vapor-flow (LCVF) model, and two-phase-flow model, enabling detailed predictions of operational limits such as capillary and dryout thresholds.

In FY2025, the full-core HPMR heat-pipe model was upgraded from using effective conductance model to adopting the advanced LCVF model, alongside introduction of a sodium working fluid variant of the HPMR concept. The LCVF model's steady-state and transient behavior within the multiphysics framework was exercised to confirm compatibility and consistency. Notably, a multiphysics HPMR startup model was developed on the upgraded configuration, enabling analysis of transients that were not achievable with the prior effective conductance approach.

2.4.2 SAM/THM

The System Analysis Module (SAM) [14] is a modern, MOOSE-based system-analysis tool developed under the NEAMS program for advanced non-LWR safety analysis. As a MOOSE application, SAM enables flexible coupling with other MOOSE-based codes and has direct access to framework capabilities and physics modules, including the Navier–Stokes Module and the Thermal Hydraulics Module (THM) [15].

Its core capability lies in assembling a network of coupled components, for instance, pipes, junctions, and valves. THM provides several new systems to MOOSE to enable and facilitate thermal hydraulic simulations, most notably the Components system, which provides a higher-level syntax to MOOSE's lower-level objects. This system is extensible by the user, but the current library primarily includes components based on a one-dimensional, single-phase, variable-area, compressible flow model, as well as heat conduction.

Full-core GCMR modeling was performed in Section 4 using THM through SAM. The single coolant channel model follows the approach and models established in FY2024, whereas the balance of plant model was developed by adapting a similar model available in the Virtual Test Bed (VTB) [16].

2.5 Moderator Performance

2.5.1 SWIFT

SWIFT [17] is a MOOSE application dedicated to simulating the performance of hydride-based moderator. SWIFT assessment was first conducted in FY2023 and FY2024. The SWIFT-based hydride performance analyses have been made for both full core HPMR and GCMR models in FY2024. In FY2025, the focus of SWIFT-based analyses was focused on its impact on the GCMR behavior during both normal operation and power transients (Section 4.3).

2.6 Multiphysics Coupling

The NEAMS codes—Griffin, SAM/THM, Sockeye, SWIFT, and BISON—were used to perform multiphysics simulations of the HPMR (Section 3), GCMR (Section 4), and KRUSTY (Section 5) models under both steady-state and transient conditions. Figure 2-1 shows the MOOSE MultiApp architecture used in FY2025 analyses, with Griffin as the parent application governing neutronics. This MultiApp/Transfer system enabled seamless data exchange between Griffin, its child application (BISON), and its grandchild applications (SAM/THM, Sockeye, and SWIFT). Although SWIFT can intrinsically solve diffusion-based heat conduction for moderator temperature, the temperature profile was transferred from BISON instead. SWIFT then computed the hydrogen distribution in the moderator modules and returned it to BISON. BISON aggregated the hydrogen distributions from all hydride moderator modules and passed the full-core distribution to Griffin, where it was used as a grid variable for cross-section calculations.

A major upgrade in FY2025 was the implementation of a solid mechanics model in the full-core HPMR. Unlike the fast-spectrum KRUSTY reactor examined in this project, the neutronics of thermal-spectrum reactors such as HPMR and GCMR are less sensitive to thermal expansion, so solid mechanics had not been included in earlier full-core multiphysics models. To enhance fidelity, solid mechanics was added to BISON in FY2025, enabling the child application to capture thermomechanics rather than heat transfer alone and paving the way for future full-core TRISO performance analyses. Additionally, for GCMR balance-of-plant (BOP) development, a 1D SAM/THM grandchild application was extended to cover the entire power conversion system instead of merely coolant channels in the microreactor core. For transients involving complex reactivity control—such as startup and load following—point kinetics was used in Griffin for simplicity instead of higher-fidelity methods.

Small-scale and test simulations ran on Argonne’s divisional cluster, where individual MOOSE applications were compiled separately against a shared MOOSE build and dynamically linked at runtime. Large-scale simulations were executed on INL’s HPC. On INL-HPC, cases not involving SWIFT used the precompiled BlueCRAB or DireWolf executables, while SWIFT-related cases used a user-built BlueCRAB dynamically linked with a user-built SWIFT (since SWIFT is not packaged with BlueCRAB). As the project advanced from unit-cell/assembly to full-core scale, memory demands increased substantially, making pre-split distributed meshes essential to fit within the available computational resources on INL’s HPC.

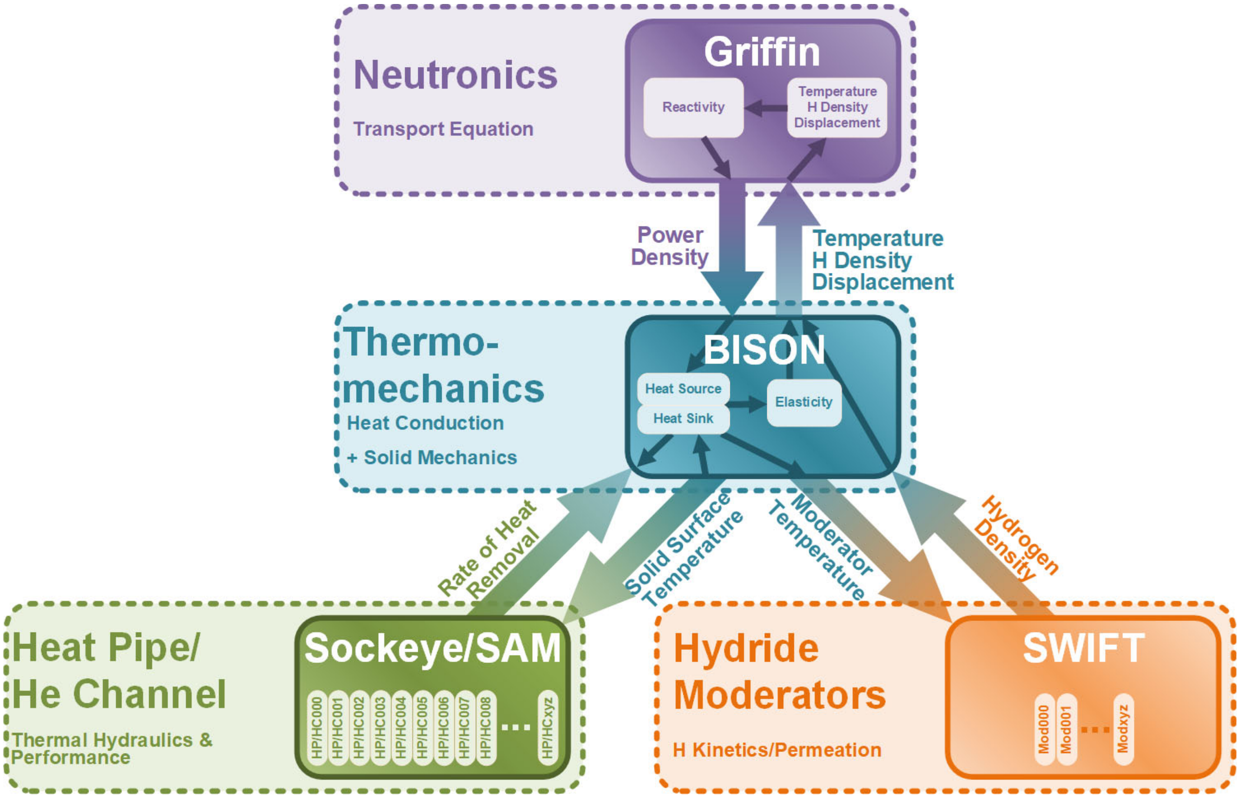

Figure 2-1 A typical MultiApp hierarchy for the high-fidelity multiphysics simulations considered in this report

3 Multiphysics Modeling of Full-Core HPMR

Over the past few years, the microreactor applications team has established a comprehensive three-dimensional, full-core multiphysics modeling suite for the HPMR concept employing potassium (K) heat pipes. The suite couples high-fidelity neutronics, heat conduction in solid components, heat-pipe performance, and hydride moderator behavior, and has demonstrated the ability to simulate both steady-state operation and a wide range of transient scenarios. This year, the team further enhanced the suite by introducing a sodium (Na) heat-pipe variant that enables leveraging more advanced mechanistic (liquid-conduction vapor-flow) heat-pipe models [18], adding an HPMR startup model that leverages the advanced heat-pipe formulation, and integrating comprehensive solid-mechanics capabilities with the full-core model.

3.1 *HPMR Mesh Update*

The HPMR mesh did not require changes in FY2025; however, new features in MOOSE's built-in mesh generation were evaluated for HPMR mesh creation. The key pilot was adopting MOOSE's batch mesh generation Action to make the HPMR mesh input more concise and organized. This Action can generate a series of meshes from a single mesh generator by varying one or more input parameters, which is ideal for repeated components that differ only slightly—such as HPMR's reflectors and control drums. Using the new Action reduced the HPMR Griffin mesh input by approximately 300 lines and consolidated parameters for similar components, making them easier to modify via ***!include*** and parameter overrides. Specifically, the HPMR BISON mesh can now be produced using ***!include*** to load the Griffin mesh input and overriding the necessary parameters, reducing the input by more than 500 lines. This update has been ported to the VTB repository's HPMR model as a demonstration. Because this update is limited to input syntax, the impact on computational time is negligible.

3.2 *Na-HPMR Variant Development*

The original HPMR concept employs potassium (K) heat pipes, initially modeled in Sockeye using an effective thermal conductivity approach. In this treatment, each heat pipe is represented as a solid with an artificially high effective conductivity in its core, and empirical correlations are applied to capture performance limits. To improve model fidelity, the heat transfer efficiency of the heat pipes should be governed by a mechanistic model rather than a lumped effective conductivity. Accordingly, use of Sockeye's liquid-conduction vapor-flow (LCVF) (previously call vapor-only (VO)) model [18], which enables advanced heat-pipe simulation capabilities (such as startup transients) and strengthens the credibility of the overall HPMR analysis, is favored. Because of these advantages, the team is transiting to use the Na-HPMR variant with the LCVF model as the main default HPMR model in future investigations.

3.2.1 Working fluid selection

Due to its higher operating temperature range and the resulting thermal efficiency benefits, sodium has been selected by several HPMR developers—including the U.S. Department of Energy's Microreactor Program (MRP) in its sponsored Single Primary Heat Extraction and Removal Emulator (SPHERE) and Microreactor Agile Non-Nuclear Experiment Test Bed (MAGNET) facilities [19]—as the preferred working fluid [20]. As a result, a number of well-designed heat-pipe experiments with advanced instrumentation have been conducted recently, providing abundant data for model validation [19, 21]. Indeed, Sockeye's LCVF model has been successfully validated against these new experimental datasets [22]. To leverage this validated capability in Sockeye and showcase the strength of the NEAMS toolset, we developed a Na-HPMR variant derived from the existing K-HPMR concept, retaining most key design parameters. To align with sodium's optimal operating regime, the Na-HPMR's nominal operating temperature is increased by approximately 100 K.

3.2.2 Griffin and Cross-section Update

Homogenized multi-group cross sections were generated for the Na-HPMR model using Serpent-2. The Serpent-2 input follows the same structure as that of the K-HPMR, with the key difference being that sodium is used as the heat pipe working fluid instead of potassium. An 11-group energy structure is employed, with parameters defined over grids of: Fuel temperature (5 values), Moderator, reflector, monolith, and heat pipe temperature (5 values), Hydrogen content (7 values), Control drum rotation (1 value: drums out).

The results obtained from Serpent-2 are consistent with expected reactor physics trends. Specifically, increasing hydrogen content within the tabulated range (from $YH_{0.5}$ to YH_2) increases K-eff due to enhanced moderation. Increasing fuel temperature consistently decreases K-eff reflecting the negative reactivity feedback caused by Doppler broadening. This multi-grid cross-section library enables analysis of both thermal reactivity feedback effects and the impacts of hydrogen redistribution within the moderator. All simulations reported here are being carried out for the central control rod–out and control drums-out configuration. Finally, the generated cross sections from Serpent-2 are converted into an XML format for compatibility with Griffin.

3.2.3 Advanced Heat Pipe Model

The effective conductivity model previously used in the K-HPMR was replaced with the LCVF mechanistic model in Sockeye. The migration was straightforward thanks to the user-friendly interface: most input blocks—including boundary conditions and analysis postprocessors—were retained, and the existing MultiApp hierarchy remained compatible with the upgraded Sockeye grandchild application. With this change, the heat-pipe component now uses LCVF, and the former performance-limitation postprocessors are no longer needed and were removed. Compared with the diffusion-based effective conductivity model, the LCVF model is more computationally demanding. In practice, enabling advanced solver options—such as the SuperLU preconditioner and automatic scaling—improved robustness and convergence.

3.3 Multiphysics Simulations of Na-HPMR

The high-fidelity, 3D full-core multiphysics model for the Na-HPMR was derived from the existing K-HPMR configuration. The baseline model comprises a three-level MultiApps hierarchy that couples Griffin for neutronics (DFEM-SN(1,3)), BISON for heat transfer in solid components, and Sockeye for heat-pipe performance. SWIFT was also integrated as a grandchild application in the Na-HPMR model as an advanced option. As established in prior work, hydride moderator effects are most consequential for long-duration events. Accordingly, because this section addresses only steady-state conditions and short-term transients (where hydrogen diffusion is marginal as observed in previous FYs), multiphysics results without SWIFT coupling are reported for simplicity.

3.3.1 Steady State

At the nominal thermal power of ~2.07 MW, the Griffin-BISON-Sockeye model predicted the steady-state operation conditions of the Na-HPMR as shown in Figure 3-1.

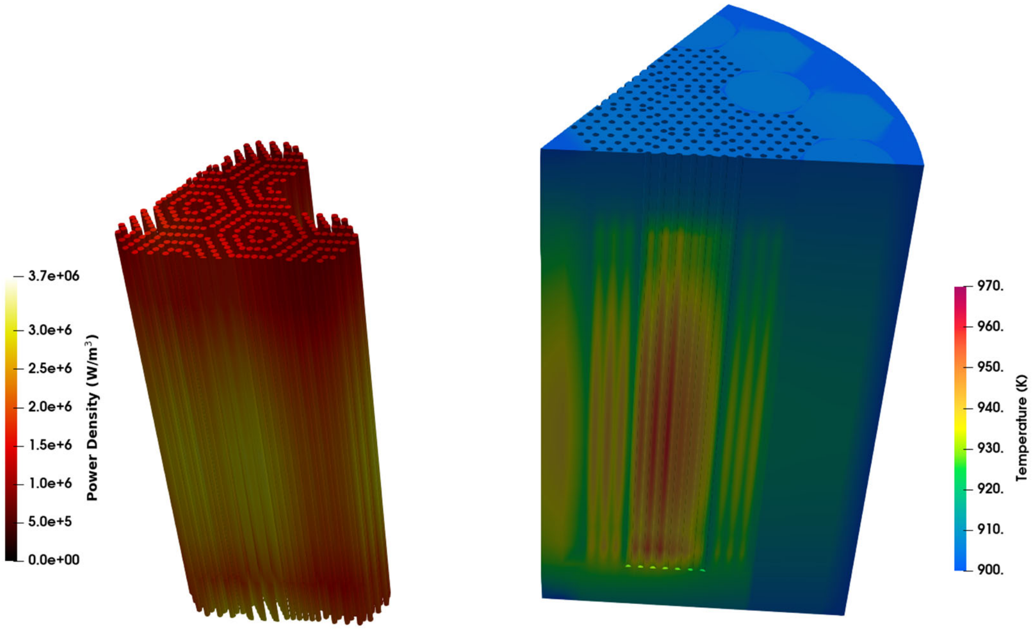

Figure 3-1 The power and temperature conditions during steady-state operation of the Na-HPMR as predicted by the multiphysics model.

The key operating condition features of the Na-HPMR are quite similar with its K-HPMR counterpart, as compared in Table 3-1. With the powerful heat removal capabilities of the heat pipes, the maximum temperature in the Na-HPMR fuel is less than 70 K higher than the heat pipe condenser region temperature (900 K).

Table 3-1 Comparison between the steady state modeling results of the K-HPMR and Na-HPMR

	K-HPMR	**Na-HPMR**
k_{eff}	1.03269	1.05589
T_{fuel} (K) (max/min/avg)	866/814/844	964/914/940
T_{mod} (K) (max/min/avg)	862/815/842	959/911/937

3.3.2 Load-Following Transient of Na-HPMR

Before applying the Na-HPMR to advanced transients enabled by the LCVF model, we first used it to reproduce several transients previously investigated with the K-HPMR. The load-following case is a "global"-level transient initiated by reducing the external heat transfer coefficient at the condenser outer surface from 10^6 W/m^{2}K to 10^2 W/m^{2}K, thereby decreasing the heat removal capability by 99.99%. This initiation method is identical to that used in the K-HPMR load-following case.

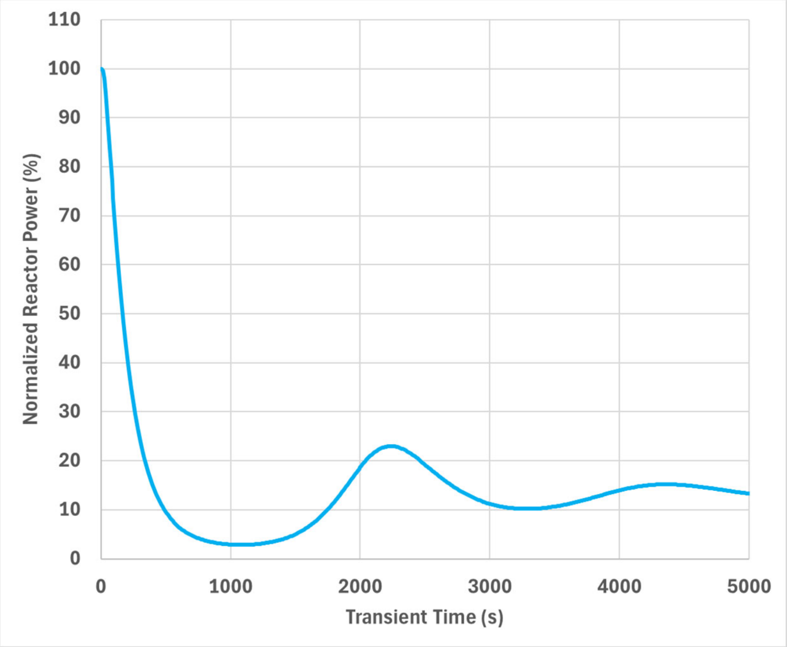

Figure 3-2 Time evolution of reactor power during a load following transient

The model predicts that the abrupt reduction in heat removal capability produces an immediate rise in core temperature. As shown in Figure 3-3, within a few hundred seconds the average fuel temperature increases by ~25 K, and the maximum fuel temperature peaks near 986 K. The resulting negative temperature reactivity feedback drives the reactor power down (Figure 3-2); within about 1,000 seconds, power falls to below 5% of its initial steady-state value. The reduced power then cools the core below the original steady-state temperature, prompting a power rebound that peaks at approximately 23% of steady state around 2,200 seconds after the transient begins. As the temperature rises again, power decreases once more. Another power rebound with ~17% peak power was predicted at around 4,200 seconds after the transient begins. These oscillations are expected to continue with diminishing amplitude until the system reaches a new, lower-power equilibrium. These results exhibit trends consistent with prior K-HPMR studies that employed the effective-conductance heat-pipe model.

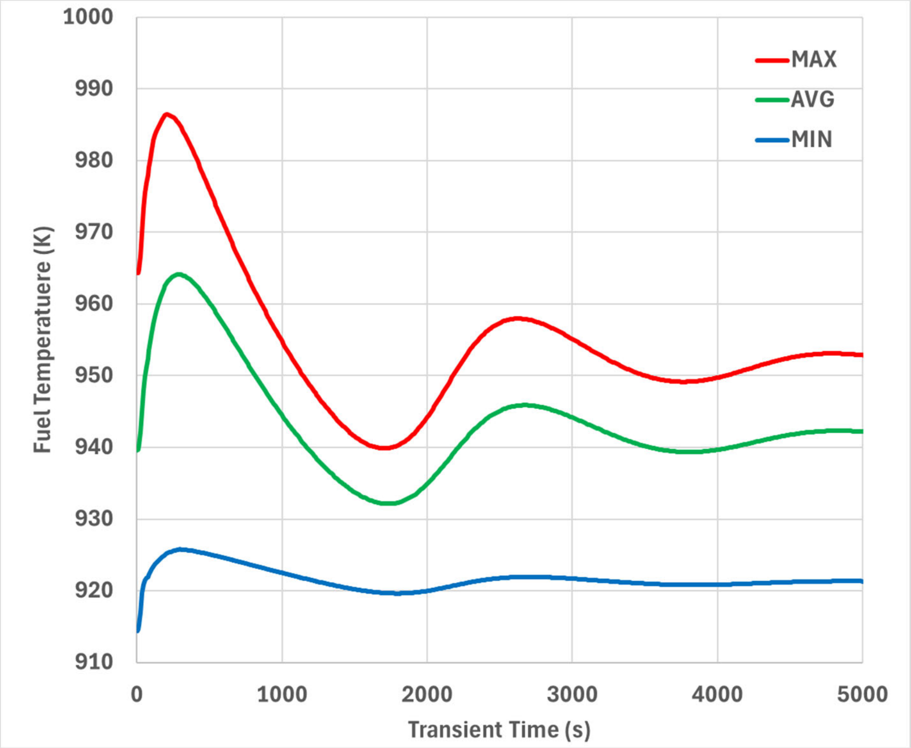

Figure 3-3 Time evolution of representative fuel temperatures during a load following transient

3.3.3 Single Heat Pipe Failure Transient of Na-HPMR

On the other hand, the single heat pipe failure case is a local-level transient initiated by reducing the external heat transfer coefficient at the condenser outer surface from 10^6 W/m^{2}K to 10^{-2} W/m^{2}K, thereby eliminating the heat removal capability of the affected heat pipe. The location of the selected heat pipe was intentionally chosen to be in the hottest region of the HPMR, which is at the center of the innermost assembly, to evaluate the worst scenario. This transient initiation method is also identical to that used in the K-HPMR load-following case.

The model predicts that the loss of a single heat pipe immediately raises the temperature in the surrounding region; within 300 seconds, the local temperature increases by approximately 10 K (see Figure 3-5). As shown in Figure 3-6, only the area adjacent to the failed heat pipe is affected. However, the impact remains highly localized because the remaining heat pipes continue to operate and remove the additional heat generated near the failed pipe.

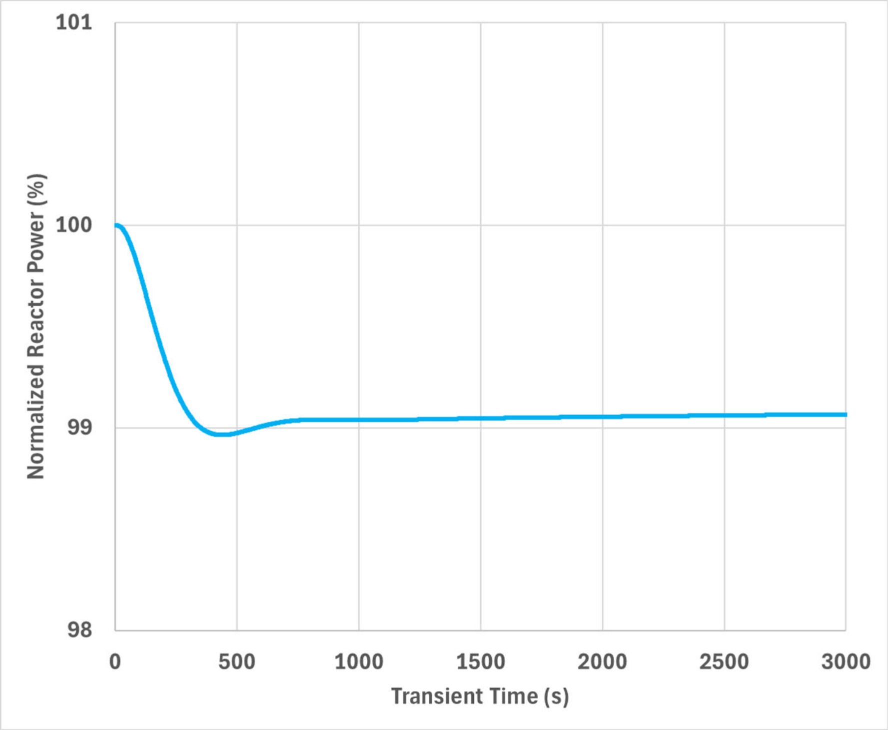

Figure 3-4 Time evolution of reactor power during a single heat pipe failure transient

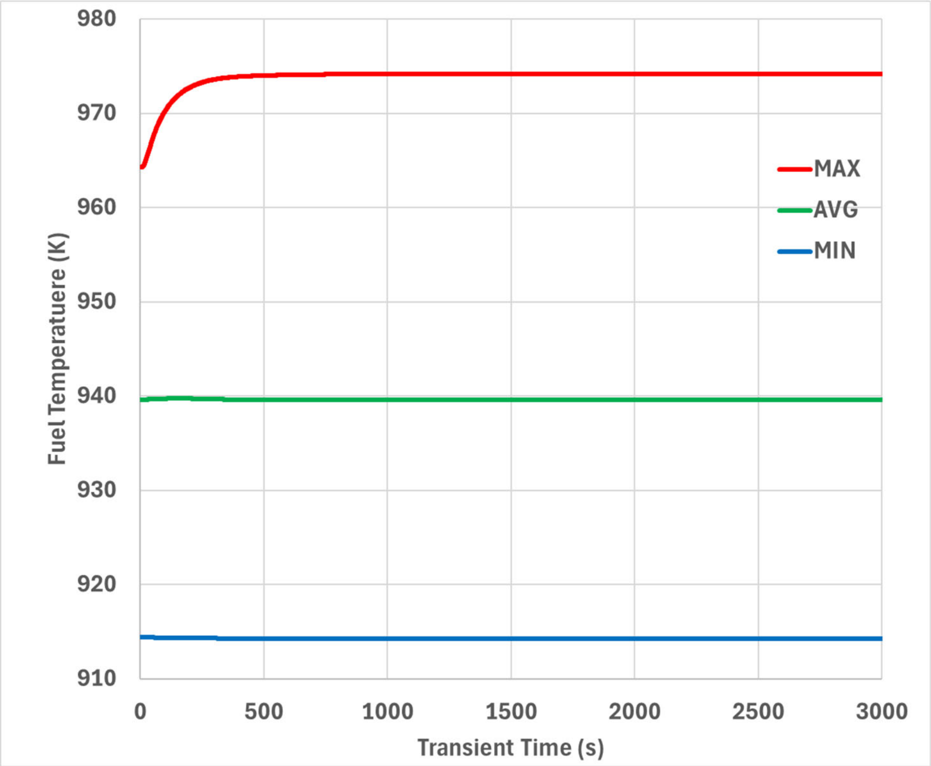

Figure 3-5 Time evolution of representative fuel temperatures during a single heat pipe failure transient

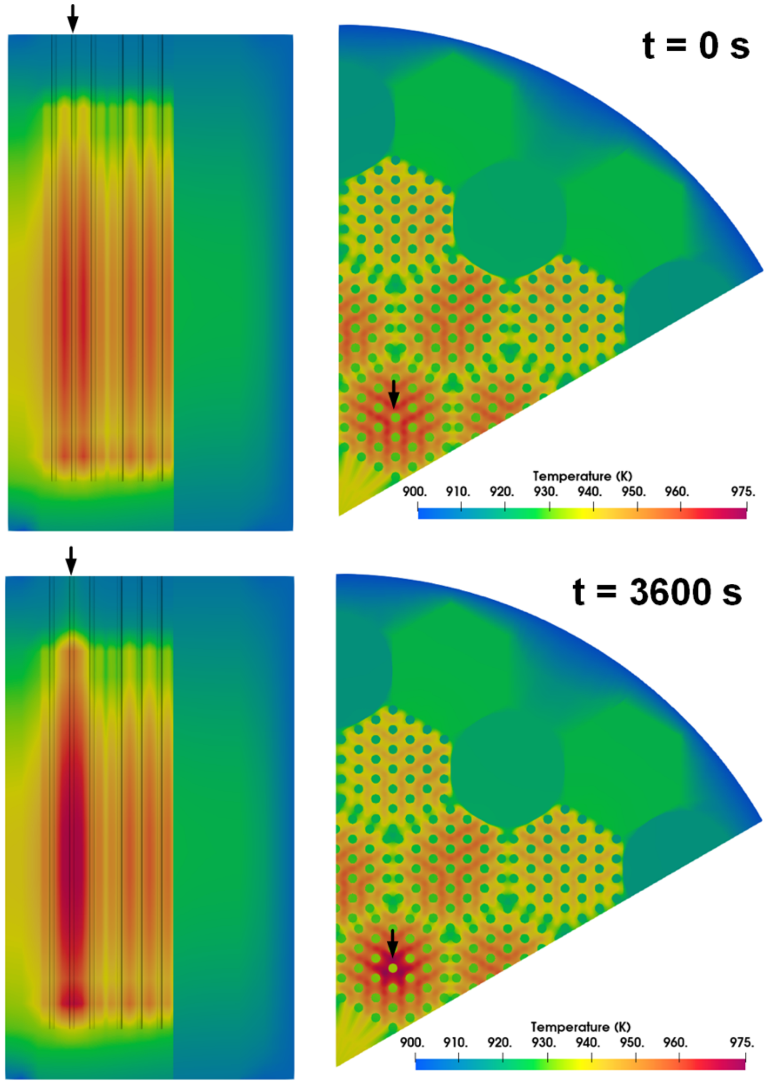

Figure 3-6 Temperature profiles of the vertical and horizontal cross sections of the failed heat pipe (marked by the arrow) at 0 s and 3,600 s after the initiation of the failure event.

Consequently, the reactor's average temperature changes only marginally over the entire transient. Because the effect is localized, the microreactor's power decreases by only about 1%, driven by the local temperature rise and the resulting negative reactivity feedback (see Figure 3-5). The Na-HPMR demonstrated strong resilience to a single heat pipe failure, owing to the large margin to operating limits for individual heat pipes at the designated power level. Under overpower conditions that reduce this margin, however, cascading heat pipe failures are expected, as demonstrated in prior studies of this project.

3.3.4 Startup Transient

A key motivation for upgrading to the LCVF heat-pipe model (as well as to Na working fluid) is to enable simulation of more advanced transients, notably HPMR startup. The startup analyzed here is not a frozen startup, in which the working fluid begins in a solid state. Instead, we assume the heat pipes initially contain liquid working fluid, and startup proceeds as a vapor front advances toward the condenser, progressively activating each pipe's heat-removal capability.

The aforementioned HPMR startup is correlated to reactor power ramping. Here a linear power ramping from 0% to 100% of the designed reactor power within 1 hour was adopted. Ideally, such a power ramping need to be simulated by a high-fidelity neutronic model with well-designed control drum rotation strategy that takes various reactivity feedback mechanism into account. Such an advanced approach would be non-trivial, time consuming, and would require a sophisticated secondary loop model. In this section, to focus on the modeling capability of the startup of heat pipes, a simplified neutronics approach enabled by point kinetics (PKE) was adopted. The high-fidelity approach mentioned above should be a long-term task for the Na-HPMR model development to capture the power profile evolution during startup and to demonstrate the capability of determining a control drum operation strategy during start up using MOOSE tools.

In the PKE-based approach, the steady-state 3D spatial power distribution of the Na-HPMR from the high-fidelity model (see Figure 3-1) is held fixed and scaled by the time-dependent power multiplier predicted by the PKE model to construct the volumetric heat source for the BISON child application. Consequently, only the neutronics portion (the main application) of the high-fidelity multiphysics model is replaced with the simplified PKE treatment. The average fuel temperature computed in BISON is then passed back to the Griffin PKE model to evaluate the temperature-feedback reactivity. Figure 3-7 shows the total reactivity required to achieve the prescribed linear power ramp, along with the corresponding external reactivity (i.e., with temperature feedback removed) that would be supplied by control drum rotation.

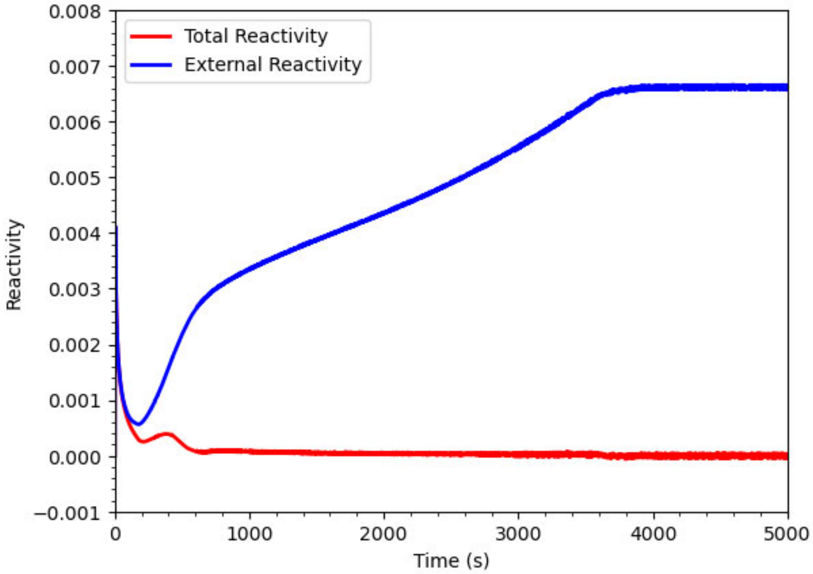

Figure 3-7 Calculated external reactivity to achieve the designated power ramping profile during the startup

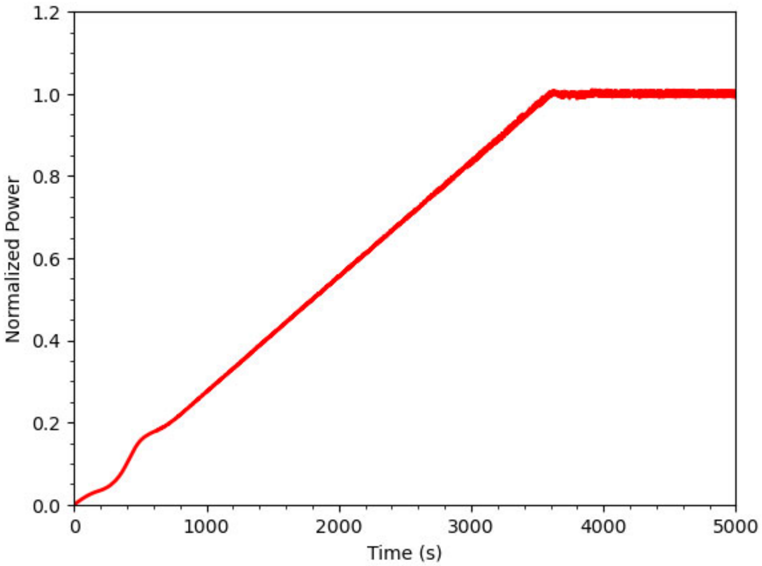

Figure 3-8 Time evolution of the reactor normalized power as a result of the calculated external reactivity during the startup

Using the prescribed reactivity, the PKE model generates the power-ramp profile shown in Figure 3-8. Aside from a brief initial deviation, the computed power-multiplier closely tracks the intended linear increase.

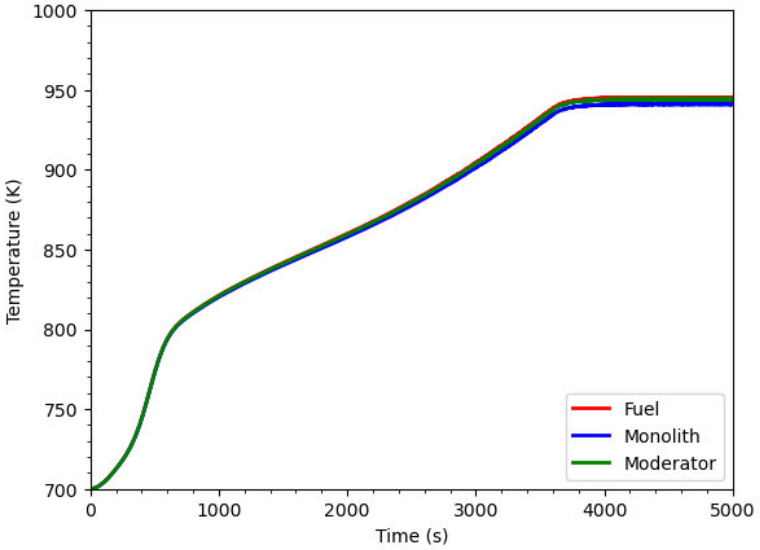

Figure 3-9 Time evolution of the calculated average temperatures of different reactor components during the startup

With the power input described above, the temperature of the system was initiated at 700 K—above sodium's melting point to prevent solidification yet below the nominal operating temperature of the Na heat pipes. To realize this initial state, we reduced the external boundary temperature at the condenser from 900 K to 700 K. To still maintain a ~900 K condenser temperature at steady state and full power with a 700 K external temperature, the heat-transfer coefficient was artificially adjusted to 152 W/m^{2}K, which holds the condenser near 900 K at approximately 1800 W of power (i.e., average heat pipe power at design power level). This is a simplified boundary-condition construct to achieve the desired temperature behavior during startup. A coupled, high-fidelity secondary-system model at the condenser will be required for a more realistic startup simulation and is planned for next year's work.

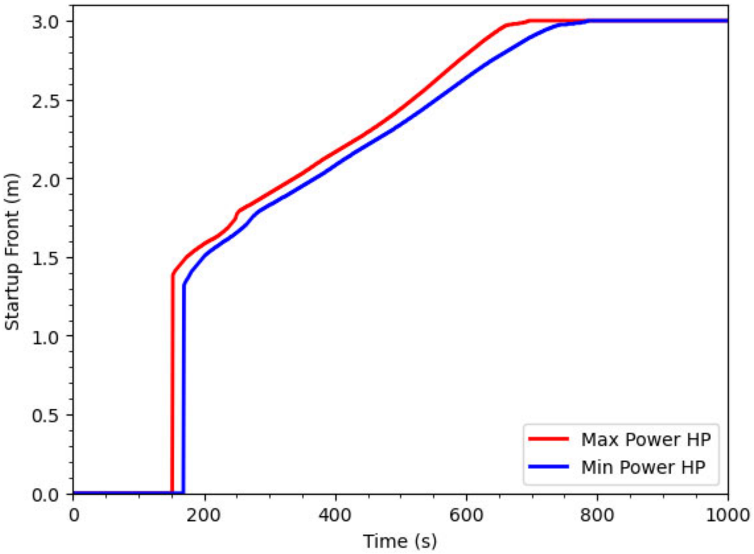

Figure 3-10 Time evolution of startup front position for the two representative heat pipes (evaporator region 0~1.8 m, adiabatic region 1.8~2.1 m, and condenser region 2.1~3.0 m)

With the modifications described above, the time evolutions of average temperatures for three representative Na-HPMR components are shown in Figure 3-9. Initially, temperatures rise rapidly because the heat pipes have not yet been activated. Around 600 seconds, the rate of increase slows, indicating heat-pipe activation. The temperatures then approach asymptotic values shortly after the power ramp ends at 3,600 seconds. The evolution of the startup front locations in representative heat pipes (Figure 3-10) corroborates these trends: the vapor fronts reach the leading edge of the condenser regions at ~500 seconds and traverse the full condenser length by ~700 seconds, coinciding with the temperature inflection in Figure 3-9. This behavior is further confirmed by the heat-removal rate evolution shown in Figure 3-11.

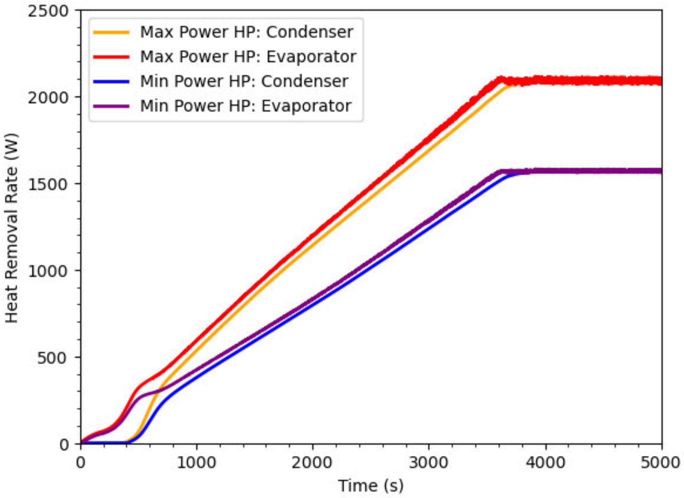

Figure 3-11 Time evolution of heat removal rate for the two representative heat pipes

This work demonstrates that the advanced LCVF heat-pipe model can be coupled with neutronics and solid heat conduction models to build a full-core multiphysics HPMR model that captures the coupled behavior during startup.

3.4 Solid Mechanics Models Implementation

Previously, HPMR model development has focused on neutronics, heat transfer, and hydride moderator behavior, while solid mechanics had not yet been fully integrated into the full-core model set. Because the reactor operates in the thermal spectrum, solid-mechanics effects—principally fuel thermal expansion—are less dominant than in fast-spectrum microreactors. Even so, incorporating solid mechanics into the full-core HPMR model improves fidelity by explicitly accounting for thermal expansion. It also enables broader structural analyses under normal operation, transient conditions, and seismic loading. In addition, the coupled solid mechanics capability provides stress fields throughout the reactor, making full-core, multiphysics-informed TRISO fuel performance assessments possible. Solid mechanics modeling for graphite was initiated this fiscal year. The initial effort focused on surveying relevant models available across MOOSE applications and completing a baseline solid-mechanics implementation for the full-core HPMR model.

3.4.1 Graphite Models in MOOSE-based Applications

In the HPMR and GCMR concepts examined in this project, graphite serves as the primary structural and matrix material. A monolithic graphite block accommodates key core components—including TRISO fuel compacts, hydride moderator modules, burnable poisons, and heat pipes (or coolant channels in the GCMR). Graphite also forms the matrix of the TRISO compacts. Graphite is therefore critical both as a thermal medium for heat conduction and as a structural material governing solid-mechanics behavior. To date, the multiphysics models have primarily used graphite material models available in BISON, focused on thermophysical properties. Recently, work has progressed in NEAMS SM&C technical area to implement a comprehensive suite of graphite solid mechanics models in Grizzly to enable structural simulations of graphite components. This subsection reviews and compares the graphite models available in both codes to inform future model and code selection for graphite-related analyses. Here, both thermophysical properties models (i.e., thermal conductivity, specific heat, and coefficient of thermal expansion) and mechanical properties models (i.e., elasticity tensor and creep) are compared with a focus on covered graphite grades and model dependence on parameters including temperature (T), fast neutron fluence (ϕ), and applied stress (σ).

Table 3-2 Thermal conductivity and specific heat models of graphite in BISON and Grizzly

BISON			Grizzly		
Class Name	Grade	Dependence	Class Name	Grade	Dependence
Graphite Matrix Thermal	A3-3 A3-27 **H-451** IG-110 PCEA NG2020	T, ϕ	N/A	N/A	N/A

As a structural analysis code, Grizzly does not include as many thermophysical models as BISON. For example, as shown in Table 3-2, only BISON provides graphite thermal conductivity and specific heat models, both of which depend on temperature and fast neutron fluence. The corresponding BISON material class applies to both TRISO-loaded and TRISO-free graphite, covering a broad range of graphite grades, including those used as the TRISO compact matrix and generic structural graphite materials.

Table 3-3 Thermal expansion models of graphite in BISON and Grizzly

BISON			Grizzly		
Class Name	Grade	Dependence	Class Name	Grade	Dependence
Graphite Grade Thermal Expansion Eigenstrain	G-348 **H-451** IG-110	T, ϕ	Structural Graphite Thermal Expansion Eigenstrain	H-451 IG-110	T, ϕ

As summarized in Table 3-3, both BISON and Grizzly contain graphite thermal expansion models that depend on temperature and fast-neutron fluence. BISON currently provides models for three graphite grades, whereas Grizzly supports two.

Table 3-4 Elasticity models of graphite in BISON and Grizzly

BISON			Grizzly		
Class Name	Grade	Dependence	Class Name	Grade	Dependence
Graphite Grade Elasticity Tensor	**H-451** NG2020	T, ϕ	Structural Graphite Elasticity Tensor	H-451 IG-110	T, ϕ

Similarly, as shown in Table 3-4, both codes have graphite elasticity models implemented. The elasticity of graphite is anisotropic in both codes and is dependent on temperature and fast-neutron fluence. Each code supports two grades of graphite.

Table 3-5 Creep models of graphite in BISON and Grizzly

BISON			Grizzly		
Class Name	Grade	Dependence	Class Name	Grade	Dependence
Graphite Grade Creep Update	**H-451**	T, ϕ, σ	Structural Graphite Creep Update	H-451 IG-110 JAEA AGC	T, ϕ, σ

BISON supports a creep deformation model only for graphite grade H-451, whereas Grizzly includes creep models for three additional graphite grades. In both codes, the creep behavior depends on temperature, fast-neutron fluence, and applied stress (see Table 3-5).

Table 3-6 Irradiation swelling/shrinkage models of graphite in BISON and Grizzly

BISON			Grizzly		
Class Name	Grade	Dependence	Class Name	Grade	Dependence
Graphite Grade Irradiation Eigenstrain	**H-451** IG-110	T, ϕ	Structural Graphite Irradiation Eigenstrain	H-451 IG-110 AGC3	T, ϕ

Last but not least, as shown in Table 3-6, the volumetric strain induced by irradiation is covered by both codes as an eigen strain, which relies on both temperature and fast neutron fluence. BISON supports both H-451 and IG-110 for this model, whereas Grizzly provides addition support for ACG3.

In summary, BISON provides a comprehensive suite of graphite thermophysical and mechanical models; notably, grade H-451 is fully supported. Consequently, if the microreactor uses H-451, BISON alone can be employed to simulate graphite solid mechanics. By contrast, while Grizzly's thermophysical coverage is incomplete, it offers broader mechanical property support by including additional graphite grades. Therefore, Grizzly is required when analyzing grades other than H-451. If both heat conduction and solid mechanics must be solved within a single application for those cases, both BISON and Grizzly classes may need to be loaded, which in turn will require dynamic library linking or a prebuilt "super" application.

3.4.2 Implementation of Solid Mechanics

The K-HPMR Multiphysics model has been updated to include a solid mechanics implementation in BISON, enabling the capture of temperature-dependent displacement changes and improving neutronics computational fidelity within the inner core region. Table 3-7 summarizes the BISON models employed for the fuel compact, graphite matrices, burnable poison absorbers, moderator envelope, and upper and lower reflectors. Since YH_2 moderator material models are not available in BISON, the thermal properties and thermal expansion coefficients were taken from open literature and were manually implemented. The solid mechanics model focuses on the fuel compact and inner core region, excluding outer reflectors and control drums. Diffusion kernels were utilized to evenly disperse displacements across these excluded components, ensuring smooth and continuous results at the interface between the modeled and excluded regions. Convective heat flux boundary conditions were applied to all external surfaces at 800K.

The current VTB model of the K-HPMR Multiphysics model utilizes a mesh that successfully converges neutronics and heat transfer calculations but failed to achieve convergence in the thermomechanics analysis due to insufficient mesh resolution. The mesh density of solid mechanics model was therefore increased by approximately 106%, which enabled successful convergence for both steady-state and transient scenarios.

Table 3-7. BISON models used in the solid mechanics simulations of HPMR.

BISON Models	Descriptions
GraphiteMatrixThermal	Thermal properties of fuel compact and monolith graphite matrices
BeOThermal	Thermal properties of Beryllium Oxide reflector and control drum
B4CThermal	Thermal properties of Boron Carbide burnable poison absorbers
SS316Thermal	Thermal properties of Stainless Steel 316 moderator envelope
GraphiteMatrixThermalExpansionEigenstrain	Eigenstrain calculation due to thermal expansion in fuel compact and monolith graphite matrices
BeOThermalExpansionEigenstrain	Eigenstrain calculation due to thermal expansion in BeO
SS316ThermalExpansionEigenstrain	Eigenstrain calculation due to thermal expansion in SS316 moderator envelope
BeOElasticityTensor	Young’s modulus and Poisson’s ratio for BeO
SS316ElasticityTensor	Young’s modulus and Poisson’s ratio for SS316

The implementation of the solid mechanics model in the K-HPMR shows minimal impact on steady-state thermal performance, as shown in Table 3-7. Under the same power output at 345.6 kW (for 1/6 core), the solid mechanics model resulted in a slightly decreased k-effective from 1.048563 to 1.048436 (a reduction of ~127 pcm). The temperature distributions remain virtually unchanged, with maximum fuel temperatures differing by less than 0.01 K and identical average and minimum fuel temperatures at 845.31 K and 817.9 K, respectively. This negligible temperature variation indicates that thermal expansion and displacement effects captured by the solid mechanics model have minimal influence on the steady-state neutronics and thermal behavior of the system. The small reduction in reactivity likely results from geometric changes due to thermal expansion, which slightly increased neutron leakage or alters the neutron spectrum, though these effects are minor enough that they do not significantly impact the reactor’s thermal performance under steady-state conditions.

Table 3-8. Comparison of key K-HPMR operating parameters with and without Solid Mechanics model implementation.

	k_{eff}	Power (kW)	T_{fuel_max} (K)	T_{fuel_avg} (K)	T_{fuel_min} (K)
w/ Solid Mechanics	1.048436	345.6	869.83	845.31	817.87
w/o Solid Mechanics	1.048563	345.6	869.84	845.31	817.85

Figure 3-12 displays the thermal and mechanical response of K-HPMR core under steady-state operation. The left shows the temperature distribution within the fuel compacts, with peak temperature of 869.83 K occurring in the central fuel region and decreasing axially to ~820 K at the top, showing heat pipes providing efficient heat removal pathways. The right illustrates the magnitude of displacements resulting from thermal expansion, with maximum displacements occurring at the top of the core and minimal displacement at the bottom boundary, which represents a fixed surface. The displacement gradient demonstrates the cumulative effect of thermal expansion along the axial and radial directions. The continuous displacement field confirms that the diffusion kernels successfully distributed the mechanical response across the domain, avoiding discontinuities at inner matrix and outer reflector and control drum interfaces while maintaining computational efficiently in the coupled Multiphysics simulation.

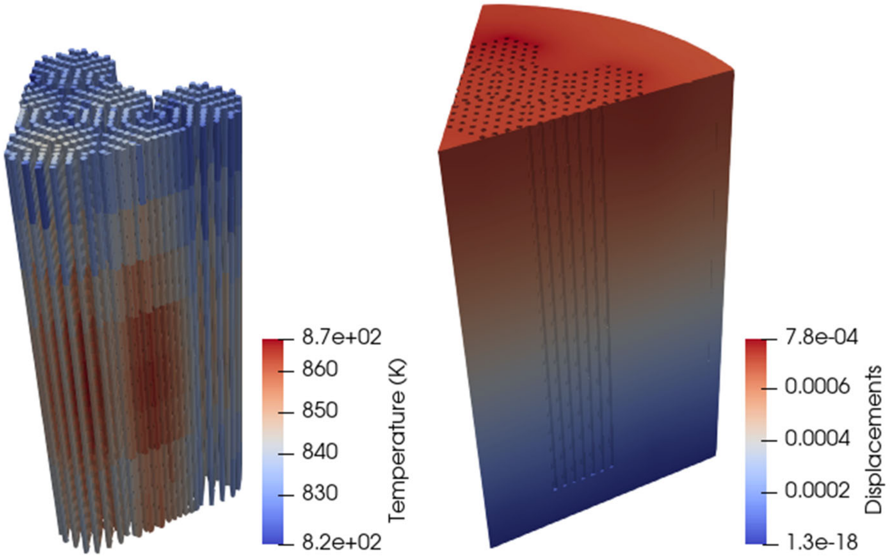

Figure 3-12. Steady-state fuel compact temperature and core displacements.

The solid mechanics model was successfully applied to two transient scenarios from the virtual test bed to evaluate the thermomechanical response of the HPMR under transient conditions [23]. These analyses demonstrate the model's capability to capture the coupled neutronics-thermomechanical-thermal-hydraulics behavior during both load-following operations and null transient conditions.

For the load-following transient, the reactor demonstrates proper passive safety characteristics through inherent negative temperature feedback mechanisms. As shown in Figure 3-13, the reactor power drops from the initial steady-state power to about 50kW within the first 200 seconds, stabilizing at this reduced power level for the remainder of the 1000-second transient. The power reduction is initiated by a decrease in heat removal capability at the secondary side, which causes the fuel compact temperatures to rise initially, as shown in Figure 3-14. The maximum fuel temperature peaks at 900 K around 100 seconds into the transient before gradually decreasing to about 860 K. The solid mechanics model captures the thermal expansion effects during this temperature excursion. While the mechanical feedback is included in the analysis,the evolution of neutronics is dominated by the strong negative temperature reactivity coefficient.-

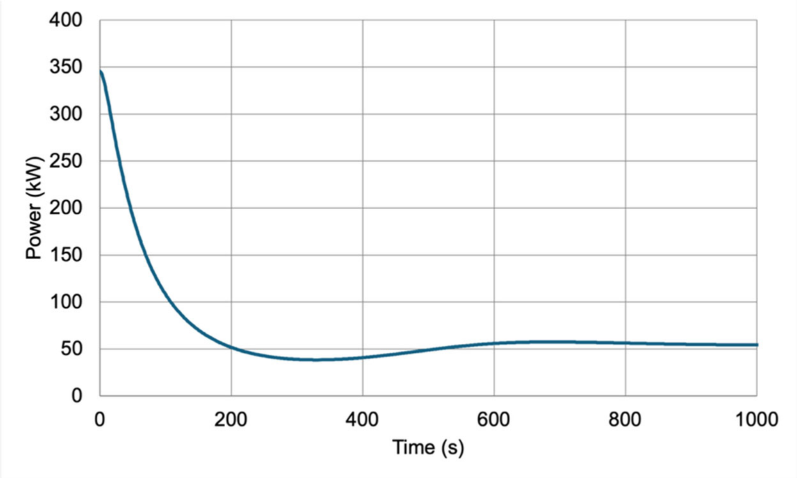

Figure 3-13. Time evolution of K-HPMR core power during the load following transient.

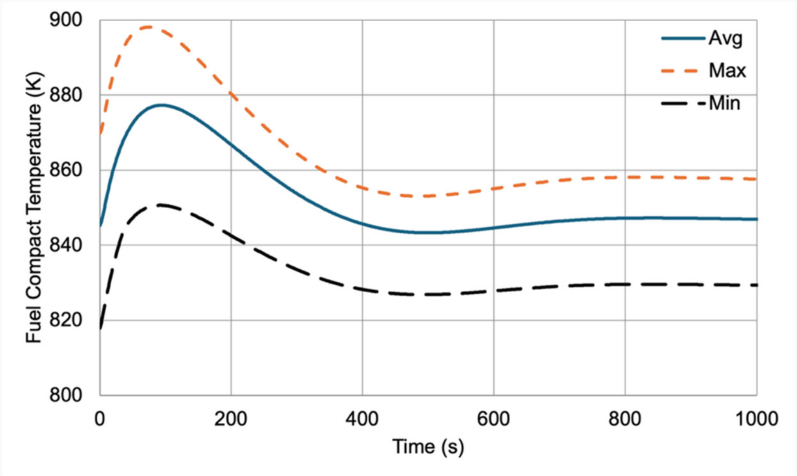

Figure 3-14. Time evolution of K-HPMR fuel compact temperature during the load following transient.

The null transient analysis, representing a perturbation-free scenario, confirms the stability of the coupled Multiphysics model with solid mechanics implementation. Figure 3-15 and Figure 3-16 show the reactor power remaining at 345.55 kW and the temperature unchanging through the 200-

second simulation. These constant values match the steady-state conditions, verifying that the solid mechanics implementation introduces no numerical oscillations or drift. The stable power and temperature during the null transient confirm proper convergence of the thermal expansion calculations and equilibrium between the coupled neutronics, thermomechanical, and thermal-hydraulics solvers.

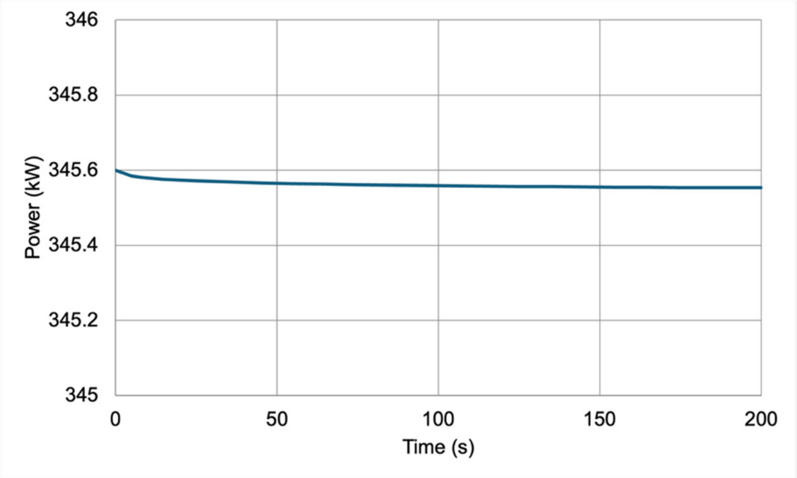

Figure 3-15. Time evolution of K-HPMR core power during the null transient.

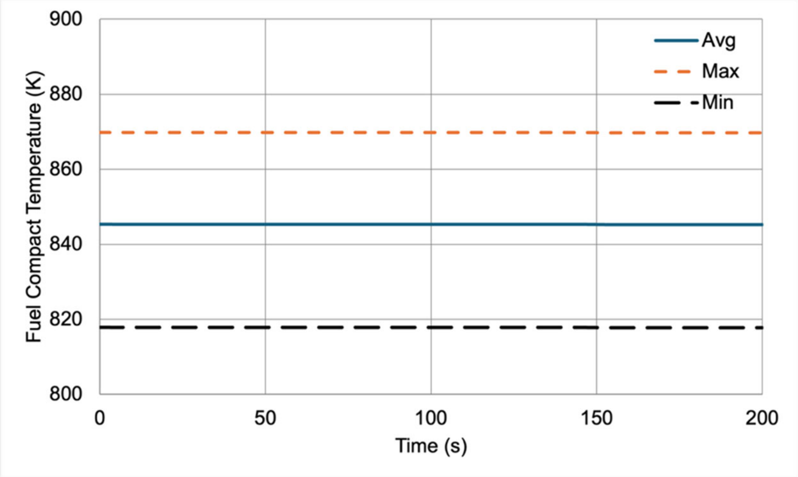

Figure 3-16. Time evolution of K-HPMR fuel compact temperature during the null transient.

3.5 *OECD-NEA Benchmark*

As part of this year's activity, the team prepared a proposal for a multiphysics microreactor benchmark through the Organization for Economic Co-operation and Development (OECD) Nuclear Energy Agency (NEA). This benchmark was motivated by several international participant requests from the Working Party on Scientific Issues of Reactor Systems (WPRS). These institutes are at various stages of development and demonstration of multiphysics modeling capability on microreactors and recognize the validation of these models is hindered by a scarcity of experimental data. This project aims to address this gap by facilitating a cross-comparison of multiphysics simulation results among WPRS participants, thereby enhancing confidence in the simulation workflows used in microreactor design and licensing. Through this benchmark, we will compare simulation results and derive best practices for steady-state and transient modeling of a heat-pipe microreactor. The project will establish a collaborative environment for institutes to exchange best practices in multiphysics modeling of these systems.

The benchmark proposal developed is based on the Na-HPMR multiphysics model published in this activity on the VTB. The benchmark proposed will be conducted in three phases over three years:

- Phase 1.A: Focus on neutronics-only comparison, evaluating K-eff and power distribution across different core configurations.
- Phase 1.B: Focus on heat-pipe analysis and comparison, evaluating heat transfer performance in steady-state and transients.
- Phase 2: Steady-state multiphysics comparison, assessing K-eff, power distribution, and temperature distribution.
- Phase 3: Transients comparison, analyzing load following and heat-pipe cascading failure scenarios.

At the WPRS, three expert groups are being involved in this proposal: Physics of Reactor Systems (EGPRS), Reactor Core Thermal Hydraulics and Mechanics (EGTHM), and Reactor Systems Multi-Physics (EGMUP). The benchmark proposal was developed and distributed to WPRS delegates for comments. Interest from 12 international institutes was already confirmed from the US, Europe, Japan, and Korea (ANL, CEA, Ibaraki University, JAEA, KAERI, Nagoya University, NCSU, GeorgiaTech, PSI, Seoul National University, Sejong University, UNIST). The proposal has now been sent to the PRG for recommendation, before seeking Nuclear Science Committee (NSC) bureau approval expected in the fall of 2025. Benchmark specifications will be developed in late 2025 and shared with participants for iteration at the beginning of Phase 1.

3.6 Summary of HPMR Work

The FY2025 HPMR effort yielded key insights into microreactor behavior through multiphysics modeling:

- Development of the sodium working fluid variant of the HPMR design indicated the efficiency of the workflow established in this project and flexibility of the MOOSE ecosystem in adopting design modifications of microreactors.
- For the sodium working fluid variant of the HPMR, the advanced LCVF heat pipe model was fully applied to both steady state and transient analyses, demonstrating seamless compatibility and consistent coupling with the other multiphysics models.
- The multiphysics Na-HPMR startup model further showcased LCVF’s unique ability to capture complex transients that the prior effective conductivity approach could not represent.
- Integrating solid mechanics into the full core HPMR models establishes a clear pathway to core-level TRISO performance assessments, while the comparative review of graphite models in BISON and Grizzly lays the foundation for graphite structural analyses planned for FY2026.

4 Multiphysics Modeling of Full-Core GCMR

Analysis of GCMR technology began in FY2022, initially focusing on the assembly model and a design based on industry concepts, followed by initial full-core modeling and assembly-level TRISO performance analyses. In FY2024, the GCMR core was redesigned to enable 1/6 reflective symmetry, and a steady-state multiphysics model incorporating hydride performance was developed. Work continued in FY2025 with several activities:

- Comprehensive transient analyses were performed to cover a range of scenarios with both global and localized effects on the GCMR; the impact of integrating the hydride performance model was also assessed.
- A balance-of-plant model was developed by coupling the existing full-core multiphysics model with an energy conversion cycle model, enabling more realistic transient analyses of the GCMR.
- The effects of fission products on load-following operation were investigated using the multiphysics model with poison-tracking capabilities in Griffin.
- A new heterogeneity treatment was developed to improve the accuracy of fuel-temperature estimates for the TRISO-compact–fueled GCMR.

4.1 Model Description and Updates

The whole-core GCMR is designed to operate at 20 MW_{th}. The core is relatively small, measuring 2.42 m in diameter and 2.40 m in height (with a 200 cm active height). It is divided into three radial fuel zones, surrounded by BeO axial and radial reflectors, and controlled by twelve drums located in the reflector. Fuel is TRISO particles (40% packing fraction, 19.75% LEU) embedded in graphite blocks. Moderator pins of $YH_{1.8}$ are coated with chromium (0.007 cm) and enclosed in FeCrAl envelopes (0.05 cm). Reactivity control is supported by burnable poison rods of Gd_2O_3 (25% packing fraction, radius 0.25 cm), distributed axially throughout the assemblies. Coolant channels (radius 0.6 cm) and a lattice pitch of 20.8 cm with pin pitch of 2.0 cm ensure efficient thermal-hydraulic performance. The GCMR was designed for cycle length of 9.5 years, and for using a Brayton power conversion cycle.

4.1.1 Energy Balance in Thermal Model

For the heat conduction simulation, a finer mesh is required to resolve heat fluxes near key interfaces and surfaces—particularly along coolant-channel walls and the reactor's exterior. This is essential for maintaining energy balance; at steady state, the total heat removed from all model surfaces should reasonably match the reactor power (e.g., >95% with linear elements). To further minimize energy imbalance (i.e., <0.1%), quadratic elements should be employed to accurately capture heat flux near critical interfaces and surfaces, as shown in Table 4-1. In this report, the linear element meshes were used with the multiphysics model to generate the reported results considering the computational resource needed.

Table 4-1 Energy balance of the GCMR multiphysics model using the refined BISON mesh

Power Type	**Unit**	**Value (Linear)**	**%**	**Value (Quadratic)**	**%**
Total Reactor Power (1/6 core)	kW	3330	100.00%	3330	100.00%
Heat Transfer to Coolant	kW	3201	96.11%	3328	99.93%
Heat Transfer to Environment	kW	0.692	0.02%	0.450	0.01%
Heat Loss on Symmetry Boundary	kW	1.501	0.05%	0.578	0.02%

4.2 Multiphysics Simulations of GCMR

In FY2024, the Griffin/BISON/SAM/SWIFT model for the GCMR experienced convergence failures during fixed-point iteration for steady-state simulations, so a manual fixed-point iteration procedure was used to obtain tentative results. Following updates to the MOOSE framework, the issue was resolved in FY2025, enabling automated steady-state multiphysics simulations. Leveraging this progress, a comprehensive suite of transient scenarios was also modeled with the established GCMR multiphysics model.

4.2.1 Steady-State Simulation

The steady-state simulation results of the multiphysics GCMR model are illustrated in Figure 4-1 and results are summarized in Table 4-2.

Set by the inlet coolant temperature, the minimum fuel temperature in the GCMR is about 900 K. The fuel temperature increases with axial height, reaching roughly 1,200 K near the coolant outlet. Because the coolant channels are densely distributed, the moderator temperature is comparable to the fuel temperature. Notably, in a radial cross-section the maximum temperature is not at the geometric center; instead, it is predicted in the mid-core region, primarily due to differences in assembly designs across radial zones.

It is noteworthy that inclusion of SWIFT for modeling hydrogen migration yields a k_{eff} approximately 600 pcm higher than the model without SWIFT (i.e., assuming a flat axial hydrogen distribution). This increase stems from the pronounced axial temperature gradient and the resulting hydrogen redistribution which impacts neutron interaction cross sections (see Figure 4-1).

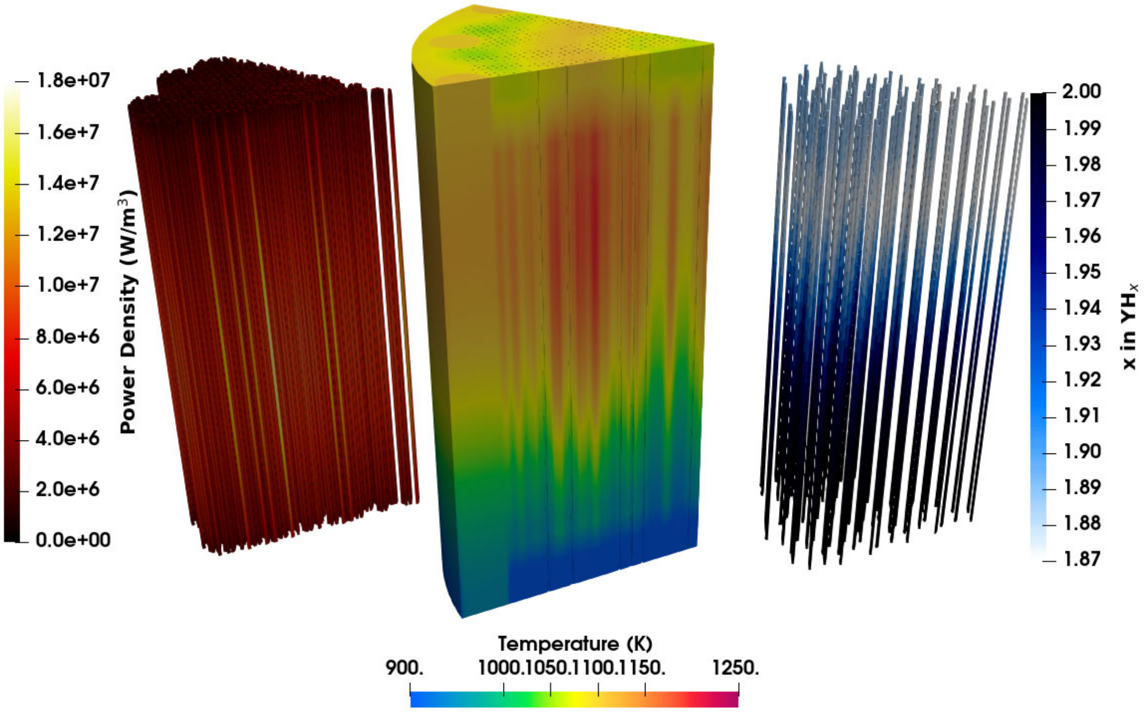

Figure 4-1 Steady-state operation status of the full-core GCMR

Table 4-2 Key predicted parameters by the GCMR models

Parameter	w/ SWIFT linear	w/o SWIFT linear	w/o SWIFT quadratic
Power (MW_{th}, 1/6 core)	3.33	3.33	3.33
$T_{fuel,avg}$ (K)	1096	1096	1100
$T_{fuel,max}$ (K)	1225	1226	1231
$T_{fuel,min}$ (K)	911	911	912
$T_{mod,avg}$ (K)	1074	1073	1076
$T_{mod,max}$(K)	1180	1181	1185
$T_{mod,min}$ (K)	912	912	912
k_{eff}	1.035701	1.029007	1.0288574

4.2.2 Comprehensive Transients Simulations

Using the steady-state solution as initial conditions, four transient scenarios were modeled with the multiphysics model with SWIFT integrated: three with global effects—coolant depressurization, loss of coolant velocity, and a drop in inlet coolant temperature—and one with localized effects—a single coolant-channel blockage. The multiphysics model successfully handled all of these scenarios. It is important to note that decay heat was not considered in these simulations, based on the assumption of a fresh microreactor core at the onset of the transient. This assumption might lead to an underestimation of residual heat when a microreactor core with an extended and stable power history reaches low power during transients. Incorporation of decay heat is recommended for future transient simulations and should be coordinated with the planned depletion modeling efforts for this project.

4.2.2.1 Coolant Depressurization

The coolant-depressurization transient is modeled as a linear drop in outlet pressure from 7 MPa to ambient (0.1 MPa) over 13 seconds, accompanied by a simultaneous reduction in coolant velocity from 15 m/s to 0.1 m/s. This event substantially reduces the reactor's global heat-removal capacity, driving temperatures upward. In turn, negative temperature reactivity feedback is expected to reduce reactor power and ultimately arrest the temperature rise. This inherent safety response should be captured by the multiphysics GCMR model.

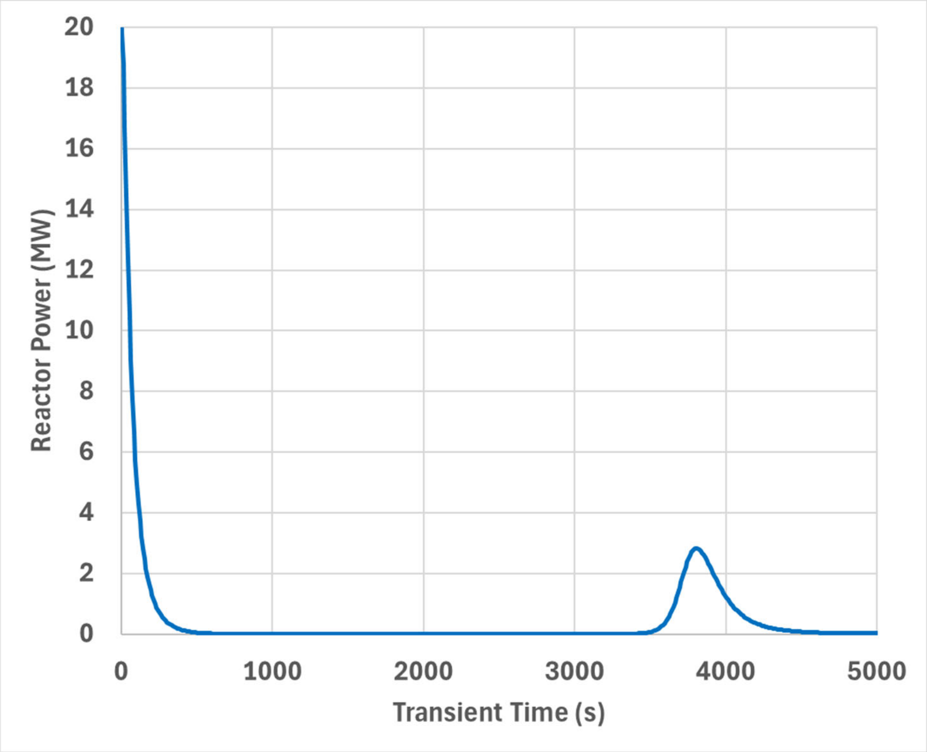

Figure 4-2 Time evolution of the reactor power during a coolant depressurization transient

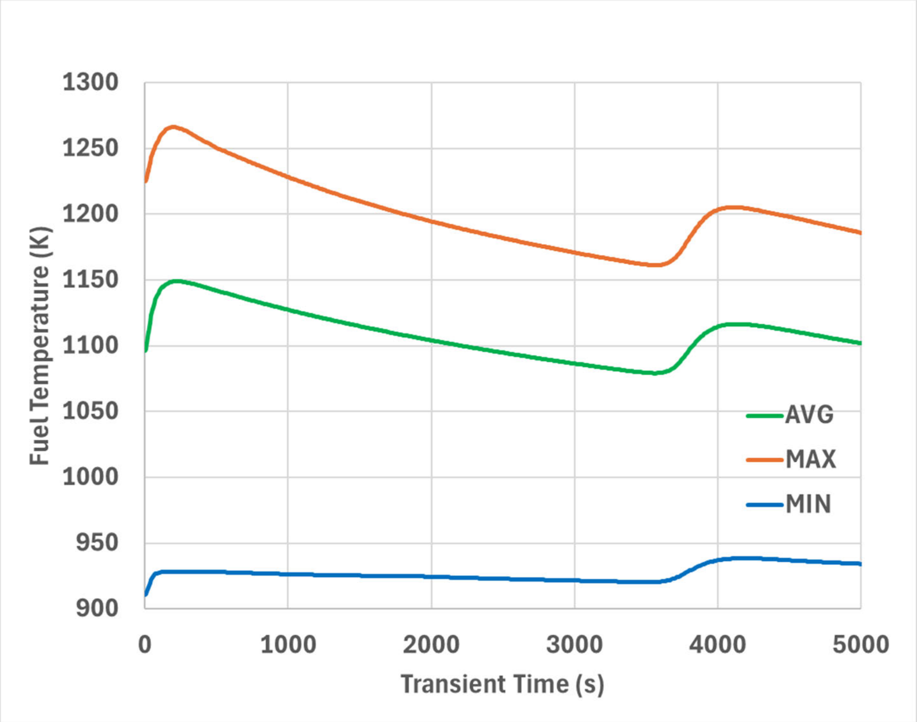

Figure 4-3 Time evolution of the representative fuel temperature during a coolant depressurization transient

As shown in the Figure 4-2, the multiphysics model predicts that under coolant depressurization the GCMR loses nearly all of its operating power within ~400 seconds. The maximum fuel temperature initially rises by ~50 K due to reduced cooling, then declines as power falls (see Figure 4-3). After roughly 2,000 seconds, the average fuel temperature drops below its steady-state value. The continued cooldown reverses the sign of the temperature reactivity feedback, producing a secondary power peak of ~5 MW at ~3,800 seconds. The associated temperature increases then reinstates negative feedback, and the power decreases again shortly thereafter.

4.2.2.2 Loss-of-Coolant Velocity

The loss-of-coolant-velocity transient is similar to depressurization, featuring simultaneous reductions in coolant velocity and pressure; however, the pressure remains a substantial fraction of its initial value. In this case, the coolant velocity drops linearly to zero within 10 seconds, while pressure decreases from 7 MPa to 4.67 MPa. The complete stall of coolant flow effectively eliminates loop heat removal, causing temperatures to rise and triggering negative temperature reactivity feedback that rapidly reduces reactor power. The GCMR multiphysics model is expected to capture this behavior.

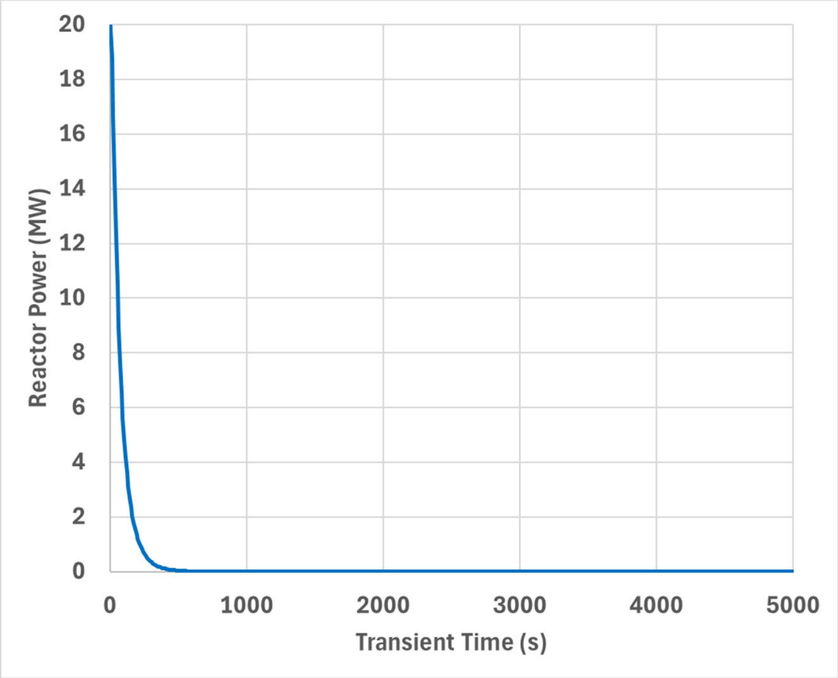

Figure 4-4 Time evolution of the reactor power during a loss of coolant velocity transient

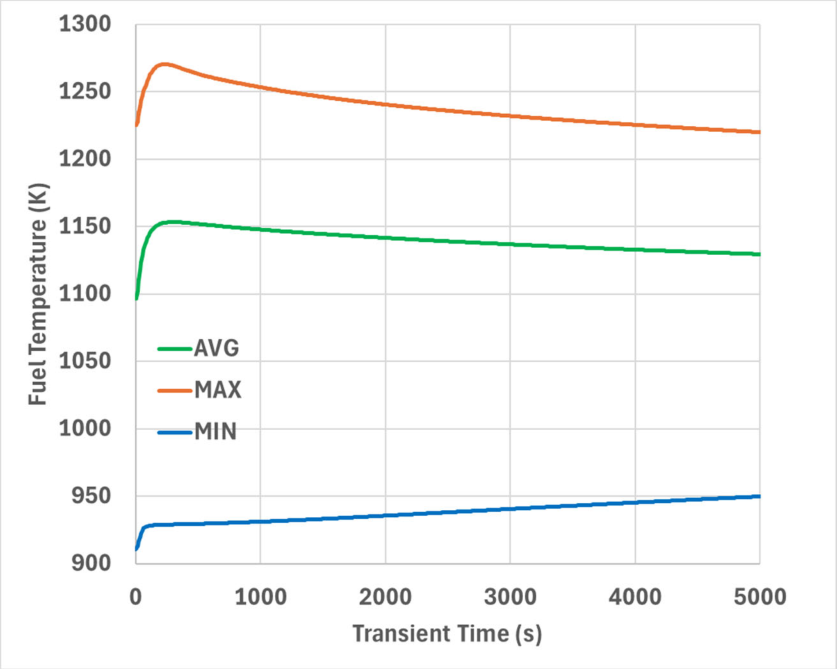

Figure 4-5 Time evolution of the representative fuel temperatures during a loss of coolant velocity transient

As shown in Figure 4-4, the model predicts a rapid drop in power to nearly zero within ~500 seconds, driven by the temperature increase shown in Figure 4-5. As in the depressurization case, the maximum fuel temperature rises by ~50 K early in the transient. However, whereasdepressurization preserves some cooling capacity and allows slow heat removal via the coolant, the loss-of-velocity transient completely stalls flow and eliminates loop heat removal. Consequently, heat must dissipate through the reactor's insulated external surfaces at an extremely low rate. The resulting cool-down is much slower than in the depressurization case: after 5,000 seconds, the average fuel temperature remains about 30 K above steady-state (see Figure 4-5). Accordingly, no secondary power peak is predicted within the 5,000-second simulation window.

4.2.2.3 Coolant Inlet Temperature Drop

The coolant inlet temperature drop transient differs from the previous two cases. Instead of reducing coolant velocity and pressure, the inlet temperature is decreased linearly by 60 K over 10 seconds. This change introduces positive neutronic feedback and is expected to increase reactor power. The multiphysics model should predict the resulting power and temperature evolution to assess whether the GCMR remains within safe operating limits during this reactivity insertion event.

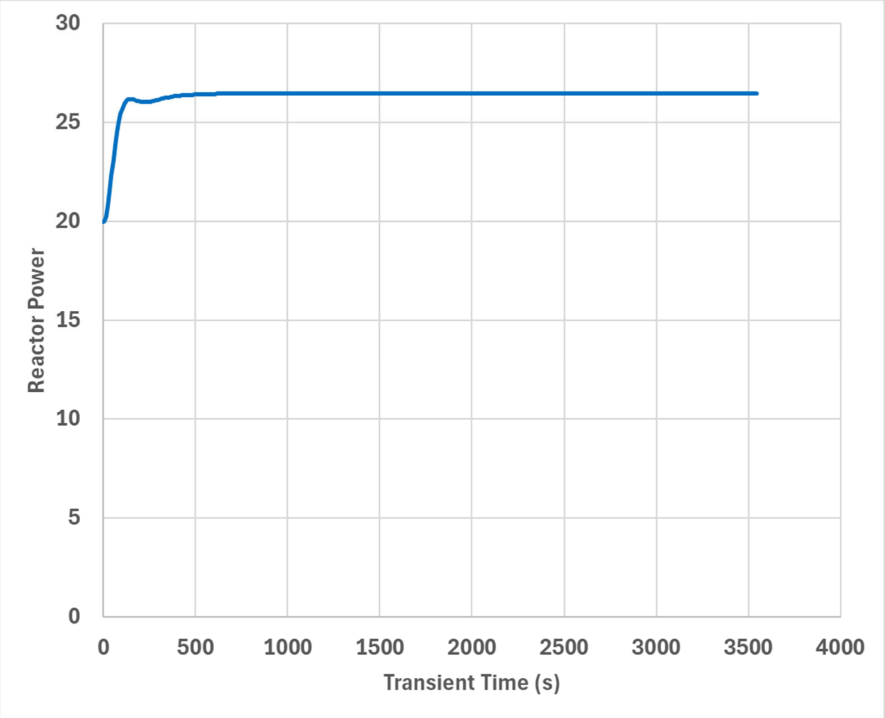

Figure 4-6 Time evolution of the reactor power during a coolant inlet temperature drop transient

According to the multiphysics model, the reduced inlet temperature and resulting positive reactivity drive a rapid power increase over a few hundred seconds, approaching an asymptotic value of ~27 MW (see Figure 4-6). Meanwhile, the minimum fuel temperature drops by ~60 K, mirroring the inlet-temperature reduction, while the maximum fuel temperature rises by ~30 K due to the higher power (see Figure 4-7). The average fuel temperature remains close to its original level, consistent with the microreactor settling into a new equilibrium.

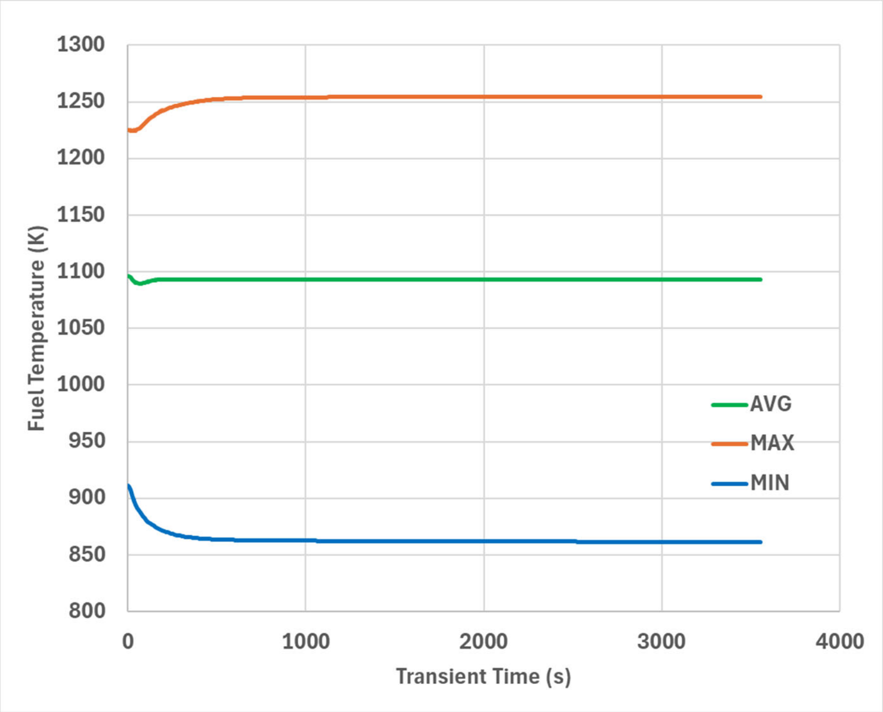

Figure 4-7 Time evolution of the representative fuel temperatures during a coolant inlet temperature drop transient

4.2.2.4 Single Coolant Channel Blockage

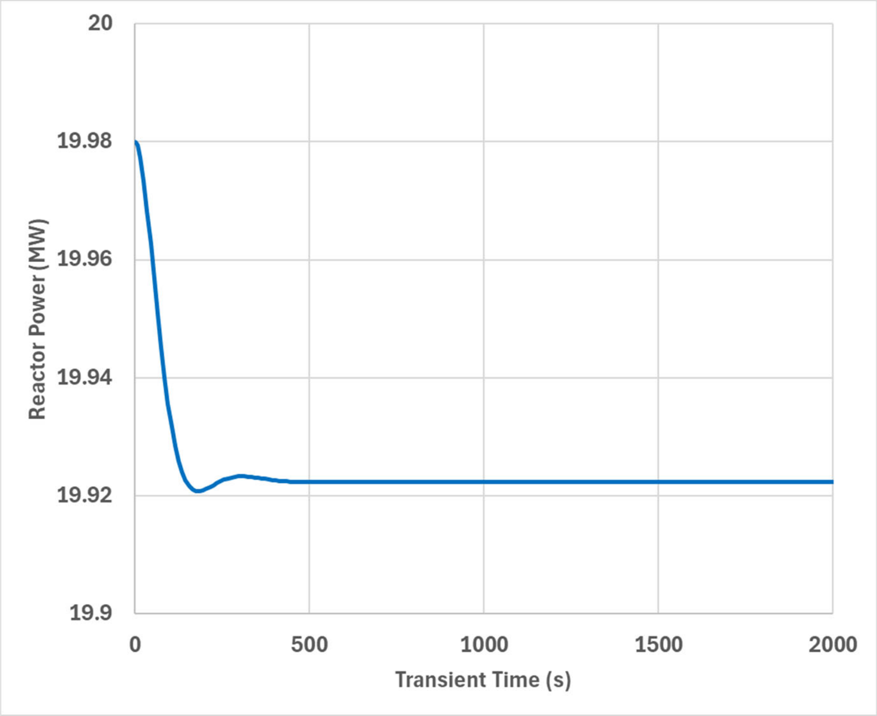

Figure 4-8 Time evolution of the reactor power during a single coolant channel blockage transient

The single coolant channel blockage transient is modeled by setting the velocity in one coolant channel to zero (out of 440 channels in the 1/6-core model), thereby eliminating heat removal in that channel. To emphasize the blockage effect, the selected channel is in the mid-core radial region where the maximum temperature occurs. Note that, because a 1/6 symmetric model is used, this nominal "single-channel" blockage corresponds to six blocked channels in the full GCMR core.

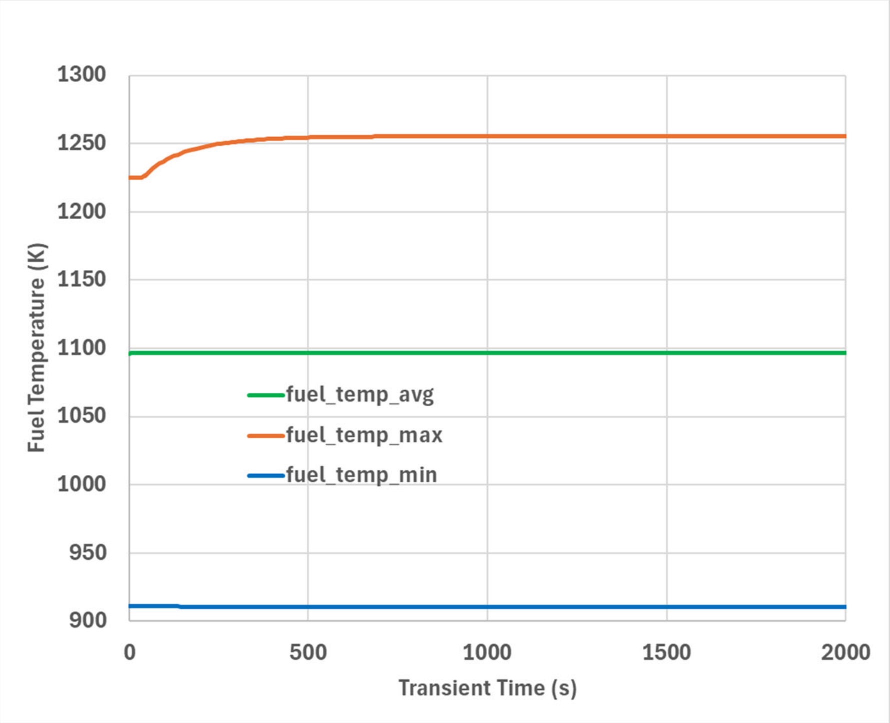

Figure 4-9 Time evolution of the representative fuel temperatures during a single coolant channel blockage transient

Figure 4-8 shows the time evolution of the normalized power, which decreases by less than ~0.4% in response to this localized channel blockage. As indicated in Figure 4-9, blocking a single coolant channel near the hottest region increases the maximum fuel temperature by ~30 K. The average fuel temperature changes by less than 0.1 K over the simulation. Overall, a single-channel blockage causes only a slight local temperature rise, with adjacent channels compensating by removing the excess heat (see Figure 4-10).

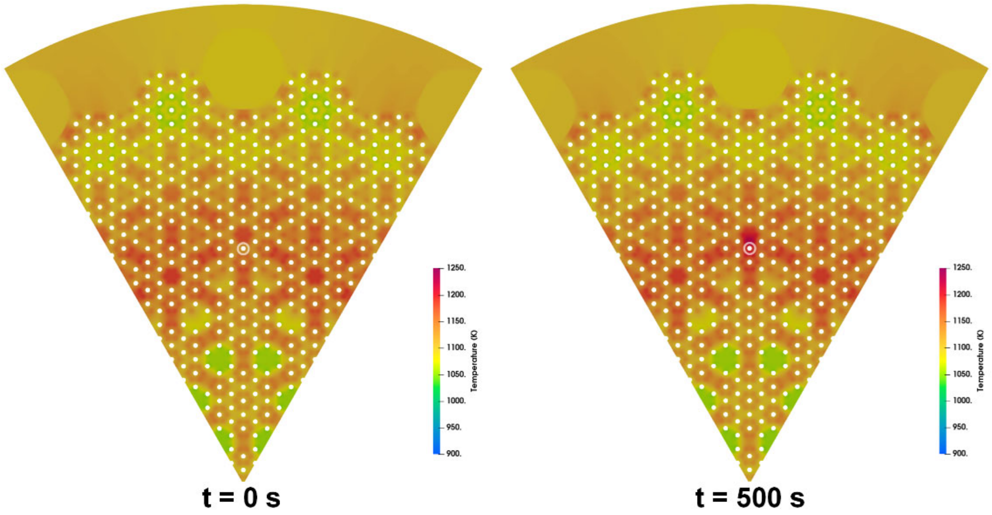

Figure 4-10 The temperature change at the midplane of the core during a single coolant channel blockage transient. The blocked channel is marked by the white circle.

4.3 Performance of Hydride

The steady-state and transient models discussed in Section 4.2 involved hydride performance modeling using SWIFT. The performance of the hydride during these conditions is discussed in this section.

4.3.1 Hydrogen Redistribution at Steady State

YH_{2-x} was selected as the moderator for the GCMR (as well as the HPMR). Because metal hydrides undergo thermal dissociation at elevated temperatures, a sufficient hydrogen partial pressure in the surrounding gas gap is required to maintain thermodynamic equilibrium with the hydride and retain most hydrogen in the solid phase. To keep the required H_2 partial pressure within practical limits—and thereby ease mechanical-strength and hydrogen-permeation requirements on the enclosure—the stoichiometric deficiency x must be optimized. For the GCMR concept studied in this project, $YH_{1.94}$ was chosen. A nonzero x also makes the moderator susceptible to hydrogen redistribution under temperature gradients, driven by the temperature dependence of hydrogen's chemical potential.

As illustrated in Figure 4-1, during normal operation the upward coolant flow from the bottom of the GCMR core produces an axial temperature gradient, with temperature increasing with elevation. Consequently, hydrogen migrates toward the cooler lower region. Near the bottom of the microreactor, the hydride stoichiometry approaches YH_2, whereas at the hottest elevations it can drop to about $YH_{1.87}$. This redistribution affects neutronics: as indicated in the table, hydrogen migration increases reactivity. Therefore, during initial startup, the resulting hydrogen redistribution introduces additional reactivity that must be taken into account in the reactor control strategy.

4.3.2 Hydrogen Redistribution during Transient

During transients, when the axial temperature gradient in the microreactor changes—either globally or locally—hydrogen will redistribute to reflect the new gradient. Although hydrogen migration is relatively slow compared with neutronic kinetics and lags the temperature change, it can still have a non-negligible effect on microreactor performance over longer transient timescales.

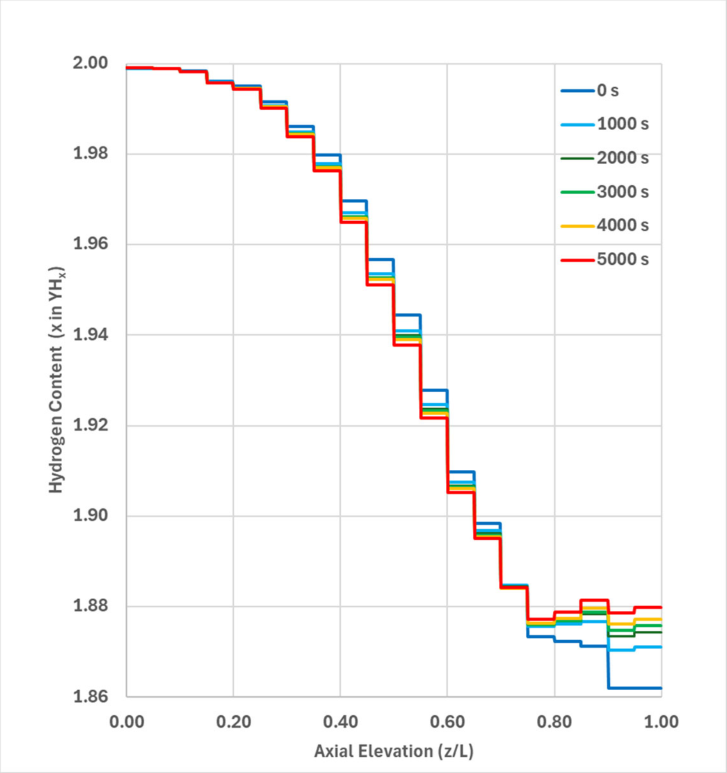

Figure 4-11 Hydrogen redistribution in a typical hydride moderator module during a coolant depressurization transient

During the coolant depressurization transient as described in Section 4.2.2.1, the reduction in cooling capacity substantially diminishes the axial temperature gradient, prompting hydrogen to migrate back toward higher elevations in the core. As shown in Figure 4-11, within 5,000 seconds of depressurization, hydrogen slowly shifts upward; while the change remains modest over this interval, it is expected to continue over longer times and become increasingly pronounced. When hydrogen redistribution is accounted for in both steady-state and transient analyses, the multiphysics model predicts a power evolution that differs slightly from a model assuming a uniform, constant $YH_{1.94}$ stoichiometry (see Figure 4-12), further underscoring the importance of moderator-hydrogen redistribution in high-fidelity multiphysics modeling. A similar trend is observed in the localized-effect transient, as shown in Figure 4-13.

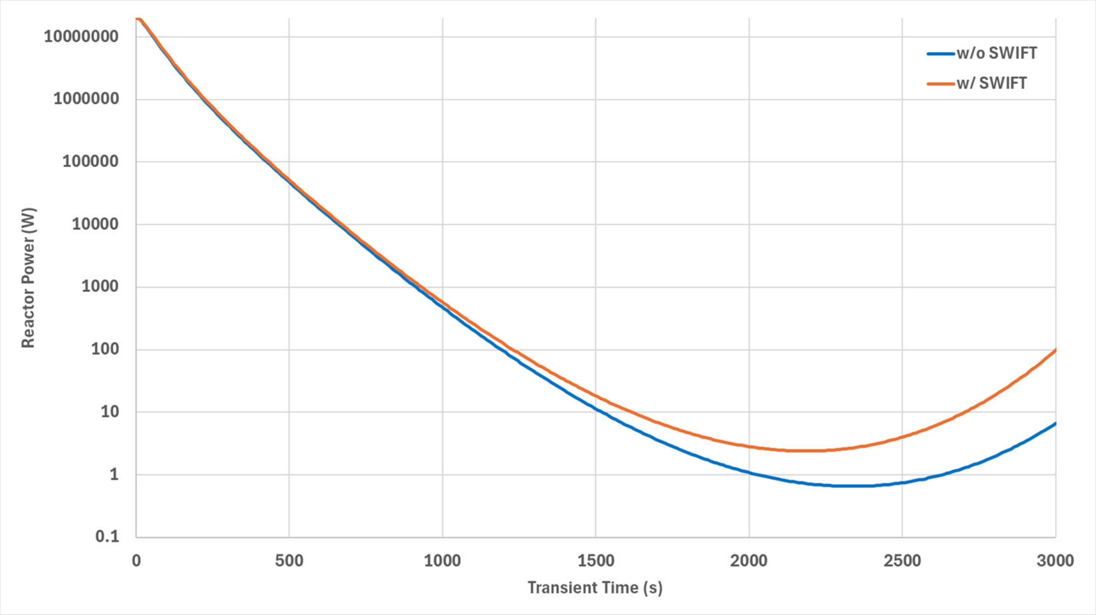

Figure 4-12 The time evolution of reactor power comparison between multiphysics models with and without hydride performance model (SWIFT) during a coolant depressurization transient

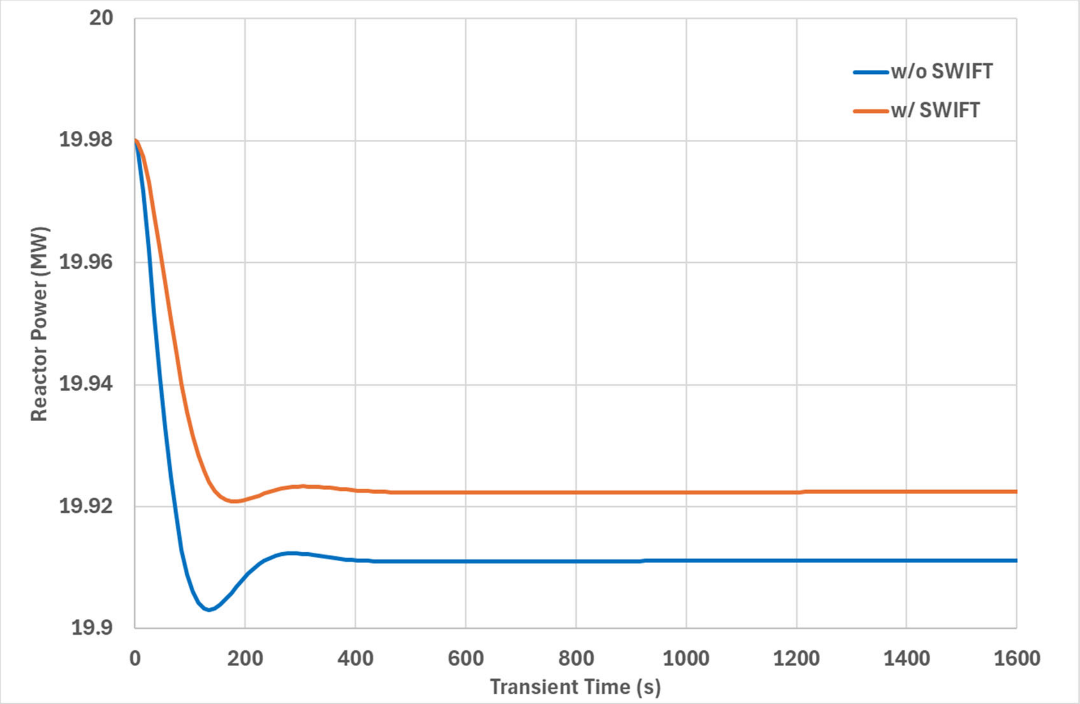

Figure 4-13 The time evolution of reactor power comparison between mutiphysics models with the without hydride performance model (SWIFT) during a single coolant channel blockage transient

4.4 Balance of Plant Model Development

4.4.1 Brayton Cycle Model

The power conversion cycle of the GCMR utilizes a Brayton cycle, circulating high-temperature and high-pressure (7 MPa) helium coolant. The cycle has been optimized based on the specifications of the 20 MWth GCMR concept investigated in this project, the details of which can be found in Ref. [12].

This GCMR BOP model is developed with the Thermal-Hydraulics Module (THM). The core geometry of GC-MR is simplified to be able to use a 1D-2D representation. Only one coolant channel is used representing all the coolant channels in the core. It is coupled to a single heat structure representing the moderator, graphite and fuel as shown in Figure 4-14. A cylindrical heat structure, with a coolant cylinder in the middle of a hollow graphite and moderator cylinder, itself in a hollow fuel cylinder are applied to model the core. The parameters are defined to preserve their total volume.

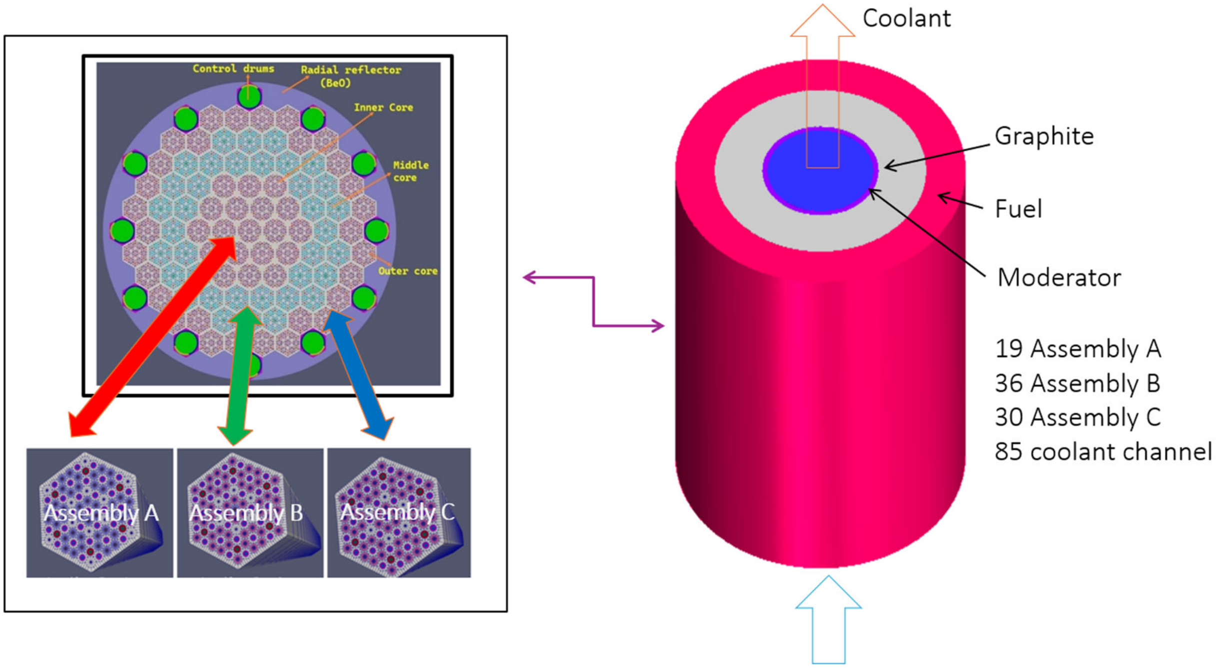

Figure 4-14 Sketch for core simplification

An open-air recuperated Brayton cycle is used as secondary loop. Air enters the loop by a compressor. The air is then heated first by the exhaust gases in a recuperator and secondly in a heat exchanger. In this component, 20 MW_{th} are transferred from the primary to the secondary loop. The gases go through a turbine, spinning the generator that delivers electricity. The turbine rotation also drives the compressor rotation. The exhaust gases transfer a part of their residual heat in the recuperator and are finally released outside. A motor is used to launch the compressor and the turbine, which are on the same shaft. This shaft is initially at rest and reaches a rotation speed during the steady state. To do this, the motor torque increases quickly during the first few seconds and then decreases slowly to zero once the turbine is launched.

The startup transient is tested on this system. A constant 20 MW_{th} power is imposed in the core. The goal is to see how the system reaching its normal operating conditions.

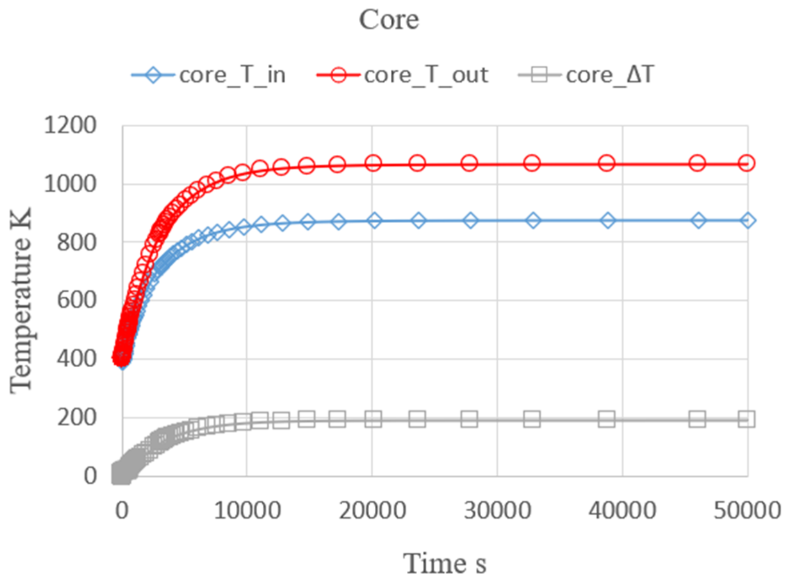

Figure 4-15 Core temperature during transient

Figure 4-15 shows the core temperature change during transient. The inlet and out core temperature of the core reach design parameter within 20,000s and keep steady. At first transient stage, the PID controlled motor increased shaft speed from 0 to approximately 80,000 RPM. This is followed by Figure 4-16 which displays the shaft speed over the course of the entire transient. The shaft speed finally keeps steady at approximately 130,000 RPM.

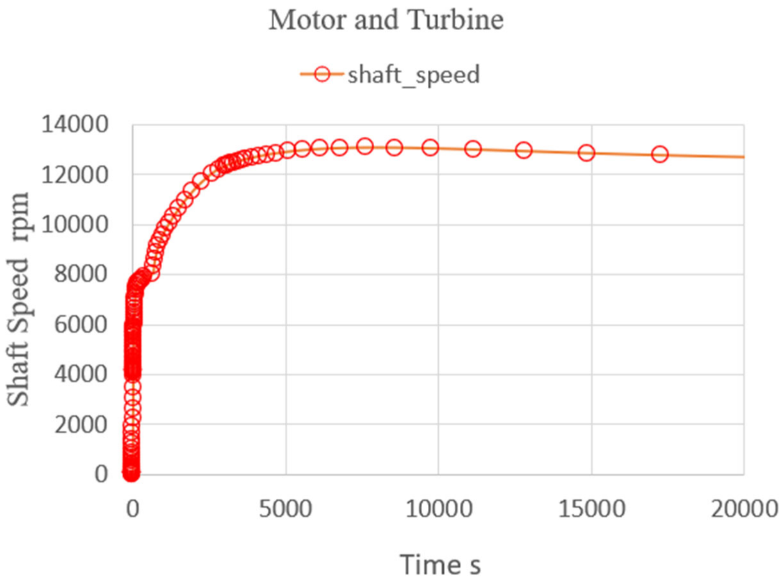

Figure 4-16 Shaft speed during transient.

The shaft speed is quickly ramped up by the PID and then linearly increases as the working fluid is heated and begins working on the turbine to produce shaft torque. When the motor and turbine provide the same amount of torque (150 N·m) which initiates the motor shutdown function. A comparison of the motor and turbine torques is shown below in Figure 4-17.

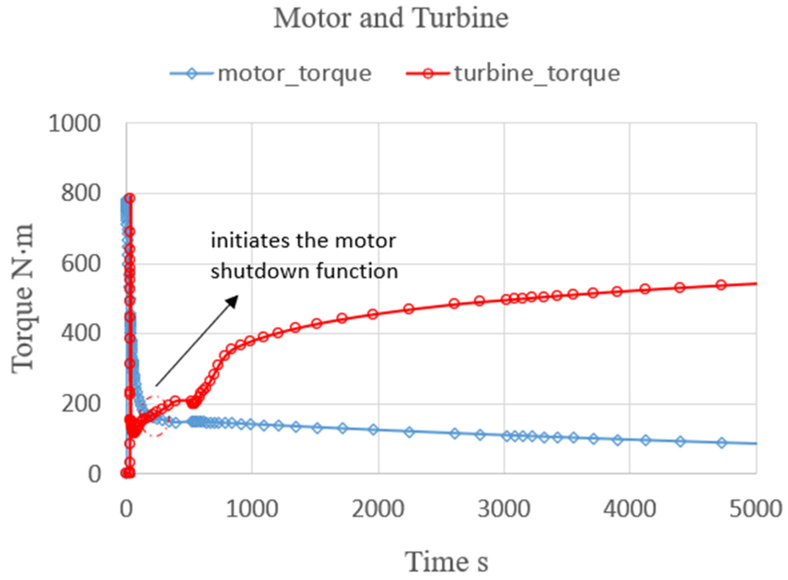

Figure 4-17 Comparison of the motor and turbine torques

Finally, coolant temperatures across key points of the secondary loop are displayed in Figure 4-18. All the temperatures reach steady state within 20,000s. The air in the cold leg is heated by the recuperator.

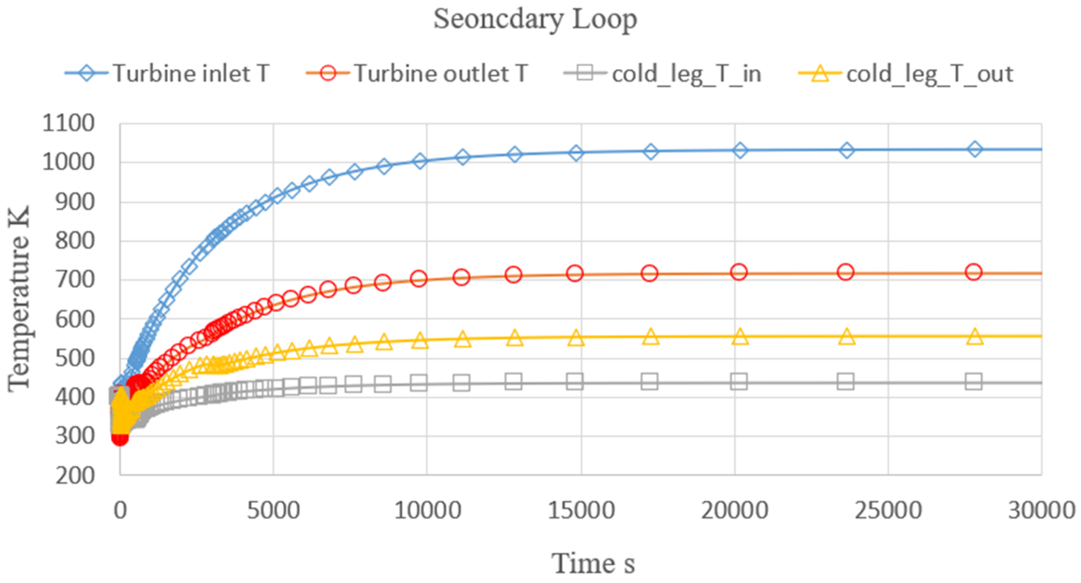

Figure 4-18 Coolant temperatures across key components

4.4.2 Coupling with the Full-Core Multiphysics Model

This section describes the multiphysics model for GCMR. The THM BOP model is coupled with the BISON full-core model for the startup transient simulation. The BISON model was directly extracted from the full-core Multiphysics GCMR model as described in Section 4.1. For the startup transient, an initial prompt power increase was assumed, obviating the need to run Griffin as the main application at this stage. The power history computed by the full-core multiphysics model was applied as the volumetric heat source. Building on this successful BOP coupling, more complex scenarios can be pursued in the future that incorporate Griffin to govern neutronics.

The sketch for the coupling strategy and hierarchy of the multiphysics model are shown in Figure 4-19. In the GCMR Multiphysics model, the channel wall temperature or heat flux can be transferred from BISON to THM, while the fluid temperature and heat transfer coefficient are calculated by THM and transferred back to BISON.

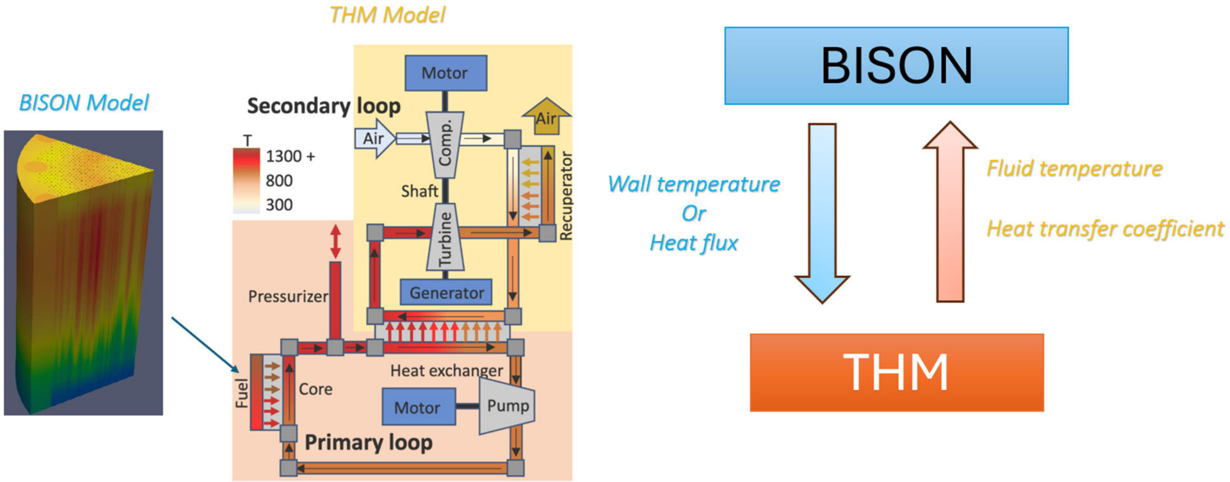

Figure 4-19 Coupling strategy and hierarchy of the Multiphysics model

As discussed in Section 4.4.1, the fuel is simplified as a cylindrical heat structure in THM standalone model. The fuel temperature from standalone THM model is a 2D representation. In multiphysics model, BISON can include detailed components in the core such as control drums, hydride moderators, and TRISO fuel compacts. Figure 4-20 shows the fuel temperature from both standalone THM model and Multiphysics model. The standalone THM model can predict a 2D fuel temperature distribution in axial and radial direction while the multiphysics model can predict the 3D fuel temperature distribution in each individual fuel pin. The multiphysics model can also give the fuel temperature distribution during a long transient event. Figure 4-21 shows the fuel temperature evolution during startup transient. This coupled calculation demonstrates the capability for long term transient scenario simulation.

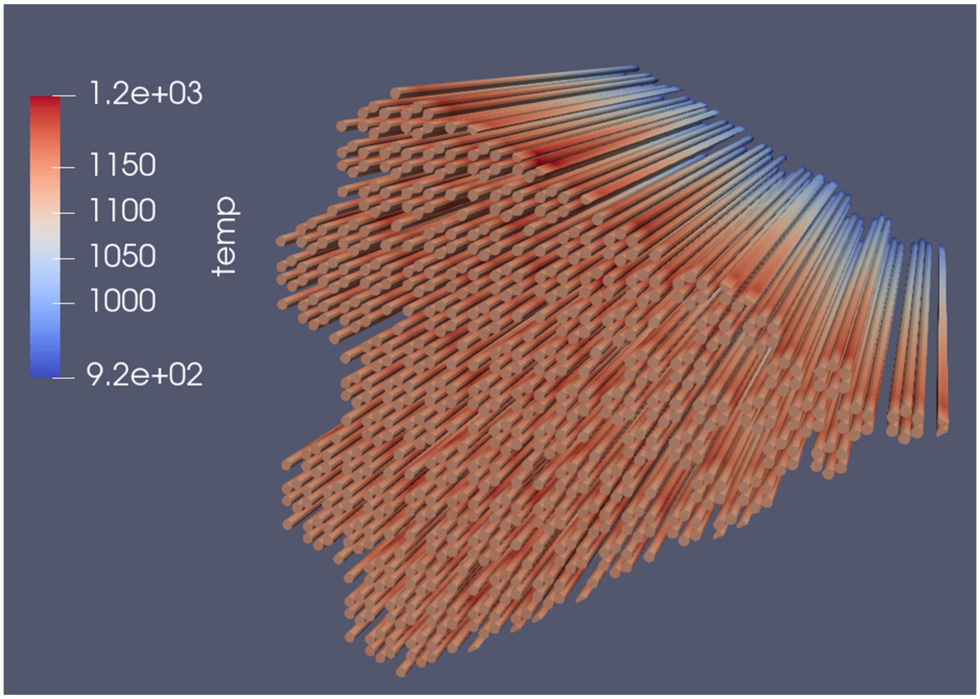

a) fuel temperature from Multiphysics model

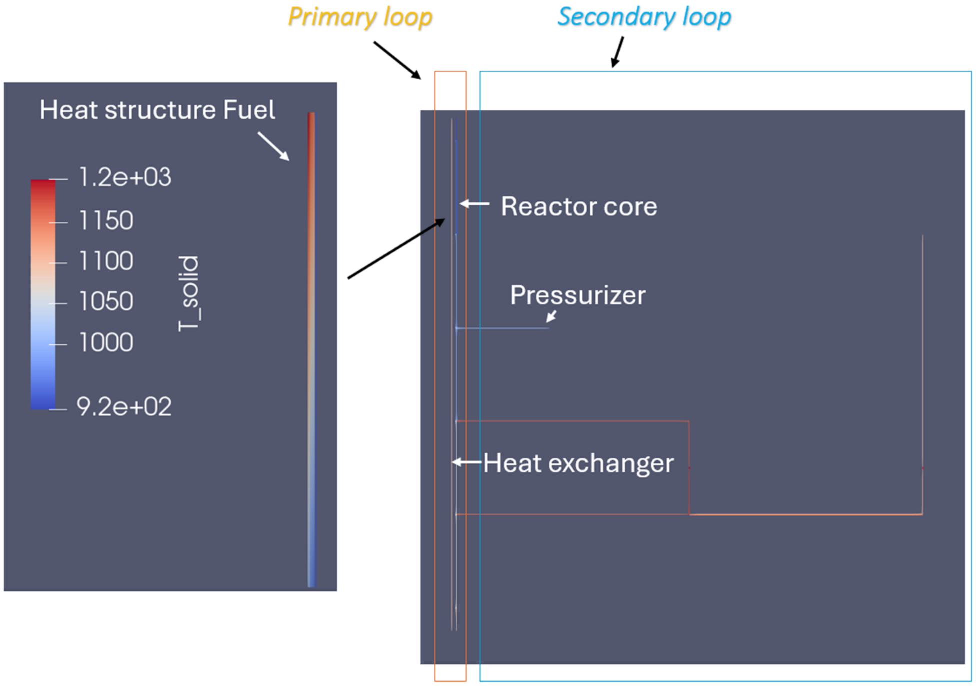

b) fuel temperature from standalone THM model

Figure 4-20 Fuel temperature from standalone THM model and Multiphysics model

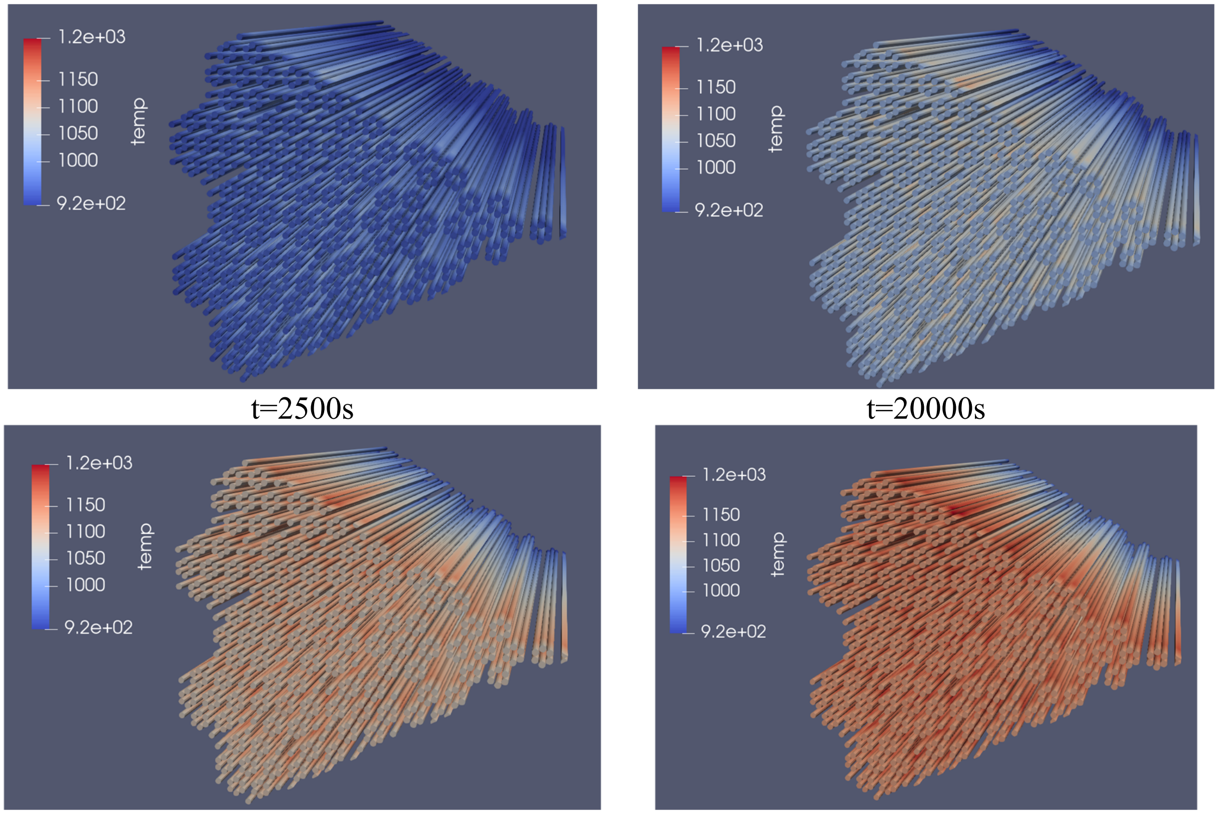

t=2500s

t=20000s

t=50000s

t=90000s

Figure 4-21 Fuel temperature evolution during startup transient

4.5 Fission Product Poisoning Effects

During transients, especially long-term transients such as load following operation in thermal reactors, fission product poisoning is driven mainly by Xe-135 and Sm-149. After a power decrease, I-135 continues decaying to Xe-135, creating a transient xenon peak that adds negative reactivity and can hinder power recovery; after a power increase, xenon “burnout” briefly provides positive reactivity until a new equilibrium is reached. Sm-149 accumulates more slowly and persists (especially post-shutdown), contributing longer-term negative reactivity. Even in microreactors with strong thermal feedback, these poisons constrain ramp rates and demand adequate control worth, potential burnable absorbers, and thus require multiphysics modeling to support transient planning and management.

4.5.1 Simple Fission Product Effects Model

MOOSE’s ODETimeDerivative and ParsedODEKernel were used to find out the time-dependent variations of xenon X(t) using Eqs. (4-1) and (4-2), where I(t) is iodine concentration at time t, γ_x is the xenon fission yield, γ_I is the iodine fission yield, λ_x is the xenon decay constant, λ_I is the iodine decay constant, and Σ_f is macroscopic fission cross-section, σ_a^x is microscopic absorption cross-section of xenon.

$$\frac{dX(t)}{dt} = \gamma_X \Sigma_f \varphi(t) + \lambda_I I(t) - \lambda_X X(t) - \sigma_a^X \varphi(t) X(t) \tag{4-1}$$

$$\frac{dI(t)}{dt} = \gamma_I \Sigma_f \varphi(t) - \lambda_I I(t) \tag{4-2}$$

This step was necessary to include xenon-induced reactivity feedback in the time-dependent net reactivity during Griffin PKE calculations. which can be estimated using xenon worth at 100% (ρ_{X0}^{100P}), xenon concentration at 100% power (X_0^{100P}**),** the intial xenon concentration (X_0), and is the time-dependent xenon concentration X(t) as shown in Eq. (4-3). Serpent-2 code was used to obtain the required parameters to solve Eqs. (4-1), (4-2), and (4-3). While intial xenon and iodine concentrations are found using Eqs. (4-4) and (4-5).

$$\Delta\rho_{Xe}(t) = \rho_{X0}^{100P} \frac{X(t) - X_0}{X_0^{100P}}, \tag{4-3}$$

$$X_0 = \frac{(\gamma_I + \gamma_X)\Sigma_f \varphi_0}{\lambda_X + \sigma_a^X \varphi_0}, \tag{4-4}$$

$$I_0 = \frac{\gamma_I \Sigma_f \varphi_0}{\lambda_I}, \tag{4-5}$$

Achieving programmed power variation is essential for realistic load-follow simulations. In a coupled MultiApp Griffin–BISON–SAM framework, programmed power changes are realized by adjusting the control drums or rods to meet the required power demand.

When using the Griffin PKE model, the external reactivity term (ρ_{ext}) must be actively controlled to offset internal reactivity feedback effects arising from xenon poisoning and temperature variations. For a programmed power profile, $P_{demand}(t)$, the objective is to have Griffin automatically adjust $\rho_{ext}(t)$ such that the point-kinetics power solution $P_{PKE}(t)$ follows the demanded power.

One possible approach is to search, using the MultiApp system (Griffin (PKE)–BISON–SAM), for the external reactivity history that produces the desired power profile. However, such direct search is computationally expensive. To make this process more efficient, the temperature distribution corresponding to the required power demand is first obtained from a BISON–SAM simulation. This temperature field is then used to calculate the thermal reactivity feedback, which is combined with the PKE reactivity terms, including xenon-induced reactivity and the external reactivity component. To reduce cost, Griffin was coupled with a simplified "dummy" main App designed specifically to search for the external reactivity that ensures the PKE-estimated power matches the demanded power. This approach is computationally inexpensive compared to a full Multiphysics search. The search used in the dummy App is done through a sigmoid function:

$$Sigmoid\ (\varepsilon) = \frac{2}{1 + e^{-5\varepsilon}} - 1 \tag{4-6}$$

where,

$$\varepsilon = \left|\frac{\mathrm{P_{Demand}} - P_{PKE}}{\mathrm{P_{Demand}}}\right|$$

$$\rho_{ext}^{m+1} = \begin{cases} \rho_{ext}^{m}[1 + 0.002(1 - Sigmoid\ (\varepsilon)], & \mathrm{P_{Demand}} > P_{PKE} \\ \rho_{ext}^{m}[1 - 0.002(1 - Sigmoid\ (\varepsilon)], & \mathrm{P_{Demand}} < P_{PKE} \end{cases} \tag{4-7}$$

When the error ε is small (ε→0), the sigmoid term tends to zero, so the correction factor approaches 0.002, giving a gentle but effective adjustment that removes residual mismatch. For large errors (ε→∞), the sigmoid approaches one, making the correction factor vanish, which keeps the update conservative and prevents instability. The direction of the correction follows the error sign: ρ_{ext} increased if the target power is higher than the achieved power and decreased otherwise.

Figure 4-22 through Figure 4-25 illustrate the dynamic behavior of the reactor during the 100-50-100 load-following simulation. Figure 4-22 shows the time evolution of the normalized reactor power, while Figure 4-23 presents the total reactivity required to achieve this programmed power profile. With such a load-following power profile for the two-day operating period, the average temperature of the fuel is illustrated in Figure 4-24. Figure 4-25 separates the contributions from xenon poisoning and temperature feedback. As the reactor power decreases, the core temperature also decreases. Because the system has a negative temperature reactivity coefficient, this results in a positive thermal reactivity feedback as power decreases. In contrast, the xenon reactivity evolves more slowly, reflecting the delayed buildup and decay of xenon. Over the two consecutive days of load-following operation, the combined internal reactivity feedbacks remain below 200 pcm in the microreactor core. To achieve the desired power ramps, an external reactivity component is actively controlled, compensating for these internal effects and providing the necessary positive or negative reactivity to track the programmed up and down power transients, as shown in Figure 4-23. It is also pronounced that the fission products effects play a non-negligible role in long-term transients.

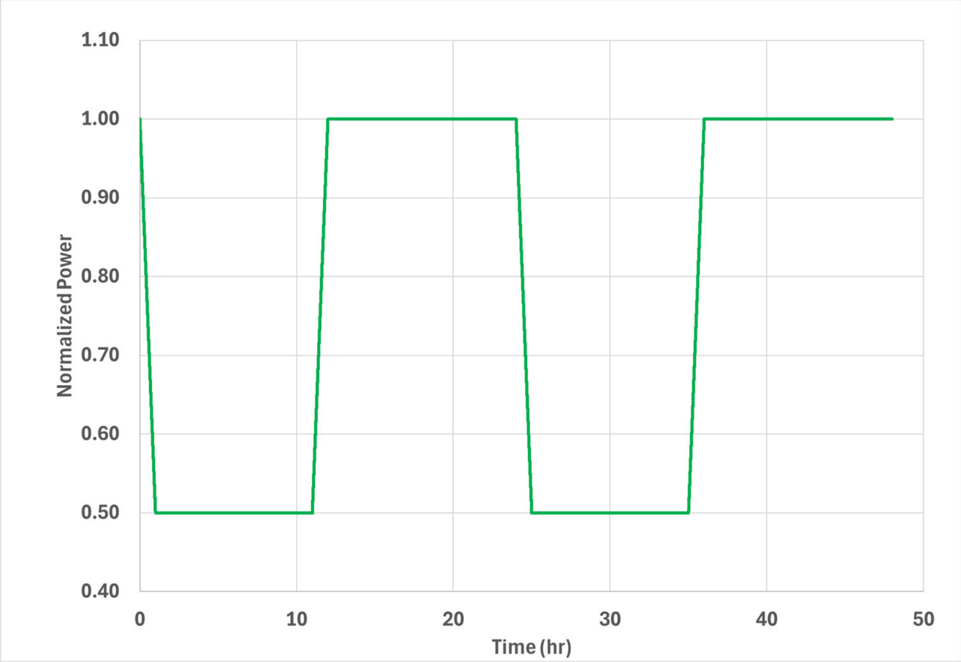

Figure 4-22 Time evolution of the normalized reactor power used for the load-following simulation

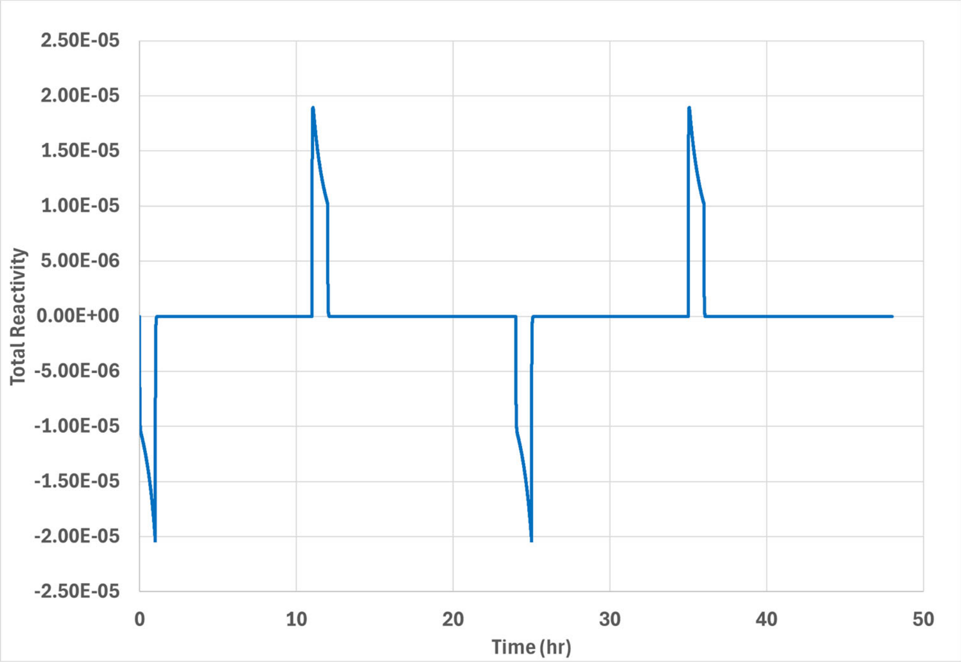

Figure 4-23 Time evolution of total reactivity that is needed to achieve the power evolution shown in Figure 4-22

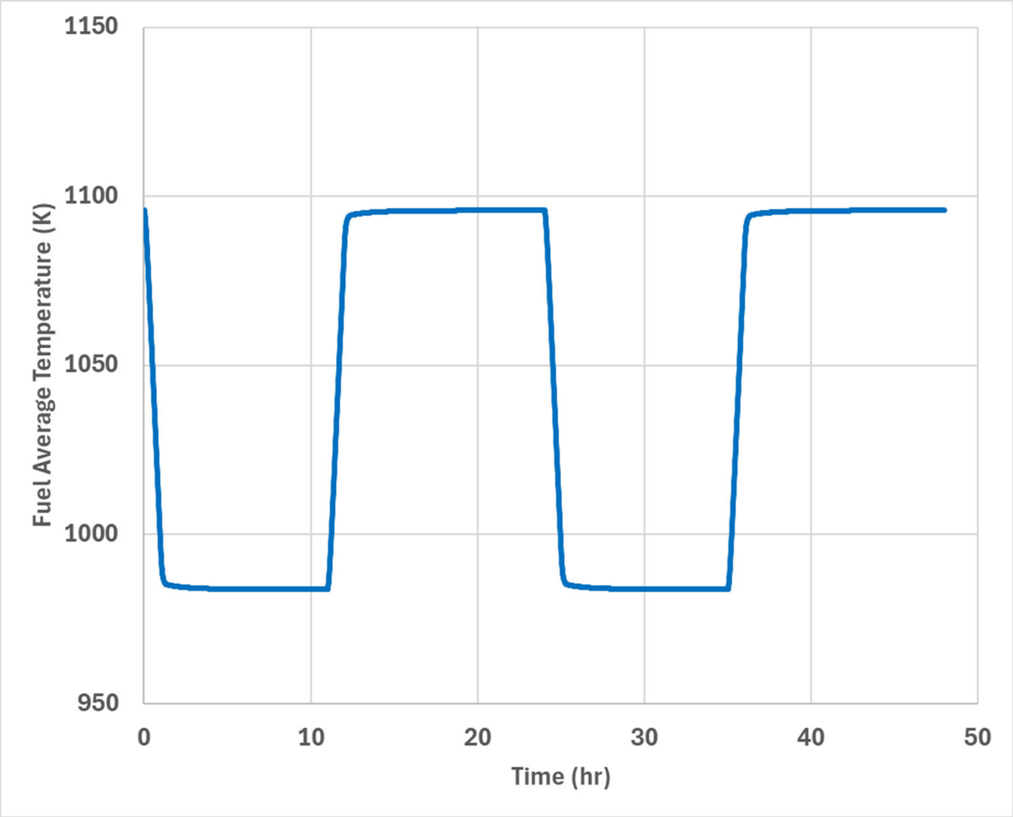

Figure 4-24 Time evolution of average fuel temperature during the load-following event

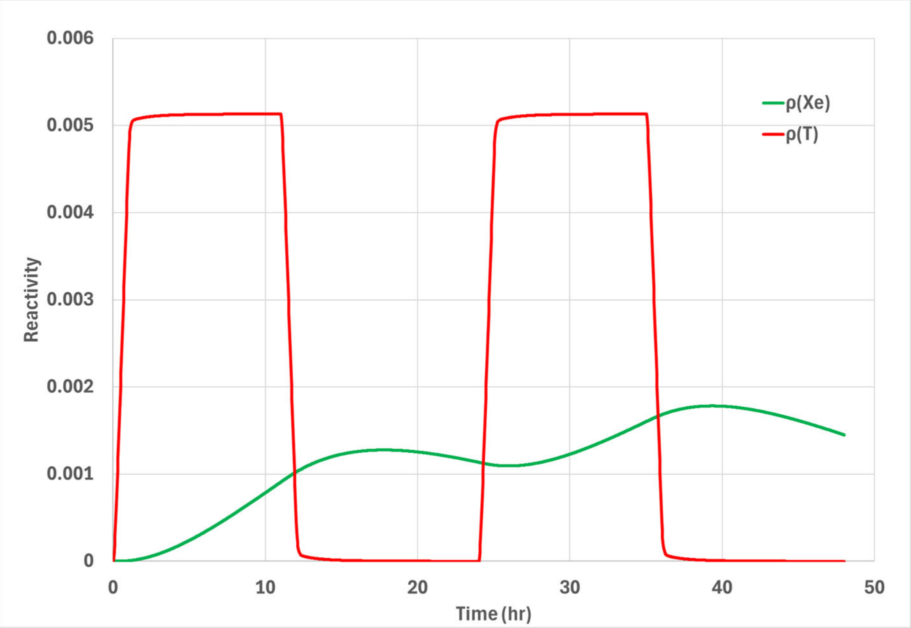

Figure 4-25 Time evolution of reactivity values contributed by Xe poisoning and temperature

4.5.2 High-Fidelity Fission Product Effects Model

As a simplified approach, the PKE based fission product effect model neglects the spatial distribution of the tracked species and their evolution during transients. Capturing these effects requires space dependent modeling. Previously, Griffin supported poison tracking only in its diffusion solver. In FY2025, following coordination with the Griffin development team, the capability was extended to the high fidelity DFEM–SN transport solver. In this section, fission product effects are evaluated by enabling poison tracking within the high fidelity, full core GCMR multiphysics model.

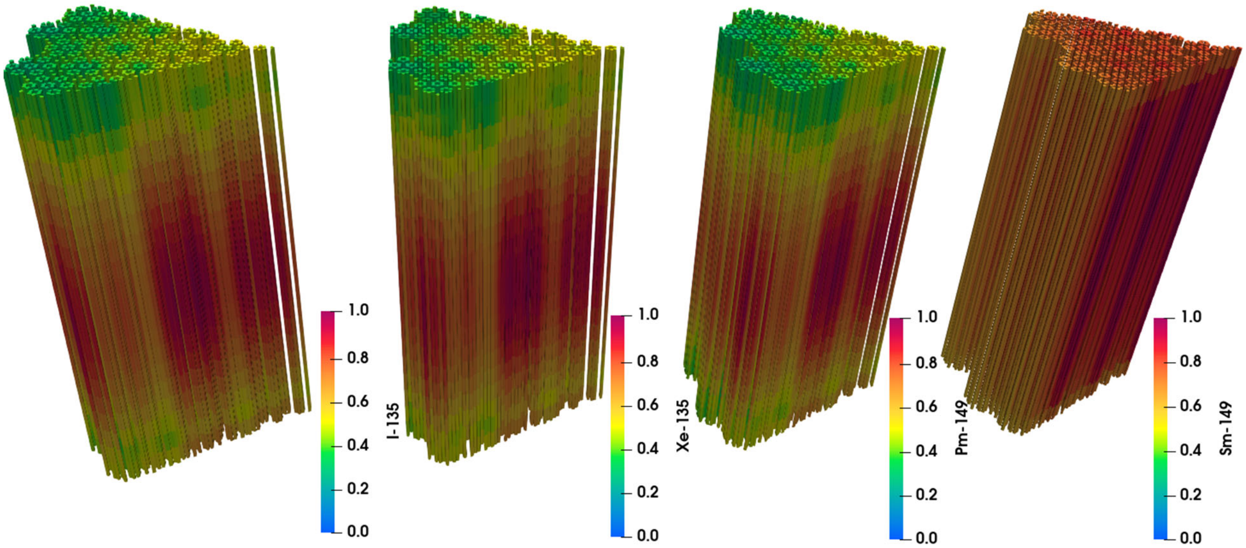

Figure 4-26 The normalized concentration profiles of the four key isotopes (from left to right: I-135, Xe-135, Pm-149, and Sm-149) involved in poison tracking as predicted in the GCMR at steady-state.

Two decay chains, I-135/Xe-135 and Pm-149/Sm-149, were tracked in the multiphysics model. The normalized distributions of these isotopes at steady state are illustrated in Figure 4-26. While the distributions I-135, Xe-135, and Pm-149 are highly correlated to the shape of the neutron flux, Sm-149 distribution has a much weaker space dependence. This is consistent with the theory that the equilibrium Sm-149 concentration is mainly dependent on the fission yield of Pm-149, fission cross-section, and absorption cross section of Sm-149.

For the full-core transient simulation with poison tracking, a load-following event was initiated by increasing the helium coolant inlet temperature by 50 K using the similar approach described in Section 4.2.2.3. The increase in inlet coolant temperature was designed to trigger temperature feedback to drop the power so that the evolution in poison species can be assessed. Preliminary results from the transient simulation are shown in Figure 4-27. An increase in inlet coolant temperature causes a roughly 25% drop in reactor power within tens of minutes. Consequently, the concentrations of the four tracked isotopes begin to evolve toward new equilibria corresponding to the reduced power level. Because the preliminary run duration is shorter than the half-lives of these isotopes, the simulated concentration changes remain limited (see Figure

4-27(d)). Nevertheless, as shown in Figure 4-27(a), the evolution of Xe-135 concentration is spatially dependent, driven by the local isotope distributions and neutron flux profile. The high-fidelity simulation with poison tracking captures these spatial details that a PKE-based approach is incapable of.

Ideally, a direct comparison between the PKE-based approach and space-resolved, high-fidelity models would be preferable to delineate when a PKE solver is sufficient to capture microreactor kinetics and when fully coupled, high-fidelity modeling is required for poison tracking analyses. In practice, however, while external reactivity can be prescribed in a PKE formulation to reproduce an arbitrary target power history, achieving the same power evolution in high-fidelity models is more challenging: power emerges from the coupled multiphysics solution, and the motion of individual control drums must be determined to realize a specified trajectory under space-resolved feedback. Within the current MOOSE infrastructure, attaining comparable power control capability across PKE and high-fidelity multiphysics models remains challenging.

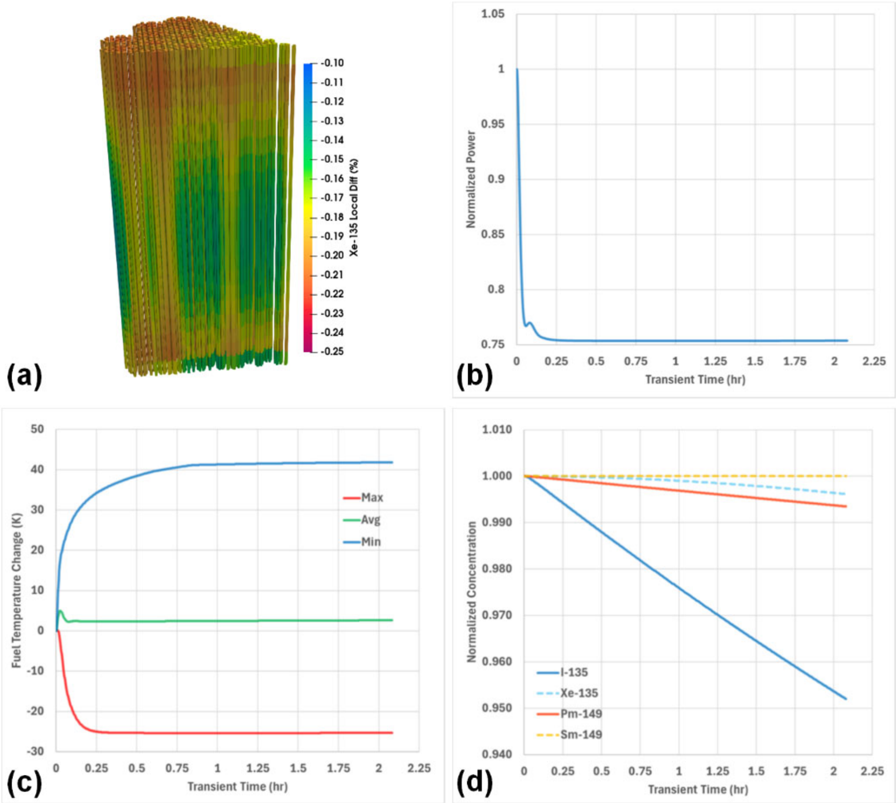

Figure 4-27 The 7,500-second preliminary high-fidelity transient simulation results with poison tracking: (a) local percentage change in Xe concentration; (b) time evolution of reactor power; (c) time evolution of fuel temperature; (d) time evolution of normalized concentration of the four tracked isotopes.

Beginning in FY2026, a unified workflow will be developed within the MOOSE ecosystem to streamline reactivity control for both PKE-based and high-fidelity models. Once complete, these tools will preserve the simplicity of PKE-based power control and will enable determination of control-drum rotation strategies that realize designated power history, thereby enabling rigorous comparisons between the two approaches.

4.6 *Heterogeneous TRISO Modeling*

Many microreactor concepts aim to utilize TRISO fuel particles embedded in graphite compacts. This fuel form has many advantages over traditional oxide fuels, namely functional containment of fission products and low rates of fuel failure during accident scenarios. The explicit heterogeneous modeling of TRISO fuels for full core reactor analysis remains out of reach due to the length scale difference of the regions in TRISO particles compared to the fuel compacts. Heat conduction models employed in BISON do not resolve this heterogeneity and instead use effective thermal conductivity models. The BISON team has demonstrated that these models are effective for the high packing fractions employed by microreactor vendors for steady-state problems with fixed temperature boundary conditions [24]. Recent work has shown that this is not the case when considering non-uniform power distributions where the effects of particle clustering and localized energy deposition dominate [25]. This is often the case in transient analyses, where the low thermal conductivity of the fuel and buffer slow heat transport out of the kernel resulting in significant kernel temperature rises compared to the compact temperature. Based on these published results in [25], an investigation was carried out to compare various TRISO homogenization strategies against a fully heterogeneous reference model. These results indicated a new temperature treatment was required. A fast-running multiscale approach using Heat Source Decomposition (HSD) was developed based on the work in [26, 27] to improve maximum kernel temperature predictions in the GCMR VTB model (see more details in Appendix).

4.6.1 Small Scale GCMR Compact Model

A small-scale multi-physics model of a GCMR fuel compact using Griffin and BISON was developed. This model uses 2774 TRISO particles embedded in a 1.1 cm tall slice of a single fuel compact. The temperature predicted by BISON and power density from Griffin can be found in Figure 4-28 for a total power of 24 W. A detailed description of the heterogeneous model can be found in Appendix A-1.

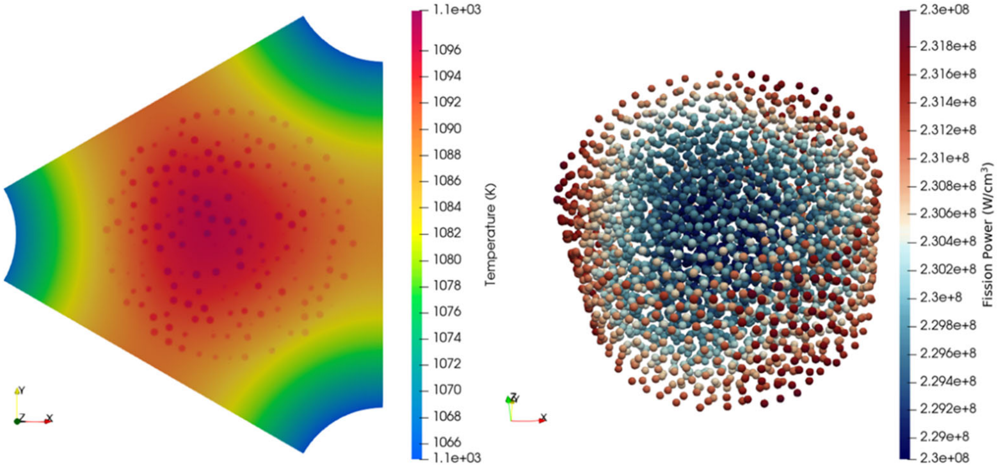

Figure 4-28 Steady-state heterogeneous TRISO model using nonlinear material properties. Left: temperature (K). Right: power density (W/m^3)

Comparisons between maximum kernel temperatures and k_{eff} were performed for different homogenization approaches with and without HSD. A summary of these comparisons can be found in Table 4-3 for two different total compact powers, where the heterogeneous TRISO model is compared against the previous BISON approach and the newly developed HSD approach. A detailed description of the previous BISON model and the tested homogeneous / HSD models can be found in Appendix A-2. This work determined that the previous approach underpredicted fuel temperatures and temperature reactivity effects.

Table 4-3 Comparison of integral metrics between the heterogeneous model (Figure 4-28), previous BISON model, and the new HSD treatment for two scenarios (Note that two compact power levels are involved)

Parameter (24W/120W)	Heterogeneous Model (24W/120W)	Previous BISON Model (24W/120W)	New Semi-Explicit HSD Model (24W/120W)
Max. T_{kernel} (K)	1099.0/1499.7	1091.1/1457.8	1102.0/1478.1
Δk_{eff} (het. - other) (pcm)	N/A	-55/-213	-34/-124

The different models were further tested against a single-physics transient where the power was ramped from 24 W to 240 W over 9 seconds. This power ramp was used as a surrogate for reactivity transient due to the small size of the compact. The results can be found in Figure 4-28 where the agreement between the semi-explicit HSD model and the fully heterogeneous model is excellent compared to the previous BISON model.

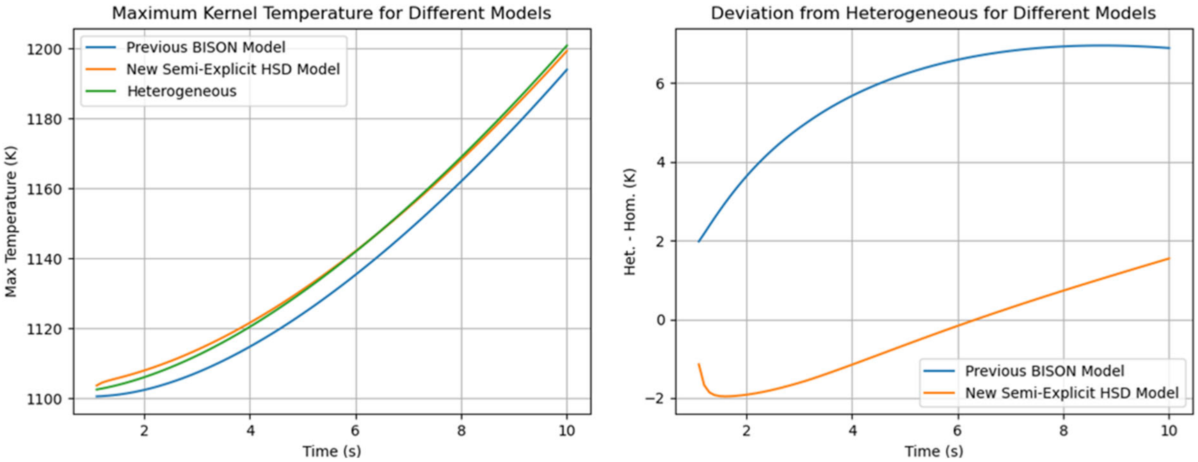

Figure 4-29 Comparison of the heterogeneous, previous BISON model, and new HSD treatment for a single-physics ramp transient.

4.6.2 Whole Core Improved Heat Conduction Model

The HSD treatment has been implemented in a modified form of the transient whole core GCMR model, where Griffin DFEM-SN is used to solve for steady-state power and Griffin PKE is used to solve for the power amplitude during reactivity transients. Additional details on the modified whole core model can be found in Appendix A3. Both 30 cent and 50 cent reactivity step insertions are tested to determine the impact of the new TRISO treatment; the results for the normalized power can be found in Figure 4-30, where the previous BISON model yields a larger peak power than the new TRISO treatment.

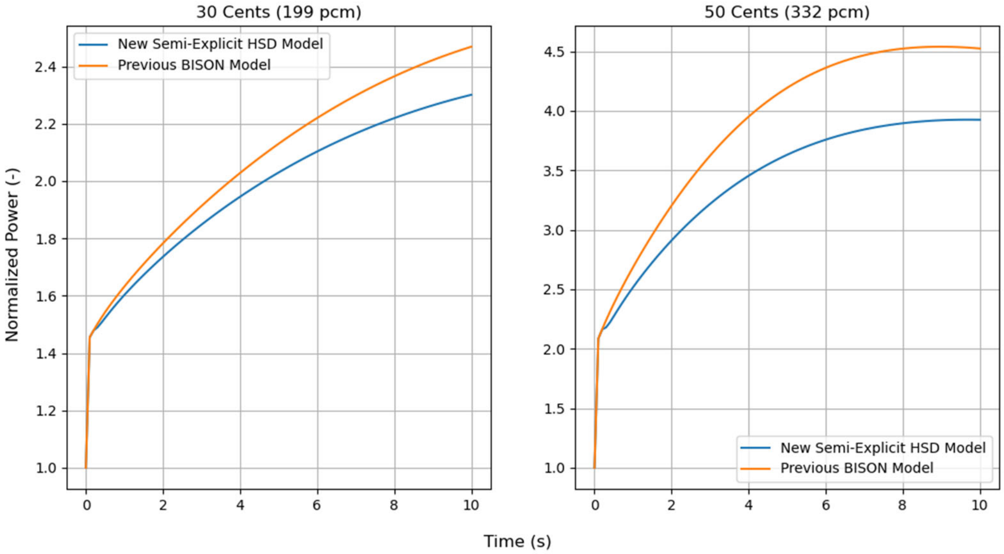

Figure 4-30 Normalized power for the modified whole-core GCMR model with both TRISO treatments

The heterogeneous treatment approaches for TRISO compact fuel based on HSD, as examined in this section, are more computationally costly than the original homogenized method. However, they offer improved accuracy in capturing maximum fuel temperature, particularly in high-power scenarios—such as reactors designed for elevated TRISO power density and transient conditions involving significant power excursions. In such cases, adopting heterogeneous approaches would be necessary.

4.7 Summary of GCMR Work

Extensive FY2025 work on the GCMR concept yielded key achievements and lessons learned, summarized below:

- The steady-state, full-core multiphysics model of the GCMR developed in FY2024 was extended to support time-dependent simulations. A suite of transients was modeled to demonstrate the capability. The impact of hydride moderator performance was also systematically evaluated by comparing results with and without SWIFT.
- A Brayton cycle balance-of-plant model tailored to the GCMR specifications was developed and coupled to the existing full-core multiphysics model to enable more realistic transient simulations.
- Fission-product poisoning effects were assessed using both simplified (PKE–based) and high-fidelity Griffin solvers within the multiphysics framework, demonstrating the necessity of poison tracking for long-duration transients.

- A workflow to incorporate TRISO heterogeneity into the full-core GCMR multiphysics model was developed and benchmarked against the conventional homogeneous approach, highlighting cases where the new method is significantly improves transients accuracy.

5 Validation Using KRUSTY

In FY2025, validation has been continued based on the previous successful development of the baseline simulation approach for the KRUSTY reactivity insertion warm critical tests in FY2024. The focus of this year was to develop an automated approach to model the 30₵ reactivity insertion test and to expand the data analyses on the model prediction data. The code validation based on the KRUSTY reactivity insertion tests has been successfully completed with a focus on the 15₵ and 30₵ tests. Future validation based on KRUSTY will move to nuclear system tests.

5.1 Methodology and Model Improvements

5.1.1 Methodology

MOOSE-based applications and modules were used to develop the KRUSTY multiphysics model. High-fidelity finite element methods (FEM) were used for both neutronics and thermomechanics solvers, including the MOOSE Reactor module to generate the unstructured mesh model, Griffin for neutronics, and MOOSE Heat Transfer Module and BISON for heat transfer and thermo-mechanics. These applications/modules are coupled through the MOOSE MultiApp System, a native MOOSE object permitting in-memory physics coupling and data transfers. To support neutronics calculations in the multiphysics simulation, a hybrid approach which combines both deterministic-generated MC^2-3 and Monte Carlo-generated Serpent multigroup cross sections was used. Reactor transient power was calculated by solving the time-dependent Boltzmann equations. The multiphysics model was run using the pre-compiled MOOSE multiphysics application BlueCRAB using the INL HPC cluster.

5.1.2 Model Improvements

The 30₵ test is initiated by a prompt initial 15₵ reactivity insertion (similar to the 15₵ test). An additional 15₵ reactivity was added to the core incrementally when the reactor power peaked and then dropped at about 3 kW. With small reactivity inserted into the core, the reactor power was maintained around 3 kW for about 150 s. In FY2024, the second-stage reactivity insertion was achieved with a manual, trial-and-error method to complete the 30 ₵ insertion simulation, which was a tentative, preliminary solution.

In FY2025, building on the FY2024 tuning, an automatic feedback control approach was developed. The controller activates only after the reactor power peaks and begins to decline: the radial reflector is raised by approximately 0.126 mm each time the quarter-core power drops below 750 W. With this mechanism, the quarter-core power was maintained within the 750–760 W band for roughly 150 seconds in simulation. The total reflector displacement during the second stage was 1.638 mm, yielding a cumulative 3.085 mm insertion over the full 30 ₵ test. The total reactivity added in the model was about 29.7 ₵, closely matching the 29.9 ₵ observed experimentally.

In addition, during the KRUSTY warm critical tests, temperatures were measured by attaching thermocouples at three axial locations along the fuel's heat-pipe groove surface. Although several issues were reported—such as poor attachment (biasing readings low) and significant response lag—it remains informative to compare measurements with model predictions at the same axial positions. Accordingly, in addition to the representative fuel temperatures (minimum, maximum, and average) reported previously, model-predicted temperatures at the thermocouple axial locations along the heat-pipe grooves were also reported and compared against the measurements to provide a more comprehensive basis for model validation.

5.2 *Code Validation Using KRUSTY Warm Critical Tests*

Building on the model improvements described above, the KRUSTY 15 ₡ and 30 ₡ reactivity-insertion tests were modeled and analyzed to complete the code validation. Detailed results and discussion are provided in this subsection.

5.2.1 15 cent insertion

As shown in the Figure 5-1, the total power calculated by the multiphysics model compares favorably with neutron-detector measurements. Immediately after the 1.480 mm reflector displacement, the simulated power rise rate closely matches the data, indicating that the initial reactivity insertion by shifting the radial reflectors is appropriately modeled. The power then peaks and declines due to negative temperature reactivity feedback as core temperatures increase—a behavior captured by the model. The predicted maximum quarter-core fission power is 957.4 W, only about 2% higher than the measured 937.5 W. This level of agreement suggests that the coupled thermal–neutronic model accurately represents core thermal expansion and associated reactivity feedback.

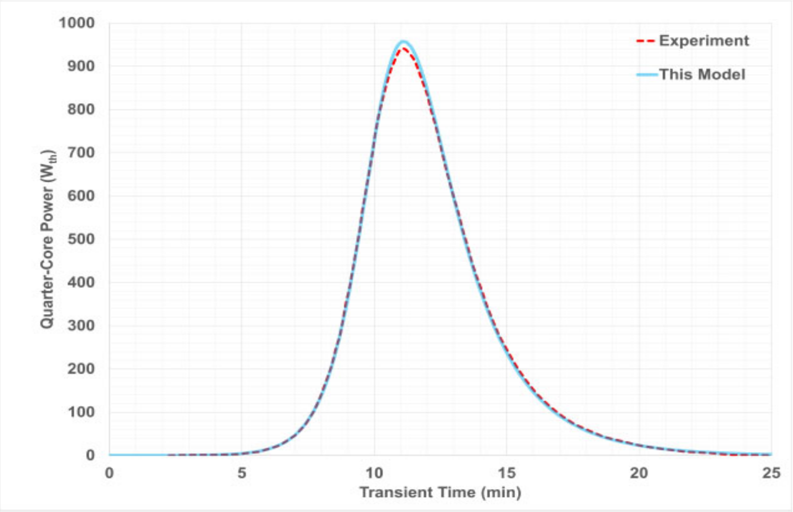

Figure 5-1 The time evolution of the predicted power (quarter-core simulation) during the 15₡ reactivity insertion test in comparison with experimental observation.

On the other hand, after the power peak, the subsequent decline driven by negative temperature reactivity feedback closely follows the measurements, further confirming the model's ability to capture feedback physics. Because the KRUSTY core was insulated during the warm critical test, out-of-core components remained near ambient while core temperatures rose, providing the source of the observed reactivity feedback. Although thermocouples monitored fuel-surface temperatures at several locations, the readings were inconsistent due to imperfect attachment and interference from the insulation. Despite these uncertainties, the model-predicted fuel temperatures are comparable to the measured values, as shown in Figure 5-2. The data also exhibit a thermocouple response lag, as noted by the experimenters.

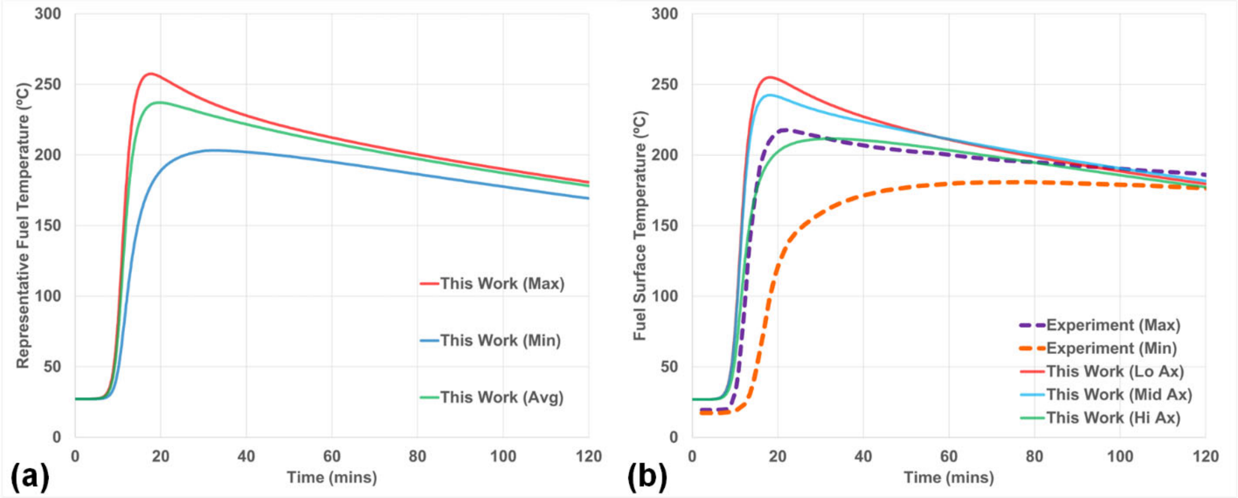

Figure 5-2 The time evolution of the predicted representative fuel temperatures during the 15 Ȼ reactivity insertion test: (a) maximum, minimum, and average fuel temperatures as predicted by the model; (b) predicted fuel temperatures at three axial elevations (i.e., “Lo Ax” - 6.25 cm, “Mid Ax” - 14.58 cm, and “Hi Ax” - 22.92 cm from the fuel bottom) along the heat pipe groove surface (corresponding to the thermocouple locations), in comparison with the reported typical temperature measured on fuel external surface

5.2.2 30 cent insertion

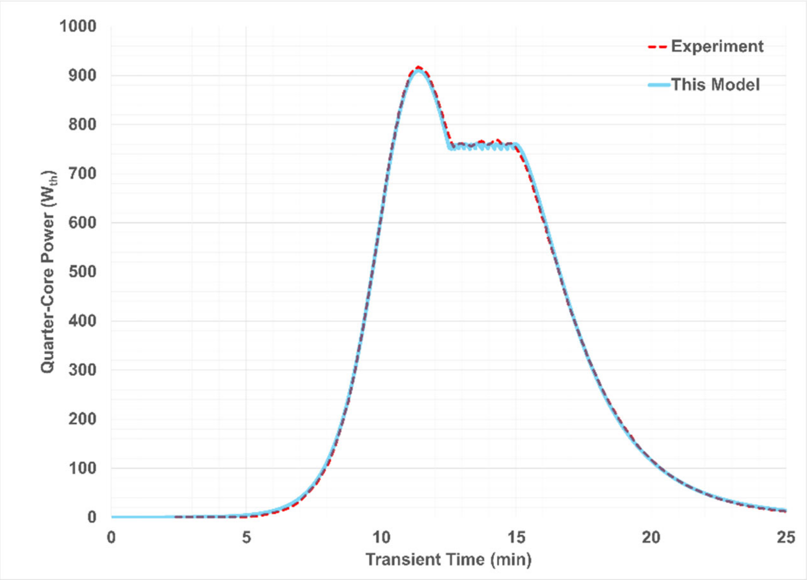

Figure 5-3 Time evolution of KRUSTY reactor power during the 30C reactivity insertion test:

model vs. experiment

The accurate prediction of the 15 ₵ reactivity-insertion experiment increases confidence in simulating its 30 ₵ counterpart, since the first stage of the latter closely mirrors the 15 ₵ case, aside from a slightly smaller external reactivity that produced a slightly lower experimental peak. As shown in Figure 5-3, the multiphysics model reproduces the first-stage power peak observed experimentally. Specifically, with about 15 ₵ inserted in the first stage, the experiment reached a peak power of ~3.65 kW (quarter-core ~913 W), slightly below the earlier 15 ₵ test. In the numerical model, the reflector displacement was accordingly reduced to 1.447 mm, yielding a predicted quarter-core peak of 913.5 W.

After the peak, when the quarter-core power fell to 750 W, the automatic reactivity-insertion mechanism described earlier maintained the quarter-core power within the 750–760 W band for approximately 150 seconds. The total reflector displacement during the second stage was 1.638 mm, resulting in a cumulative 3.085 mm insertion over the full 30 ₵ simulation. This displacement corresponds to ~29.7 ₵ external reactivity inserted and is close to the designed 30 ₵ reactivity addition reported in the litterature. The multiphysics power history agrees well with the experimental record. Finally, with no further reactivity insertion, the reactor power decreased continuously. Figure 5-3 shows that the model reproduces the observed power-decay rate.

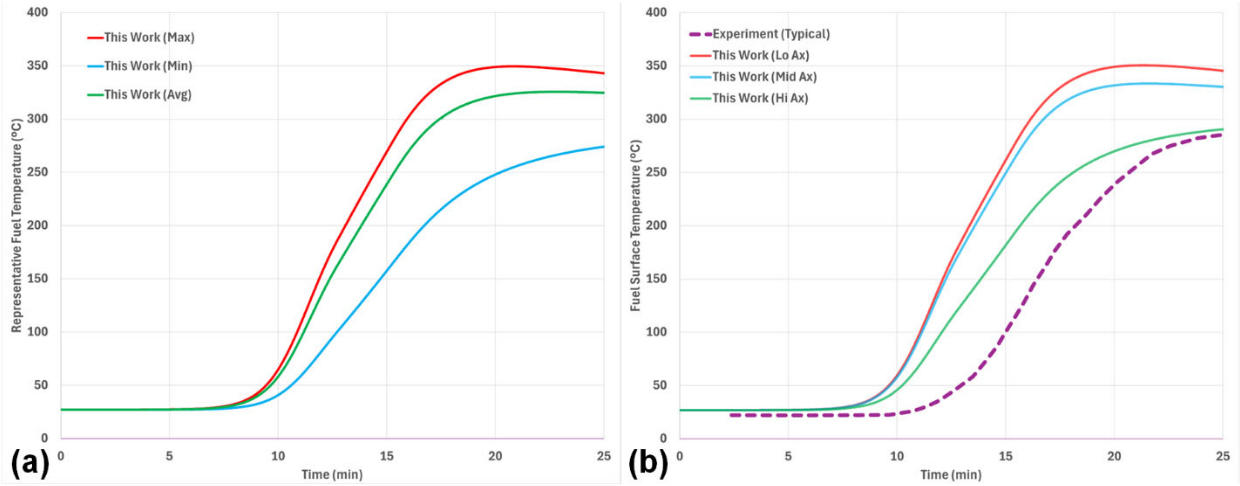

Figure 5-4 The time evolution of the predicted representative fuel temperatures during the 30₵ reactivity insertion test: (a) maximum, minimum, and average fuel temperatures as predicted by the model; (b) predicted fuel temperatures at three axial elevations (i.e., “Lo Ax” - 6.25 cm, “Mid Ax” - 14.58 cm, and “Hi Ax” - 22.92 cm from the fuel bottom) along the heat pipe groove surface (corresponding to the thermocouple locations), in comparison with the reported typical temperature measured on fuel external surface

Because reactor power was sustained for a longer period during the 30 ₵ test, the fuel reached higher temperatures. The multiphysics model predicts a rise to approximately 300 °C after about 20 minutes (Figure 5-4). The measured fuel-surface temperature likewise approaches ~300 °C but shows a pronounced lag, consistent with the experimenters’ report. This lag is also evident in the neutronic response shown in Figure 5-3, where the power peaked at 10 minutes primarily due to the changes in fuel temperature.

5.2.3 60 cent insertion

In KRUSTY warm critical experiments, the 60 ₡ test was conducted in the same way as the 30 ₡ test, except the constant thermal power at 3 kW was maintained by about 8 minutes (150 s for the 30 ₡ test). Reactivity insertion in the first stage—base case 15 ₡ run —to initiate the transient was 15.5 ₡, and total estimated reactivity insertion was 58.5 ₡. The 60 ₡ run was performed in a much longer time with experimental data reported up to 6 hours. Within this long time period, the reactor transient fully evolved, and the reactor demonstrated a passive response similar to a household thermostat, with temperature at 400 ^{0}C and power thermal power at ~100 W. Oscillation period was measured to be around 37 minutes.

The 60 ₡ run served as a steppingstone for the later nuclear system tests. It also provided a valuable scenario for further validating our Multiphysics-coupled transient model. In this FY, the same approach of modeling the 30 ₡ were tried to model the 60 ₡ test with expected longer computational time. However, the Multiphysics simulation failed at some time step when large displacement was applied in Griffin calculation.

To be specific, a convergence issue in Griffin was identified while modeling KRUSTY warm critical experiments. The failure was first observed when modeling the 30 ₡ test after the power dropped below 100 W. This issue was suspected to be caused by the large displacement introduced into the neutronic calculation. A walk-around method which used a base mesh geometry corresponding the 15 ₡ reactivity insertion solved the issue. In this case, a negative displacement was initially applied to calculate the steady state, and zero displacement was applied to initiate the transient (corresponding to the 15 ₡ run). This walk-around method is not applicable to model the 60 ₡ run as the displacement continues to grow above the threshold triggering the convergence issue again.

A Griffin standalone calculation with the displacement file confirmed that the observed convergence issue observed in the multiphysics transient is indeed due to Griffin diverging in the calculation. A modified mesh file which moved every node of the original mesh file correspondingly to a new position (the displaced value in x-, y-, z- directions) was created for a separate neutronic calculation and the result showed that the mesh after “larger” displacements is still in good quality and Griffin can converge the problem with this modified displaced mesh. A minimum working examples which recreated the problem was shared with the Griffin developers. With help from Griffin developers, the convergence problem was fixed by constructing Griffin’s Sweeper on the displaced mesh. The KRUSTY standalone neutronic model with the displaced file converged using the updates in Griffin.

Numerical simulation was restarted for the 60 ₡ test using the updated Griffin build. However, in this case, the Multiphysics simulation stalled with Griffin looped in the Sweeper at some time step (before reaching the previous displacement threshold). We are working with Griffin developers on the new issue.

5.3 Perspectives of Nuclear System Tests Modeling

Beginning in FY2026, the focus of multiphysics code validation with KRUSTY data will shift to the nuclear system tests. Unlike the warm critical reactivity insertion tests, the nuclear sytems tests were performed on the fully assembled KRUSTY reactor with all heat pipes installed and operating, providing significant heat removal and associated reactivity feedback. Consequently, the multiphysics model used for warm critical test simulations must be extended to include heat pipes, with Sockeye used to model their performance. Notably, KRUSTY employed heat pipes with a wick-free condenser region, creating a hybrid heat-pipe/thermosyphon configuration; they were also vertically oriented, making gravity effects non-negligible. In coordination with the Sockeye development team, gravity and partial-wick configuration support will be implemented in FY26. Accordingly, FY26 KRUSTY nuclear system tests will focus on steady-state and simple transient cases, with the new Sockeye features exercised near the end of FY26; more comprehensive analyses, including complex transients, will follow in FY27.

5.4 Summary of KRUSTY Work

In FY2025, a crucial code validation milestone based on the KRUSTY warm critical experiments has been completed, paving the way for simulating KRUSTY nuclear system tests in FY2026:

- The finalized full-core multiphysics modeling approach for the KRUSTY warm-critical reactivity-insertion tests demonstrated strong predictive fidelity, reproducing key operating parameters in close agreement with experimental measurements.
- A journal article summarizing the multiphysics modeling of the KRUSTY warm critical tests has been accepted for publication in *Nuclear Science and Engineering*.

6 Summary and Conclusions

In FY2025, substantial progress was made in advancing multiphysics models for three microreactor systems: HPMR, GCMR, and KRUSTY. The work emphasized addressing more complex coupled phenomena enabled by enhanced tool capabilities, rigorously verifying and validating results, providing valuable feedback to developers for improvements, and disseminating the models to support broad use in microreactor design and licensing.

6.1 Capability Demonstration

On the HPMR, a sodium working fluid variant (Na-HPMR) was developed to leverage Sockeye's LCVF model, and new full core multiphysics (Griffin/BISON/Sockeye) analyses were executed at steady state and for transients including load following, single heat pipe failure, and startup. Solid mechanics was integrated into the KHPMR in BISON, showing marginal impact on steady state reactivity and enabling future full core TRISO fuel performance assessment. Productivity in meshing was improved via the Reactor Module's batch mesh generation action, and an OECD/NEA WPRS microreactor multiphysics benchmark based on the HPMR was initiated to facilitate international collaboration in cross-code comparison.

On the GCMR, a full core Griffin/BISON/SAM/SWIFT model was advanced from steady state to systematic transients spanning depressurization, loss of coolant velocity, inlet temperature drop, and single channel blockage, demonstrating inherent safety behavior of the microreactor concept. SWIFT predicted hydrogen redistribution produced measurable reactivity shifts at steady state and during transients, underscoring its importance. A Brayton cycle BOP was coupled with the existing Multiphysics full-core model, enabling more realistic simulations for transient scenarios. The poison tracking capability in Griffin was also tested using the GCMR multiphysics model based on a 100–50–100 load follow case. A multiscale approach was developed to account for the heterogeneity in TRISO compact simulation to improve temperature fidelity.

On KRUSTY, warm critical validation progressed beyond the FY2024: the 15¢ insertion showed excellent agreement in power prediction with consistent temperature trends, and the 30¢ case employed an automated reactivity control algorithm to hold the reactor power near 3 kW full core for ~150 s, replicating the experiment procedure. A 60¢ case revealed a Griffin DFEM-SN convergence issue at large mesh displacements, which is expected to be fixed in FY2026. With warm critical validation completed, a transition to KRUSTY nuclear system tests is planned.

Multiple publications and open models were produced to disseminate methods and results to end users. A journal article summarizing the KRUSTY warm critical reactivity insertion models was accepted to *Nuclear Science and Engineering* [28]. Three conference papers were published, including contributions at ANS Winter 2024 on recent VTB models [4] and at ANS 2025 providing a summary of microreactor multiphysics modeling progress as well as a topical paper on TRISO analyses [29, 30]. Six models were ported to the Virtual Test Bed to support broad reuse: updated HPMR assembly-level TRISO analysis model (based on FY2024), KRUSTY 15¢ reactivity-insertion test model (based on FY2024), KRUSTY 30¢ reactivity-insertion test model, full-core GCMR multiphysics transient model, HPMR control drum rotation model (based on

FY2024), and Na-HPMR updated model.

Additionally, the models developed in this project and released through the VTB platform have attracted a broader user community, amplifying their impact. For example, Westinghouse has evaluated fission matrix methods using the HPMR model [31], and the U.S. DOE-NE DNCSH program has adopted the HPMR and GCMR models from this project for criticality safety analyses [32]. Additionally, the DOE NRIC Virtual Test Bed program has incorporated the GCMR core design into a multiphysics model of the DOME shield as a placeholder for future vendor designs.

6.2 User Experiences and Lesson Learned

Throughout FY2025, extensive user experience was gathered on best practices for using NEAMS tools to perform multiphysics simulations of microreactors. The MOOSE ecosystem provided a flexible framework in which established models could be upgraded to advanced formulations (e.g., the Na HPMR variant and adoption of Sockeye's LCVF model) and expanded to include additional physics (e.g., poison tracking in Griffin and balance of plant modeling with SAM/THM).

At the same time, the coexistence of multiple phenomena with disparate spatial and temporal scales in full core models made simulations computationally intensive, necessitating careful model optimization to utilize resources efficiently. Execution timing of framework objects—such as UserObjects, AuxKernels, Postprocessors, and Outputs—was found to materially affect runtime; accordingly, timings should be selected judiciously for the specific model and target phenomena. As additional physics is incorporated, the MultiApps hierarchy deepens and timestep management becomes more complex; because different physics can exhibit markedly different kinetics, timestep strategies (e.g., sub cycling and catch up) should be designed in advance based on prior knowledge of the system dynamics

6.3 Feedback to NEAMS Developers

Griffin includes poison tracking capabilities, which is an important factor influencing reactivity and control strategy during long duration transients such as load following. During FY2025 evaluations, it was noticed that poison tracking was not yet supported by the high-fidelity transport solver. In coordination with the Griffin development team, this gap was promptly addressed and support for the high-fidelity solver was added (see Section 4.5).

As mentioned in Section 5.2.3, an issue about handling meshes with large displacement field was identified when running the KRUSTY 60₵ reactivity insertion tests. A series of discussions and trials have been made between this team and Griffin developers to better understand the origins of the issue. The efforts to solve this issue will continue to the next FY.

Sockeye provides flexible capabilities for simulating heat pipe behavior under both steady-state and transient conditions, making it a crucial tool for HPMR analyses within the MOOSE ecosystem. Within this project, both the effective-conductance and LCVF models were applied successfully to the HPMR concept. By contrast, adoption in the KRUSTY multiphysics model has been limited by KRUSTY's specialized heat pipes, which require explicit treatment of gravity effects and a partial wick configuration. These feature requests have been communicated to the Sockeye development team, which has scheduled support for FY2026; corresponding integration of Sockeye into KRUSTY simulations is planned on the same timeline.

6.4 Recommended Follow-Up Work

The following additional tasks are recommended to expand on this work:

- Continued verification and validation, including extension of KRUSTY multiphysics modeling to nuclear system tests.
- Development of a comprehensive structural modeling capability for the thermomechanical response of the graphite monolith in HPMR under varied operating and transient conditions.
- Expansion of the HPMR multiphysics model to include a secondary-loop model, enabling more realistic transient analyses.
- Demonstration of online cross-section generation within existing HPMR or GCMR models.
- Porting of new models to the VTB and updating of existing VTB entries with new features where applicable.

References

[1] N. Stauff *et al.*, "Detailed analyses of a triso-fueled microreactor: Modeling of a micro-reactor system using neams tools," Argonne National Lab.(ANL), Argonne, IL (United States), 2021.

[2] N. E. Stauff *et al.*, "Multiphysics analysis of load following and safety transients for MicroReactors," Argonne National Laboratory (ANL), Argonne, IL (United States); Idaho …, 2022.

[3] N. Stauff *et al.*, "High-fidelity multiphysics load following and accidental transient modeling of microreactors using NEAMS tools: Application of NEAMS codes to perform multiphysics modeling analyses of micro-reactor concepts," Argonne National Laboratory (ANL), Argonne, IL (United States); Idaho …, 2023.

[4] N. Stauff, Y. Miao, A. Abdelhameed, Y. Cao, K. Mo, and E. Shemon, "NEAMS Microreactor Models Submitted to the VTB in 2024," presented at the 2024 ANS Winter Conference and Expo, Orlando, Florida, 2024.

[5] Y. Wang *et al.*, "Griffin: A MOOSE-based reactor physics application for multiphysics simulation of advanced nuclear reactors," *Ann Nucl Energy,* vol. 211, p. 110917, 2025.

[6] R. L. Williamson *et al.*, "BISON: A flexible code for advanced simulation of the performance of multiple nuclear fuel forms," *Nuclear Technology,* vol. 207, no. 7, pp. 954-980, 2021.

[7] B. W. Spencer, W. M. Hoffman, S. Biswas, W. Jiang, A. Giorla, and M. A. Backman, "Grizzly and BlackBear: Structural component aging simulation codes," *Nuclear Technology,* vol. 207, no. 7, pp. 981-1003, 2021.

[8] J. E. Hansel, R. A. Berry, D. Andrs, M. S. Kunick, and R. C. Martineau, "Sockeye: A one-dimensional, two-phase, compressible flow heat pipe application," *Nuclear Technology,* vol. 207, no. 7, pp. 1096-1117, 2021.

[9] E. Shemon *et al.*, "MOOSE Reactor Module: An Open-Source Capability for Meshing Nuclear Reactor Geometries," *Nuclear Science and Engineering,* pp. 1-25, 2023.

[10] L. Harbour *et al.*, "4.0 MOOSE: Enabling massively parallel Multiphysics simulation," *SoftwareX,* vol. 31, p. 102264, 2025.

[11] J. Leppänen, M. Pusa, T. Viitanen, V. Valtavirta, and T. Kaltiaisenaho, "The Serpent Monte Carlo code: Status, development and applications in 2013," *Ann Nucl Energy,* vol. 82, pp. 142-150, 2015.

[12] N. Stauff *et al.*, "Assessment and validation of NEAMS tools for high-fidelity multiphysics transient modeling of microreactors," Argonne National Laboratory (ANL), Argonne, IL (United States), 2024.

[13] C. Lee and W. S. Yang, "MC2-3: Multigroup cross section generation code for fast reactor analysis," *Nuclear Science and Engineering,* vol. 187, no. 3, pp. 268-290, 2017.

[14] R. Hu *et al.*, "SAM: A Modern System Code for Advanced Non-LWR Safety Analysis," *Nuclear Technology,* vol. 211, no. 9, pp. 1883-1902, 2025.

[15] J. Hansel, D. Andrs, L. Charlot, and G. Giudicelli, "The MOOSE Thermal Hydraulics Module,"

Journal of Open Source Software, vol. 9, no. 94, p. 6146, 2024.

[16] G. L. Giudicelli *et al.*, "The virtual test bed (VTB) repository: a library of reference reactor models using NEAMS tools," *Nuclear Science and Engineering,* vol. 197, no. 8, pp. 2217-2233, 2023.

[17] C. Matthews, A. P. Shivprasad, and M. W. D. Cooper, "Metal Hydride Simulations Using SWIFT," Los Alamos National Laboratory (LANL), Los Alamos, NM (United States), 2021.

[18] J. E. Hansel, C. d. S. B. Dutra, L. Charlot, and E. Merzari, "The liquid-conduction, vapor-flow heat pipe model in Sockeye," *Nuclear Engineering and Design,* vol. 426, p. 113359, 2024.

[19] S. Qin *et al.*, "Advanced Measurement and Visualization Techniques for High-Temperature Heat Pipe Experiments," Idaho National Laboratory (INL), Idaho Falls, ID (United States), 2022.

[20] I. Yilgor *et al.*, "Phenomena Identification and Ranking Table (PIRT) for heat pipes," *Progress in Nuclear Energy,* vol. 189, p. 105929, 2025.

[21] Z. D. Sellers, J. L. Hartvigsen, and P. Sabharwall, "High Performance Heat Pipe Power Transient Testing at SPHERE Facility," Idaho National Laboratory (INL), Idaho Falls, ID (United States), 2024.

[22] J. E. Hansel, J. L. Hartvigsen, P. Sabharwall, L. Ibarra, and B. Feng, "Sockeye validation support using the SPHERE facility," Idaho National Laboratory (INL), Idaho Falls, ID (United States), 2022.

[23] N. E. Stauff *et al.*, "Preliminary Applications of NEAMS Codes for Multiphysics Modeling of a Heat Pipe Microreactor," in *proceedings of ANS Annual 2021 meeting*, 2021.

[24] W. Jiang *et al.*, "TRISO particle fuel performance and failure analysis with BISON," *Journal of Nuclear Materials,* vol. 548, p. 152795, 2021.

[25] A. Hegazy and A. J. Novak, "Multiphysics Simulation of TRISO Fuel Compacts and the Effects of Homogenization," in *2024 International Conference on Physics of Reactors, PHYSOR 2024*, 2024: American Nuclear Society, pp. 882-891.

[26] A. Novak, "Multiscale Thermal-Hydraulic Methods for Pebble Bed Reactors," University of California, Berkeley, 2020.

[27] A. Novak, S. Schunert, R. Carlsen, P. Balestra, R. Slaybaugh, and R. Martineau, "Multiscale thermal-hydraulic modeling of the pebble bed fluoride-salt-cooled high-temperature reactor," *Ann Nucl Energy,* vol. 154, p. 107968, 2021.

[28] Y. Miao *et al.*, "Multiphysics Simulation of KRUSTY Warm Critical Experiments Using MOOSE Tools," *Nuclear Science and Engineering,* vol. accepted, 2025.

[29] Y. Miao *et al.*, "Recent Updates on High-Fidelity Multiphysics Microreactors Modeling Using MOOSE-based Applications," presented at the ANS Annual Conference 2025 Chicago, IL, 2025.

[30] S. Lee *et al.*, "Gas-Cooled Microreactor TRISO Fuel Performance Analysis," presented at the ANS Annual Conference 2025, Chicago, IL, 2025.

[31] C. Vita *et al.*, "FIM4NTRA: A Code for Neutronics Analyses Based on The Fission Matrix

Method," presented at the 2025 ANS Winter Conference & Expo, Washinton, DC, 2025.

[32] Z. Zhong, A. Abdelhameed, N. Stauff, and C. Celik, "Microreactor Assembly Transportation Cask Model for Criticality Safety Basis Assessment " presented at the 2025 ANS Annual Conferences, Chicago, IL, 2025.

[33] P. K. Romano, N. E. Horelik, B. R. Herman, A. G. Nelson, B. Forget, and K. Smith, "OpenMC: A state-of-the-art Monte Carlo code for research and development," *Ann Nucl Energy,* vol. 82, pp. 90-97, 2015.

7 Appendix A: Improved TRISO Modelling

7.1 *Heterogeneous TRISO Models*

A steady-state coupled neutronics / heat conduction heterogeneous TRISO fuel model based on the whole-core GCMR model in the VTB was developed to act as a point for comparison for various homogeneous TRISO temperature treatments. A summary of the relevant compact parameters can be found in Table 7-1. The multi-group cross sections generated for the assembly GCMR model in FY2022 are used for the Griffin neutronics model. A convective cooling boundary condition with the mean of the inlet and outlet temperature is applied to the solid/fluid boundary in the heat conduction solve, and symmetry boundary conditions are applied on the other sides of the heat conduction solve. All neutronics boundary conditions are reflective as this is a lattice cell representation of a GCMR fuel compact. BISON thermal properties are used for the UCO, SiC, and matrix; thermal properties for the buffer and PyC layers are taken to be constant with values equal to the values reported in Ref. [24].

Table 7-1 Relevant properties for the unit cell heterogeneous TRISO model

Parameter	Value
Height (total/fueled) (cm)	1.1/1.0
Radius (prism/compact) (cm)	2.0/0.8
Particle Packing Fraction	0.4
Number of Particles	2774
Particle Layer Outer Radii (kernel/buffer/iPyC/SiC/oPyC) (μm)	212.5/312.5/352.5/387.5/427.5
Material Properties (kernel/buffer/iPyC/SiC/oPyC/matrix/coolant)	UCO/C/PyC/SiC/PyC/C/He
Material Densities (kernel/buffer/iPyC/SiC/oPyC/matrix) (g/cm^3)	10.744/1.04/1.882/3.171/1.882/4.085
Coolant Channel Outer Radius (cm)	0.6
Fluid Temperature (K)	1003.4
Fluid Heat Transfer Coefficient ($W/m^2/K$)	2000
Compact Power (case 1/case 2) (W)	24/120

The geometry of the heat conduction portion of the heterogeneous compact model can be found in Figure 7-1, where the TRISO particle positions are generated with the close random packing algorithm implemented in OpenMC [33]. The mesh containing the TRISO particles was generated using the open-source capabilities of the MOOSE mesh generator suite. Generation of the compact mesh was attempted with the MOOSE mesh generator suite at the beginning of Q3 – several deficiencies of the mesh generators at that time made this impractical and so Cubit was used to generate the compact mesh. These deficiencies have since been resolved in Q3, and it is now possible to mesh the full compact geometry entirely within MOOSE. The compact and TRISO particles are meshed separately in an attempt to mitigate the need for ultra-fine boundary layers at the interface of the two different length scale domains. As Griffin DFEM-SN operates on coarse length scales, the neutronics geometry does not resolve this heterogeneity and a separate mesh is used to minimize the performance penalty when performing a transport sweep.

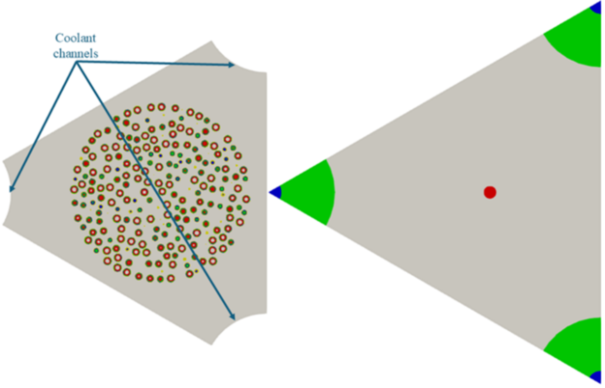

Figure 7-1 Heterogeneous TRISO model geometry. Left: heat conduction model. Right: neutronics model.

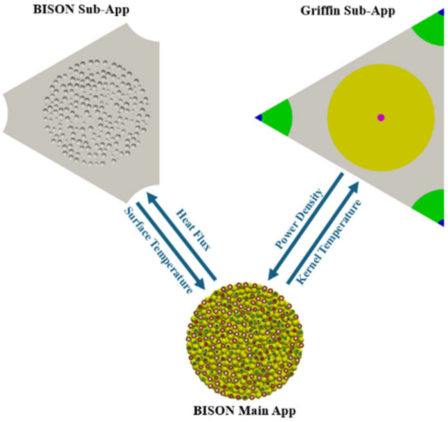

Figure 7-2 Multiphysics coupling scheme between the TRISO heat conduction, matrix heat conduction, and neutronics applications

The separation of the TRISO particles from the compact necessitates the use of a coupling strategy using the MOOSE MultiApp system, which can be found in Figure 7-2. The TRISO application acts as the main application in the hierarchy, which sends surface heat fluxes to a matrix sub-application and receives surface temperatures. The TRISO main application also transfers kernel temperatures to a neutronics sub-application and receives kernel power densities back from the eigenvalue solve. The three applications iterate in a Picard loop until convergence. This coupling scheme deviates from the approach commonly used in multiphysics simulations that use Griffin for neutronics, where other physics are solved on each transport Richardson iteration. This coupling scheme increases the number of heat conductions solves and decreases the number of transport Richardson iterations. This proves to be disadvantageous when the heat conduction solves dominate the runtime, as is the case with this heterogeneous TRISO model, and so an alternative multiphysics iteration scheme was adopted to minimize the problem runtime at the cost of added neutronics solves.

The results of the heterogeneous multiphysics calculation can be found in Figure 7-3 for a total compact power of 24 W, and in Figure 7-4 for a severe overpower case where the total compact power is 120 W. The effects of particle clustering on fuel temperature can be seen in the projection of the kernel temperatures onto the neutronics mesh for temperature feedback, which results in a slight north-west tilt in the temperature and power density distributions. The distribution of quantities of interest does not change as the power is quintupled, indicating that the nonlinearity in TRISO thermal conductivity does not have a significant impact on the solution compared to the matrix material.

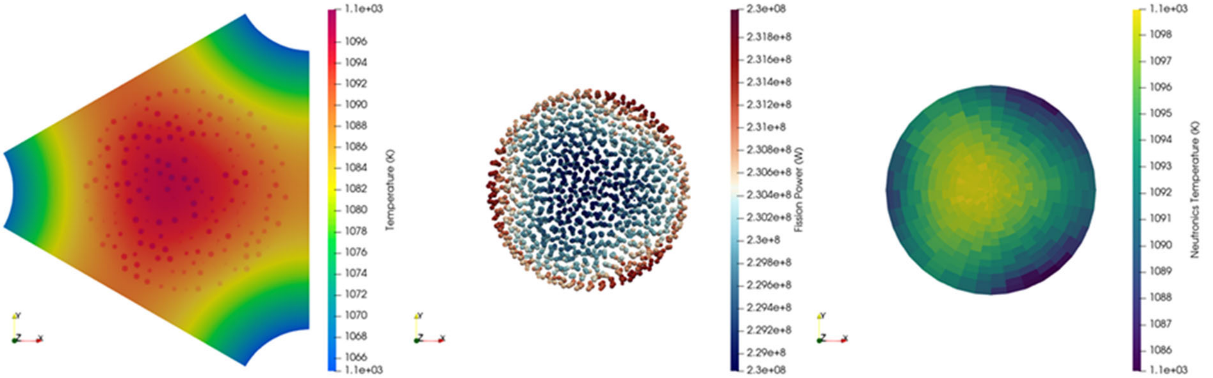

Figure 7-3 Heterogeneous compact results for 24 W (case 1). Left: temperature. Middle: kernel power density. Right: temperature projected on the neutronics mesh

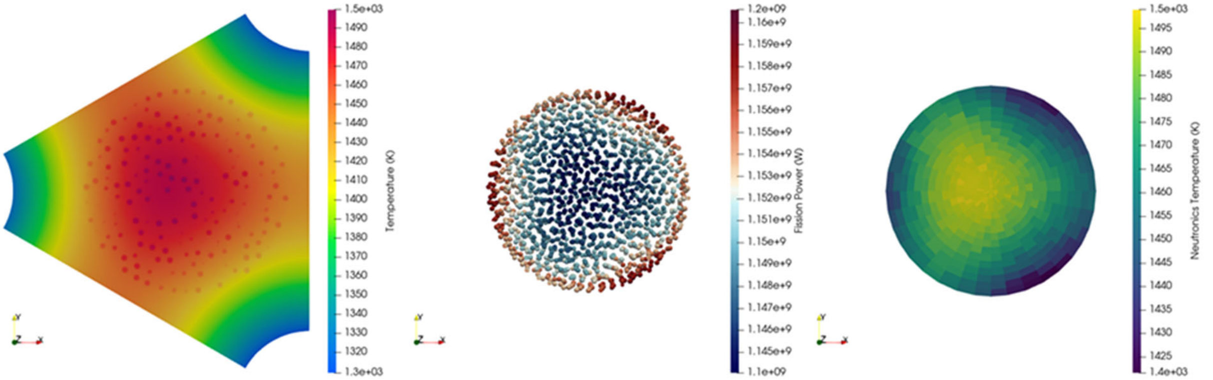

Figure 7-4 Heterogeneous compact results for 120 W (case 2). Left: temperature. Middle: kernel power density. Right: temperature projected on the neutronics mesh

In addition to the steady-state multiphysics model presented, a single-physics transient model was generated to evaluate the performance of different TRISO homogenization schemes for transient calculations. A full multiphysics transient was deemed to be impractical for this unit cell due to the lack of control devices and the required runtime of the Griffin DFEM-SN solve. The single-physics transient model uses initial conditions from a single-physics steady-state simulation where 24 W of power are distributed uniformly over all TRISO particles. Between t = 1 s and t = 10 s, the power density begins to ramp linearly from 8.65 mW/particle to 86.5 mW/particle. This corresponds to the order of magnitude increase expected from severe reactivity excursions in the GCMR concept. The results of the ramp transient can be found in Figure 7-5, where the maximum temperature of each TRISO layer is plotted alongside the maximum matrix temperature. The maximum kernel and buffer temperatures separate over the course of the transient due to the low thermal conductivity of the fuel and buffer. This temperature rise is not predicted by effective thermal conductivity models, motivating the development of improved TRISO temperature treatments for transient analyses.

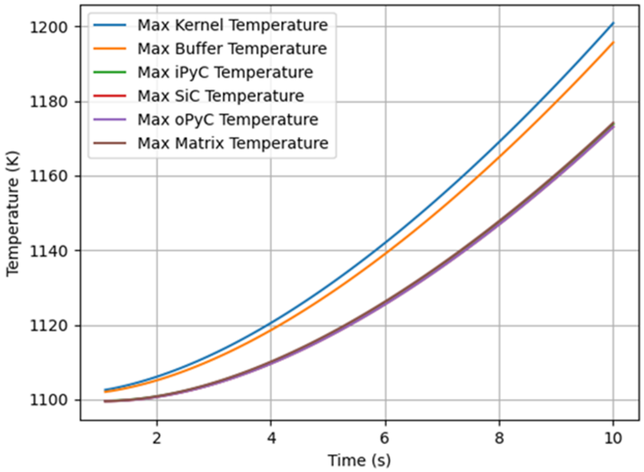

Figure 7-5 Maximum temperatures of different TRISO layers over the duration of the transient

7.2 Homogeneous TRISO Modelling

Previous multiphysics models of the GCMR use the default homogenized compact thermal property model in BISON (`GraphiteMatrixThermal`), which utilizes Differential Effective Medium Theory (D-EMT):

$$\left(\frac{k_{homogenized}(T) - k_{TRISO}}{k_{matrix}(T) - k_{TRISO}}\right)^3 \frac{k_{matrix}(T)}{k_{homogenized}(T)} = (1 - \phi_{TRISO})^3 \qquad (7\text{-}1)$$

where $k_{homogenized}$ is the thermal conductivity of the homogenized compact (W/m/K), k_{TRISO} is the thermal conductivity of a single TRISO particle (taken to be a constant in BISON) (W/m/K), k_{matrix} is the thermal conductivity of the matrix (W/m/K), and ϕ_{TRISO} is the packing fraction of TRISO particles in the compact. Eq. (7-1) requires the solution to a cubic equation to obtain the homogenized thermal conductivity. A homogenized value of the specific heat is obtained using a simple volume average:

$$\begin{aligned} C_{p,homogenized}(T) & \\ &= \phi_{TRISO} \times C_{p,TRISO} \\ &+ (1 - \phi_{TRISO}) \times C_{p,matrix}(T) \end{aligned} \qquad (7\text{-}2)$$

where $C_{p,homogenized}$ is the specific heat of the homogenized compact (J/kg/K), $C_{p,TRISO}$ is the specific heat of a single TRISO particle (taken to be a constant in BISON) (J/kg/K), and $C_{p,matrix}$ is the specific heat of the matrix (J/kg/K). The use of this homogenization strategy for steady-state calculations has been numerically verified through comparisons with heterogeneous finite element simulations, where the effective thermal conductivity of a TRISO compact is numerically determined (by imposing a temperature gradient) and compared to the homogenized thermal conductivity. Comparisons between this homogenization approach for steady-state multiphysics problems (Table 4-3) and single-physics transient problems (Figure 4-29) indicate that this is no longer sufficient when the quantities of interest are integral quantities, such as the maximum temperature of different particle layers.

Numerical experiments were performed to determine if an alternative homogenization scheme would suffice compared to the D-EMT with constant TRISO thermal properties, where a new inner homogenization scheme was tested for fully nonlinear thermal properties. This work was performed under the assumption that the homogenized thermal conductivity using constant TRISO properties resulted in a thermal conductivity that was too high, yielding lower maximum temperatures. Compact homogenization was performed in two steps: i) homogenization of the different layers of a single TRISO particle into one effective thermal conductivity function, and ii) homogenization of the TRISO particles into the matrix, yielding a thermal conductivity for the compact. The first TRISO homogenization scheme for step one considers simple volume averaging of the particle thermal conductivity (Eq. (7-3)):

$$k_{TRISO}(T) = \sum_i \phi_i k_i(T) \tag{7-3}$$

where k_i is the thermal conductivity of the i'th TRISO layer (W/m/K) and ϕ_i is the volume fraction of the i'th TRISO layer. The second TRISO homogenization scheme considers the use of harmonic volume averages (Eq. (7-4)):

$$k_{TRISO}(T) = \left(\sum_i \frac{\phi_i}{k_i(T)}\right)^{-1} \tag{7-4}$$

For the second layer of homogenization, Chiew and Glandt's extension to Maxwell's potential theory was investigated as an alternative to Eq. (7-1) as it reports similar results compared to D-EMT and can be implemented in a straight-forward manner using the `Functions` block in a BISON input file:

$$\begin{gathered} k_{homogenized}(T) \\ = k_{matrix}(T)\frac{1 + 2\beta\phi_{TRISO} + (2\beta^3 - 0.1\beta)\phi_{TRISO}^2 + 0.05\phi_{TRISO}^3 \exp(4.5\beta)}{1 - \beta\phi_{TRISO}} \\ \beta = \frac{k_{TRISO}(T) - k_{matrix}(T)}{k_{TRISO(T)} + 2k_{matrix}(T)} \end{gathered} \tag{7-5}$$

The thermal conductivity of each material in the heat conduction calculation, along with the homogenized thermal conductivity of the compact can be found in Figure 7-6. The use of a constant thermal conductivity of 4.13 W/m/K for the TRISO particles results in a far larger value of the homogenized compact thermal conductivity compared to either the simple or harmonic averages for the TRISO particle. The use of a constant value of TRISO thermal conductivity appears to have a minimal impact on the shape of the homogenized thermal conductivity curve before 1300 K, as can be seen in Figure 7-6b.

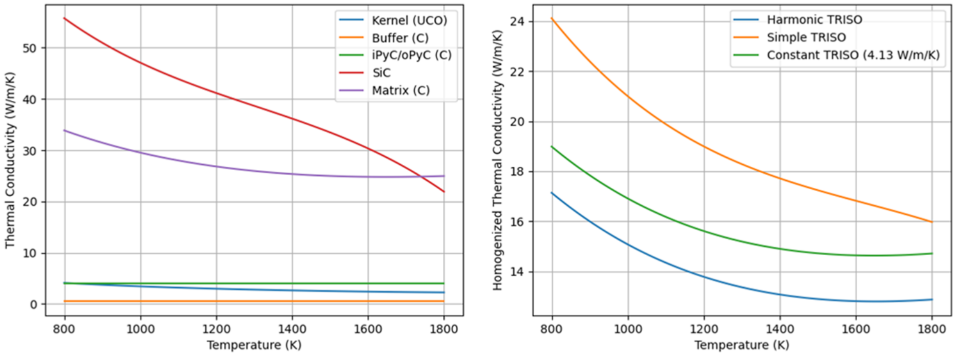

a) **b)**

Figure 7-6 Comparison between thermal conductivity and homogenized thermal conductivities. a) $k_i(T)$ as implemented in BISON. b) $k_{homogenized}(T)$ for different TRISO homogenization schemes

To facilitate the comparison of each homogenization scheme against the heterogeneous reference solution, a homogenous GCMR unit cell model was created using the parameters in Table 7-1. The BISON mesh was created using Coreform Cubit to ensure the heterogeneous element density was used in the homogenous mesh. A standard form of multiphysics iteration was employed with the homogeneous problem, where Griffin acts as the main application and BISON heat conduction (a sub-app) is solved at each transport Richardson iteration. The homogenous model and iteration scheme can be found in Figure 7-7. In addition to a steady-state homogenous model using Griffin, a transient homogenous model was also created to study the impact of heat capacity homogenization.

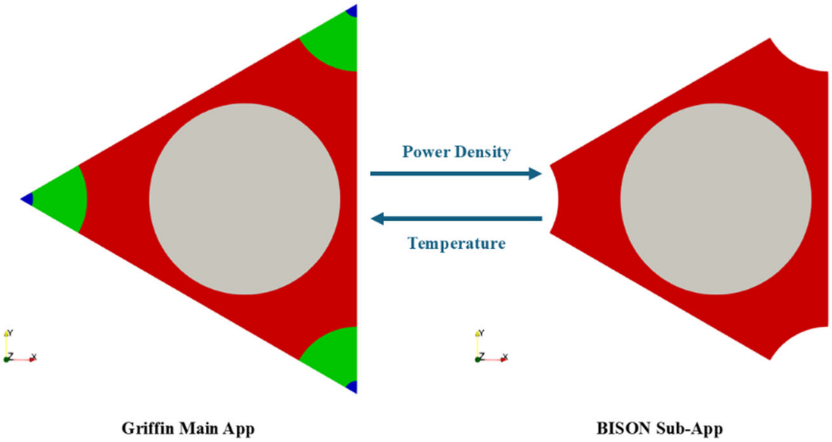

Figure 7-7 Multiphysics coupling between Griffin and BISON for the homogenous problem

Comparisons of these different homogenization approaches against the reference heterogeneous solution can be found in Table 7-2, where none of the fully homogenous compact models reach the reference. This can be attributed to the homogenous solutions only capturing the long-wavelength effects of the smeared power density, macroscopic compact geometry, and boundary conditions. The short wavelength perturbations caused by the kernel power density and localized decreases in thermal conductivity cannot be captured by these schemes, resulting in an underprediction of particle clustering effects. This can be seen in comparisons of the homogeneous temperature, power density, and projected fuel temperature (Figure 7-8). The homogenous model does not predict the north-west temperature tilt caused by particle clustering.

Table 7-2 Comparison of the maximum temperature and neutronics eigenvalue between different TRISO homogenization approaches for a total compact power of 24 W

Parameter (24 W)	**Heterogeneous**	**Simple Averaged TRISO**	**Harmonic Averaged TRISO**	**Constant TRISO**
Max. T_{kernel} (K)	1099.0	1089.2	1092.4	1091.1
Δk_{eff} (het. - other) (pcm)	N/A	-62	-50	-55

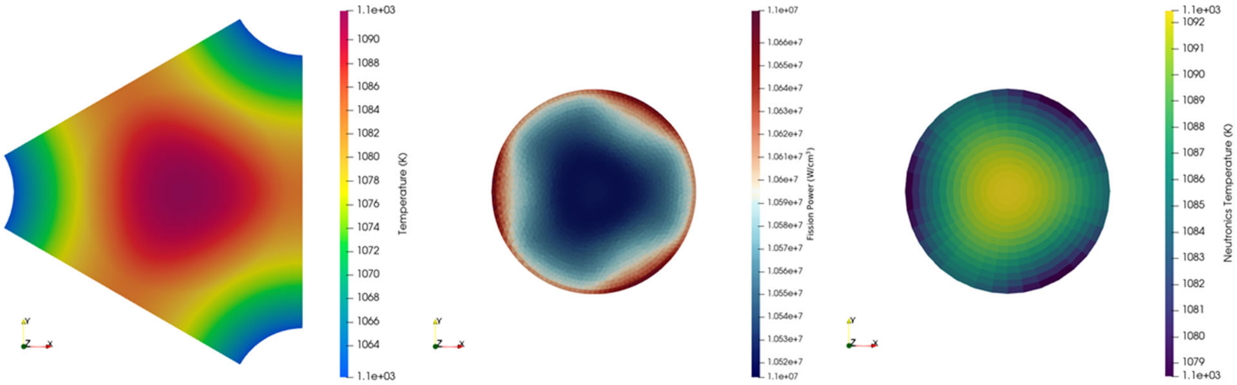

Figure 7-8 Sample homogenous results (harmonic average). Left: temperature (K). Middle: power density (W/cm^3). Right: temperature projected on the neutronics mesh (K)

In addition to comparisons with a steady-state multiphysics model, the homogenous approach was compared against the transient single-physics model to determine the effectiveness of the three homogenization strategies. Extensions to transients require a homogenization strategy for the specific heat in addition to thermal conductivity; this work chooses to employ a simple volume average for both the TRISO kernel (Eq. (7-6)a) and the full compact (Eq. (7-6)b) due to a lack of literature surrounding homogenization strategies for particles dispersed in a medium:

$$\begin{aligned} &\text{(a)} \quad & C_{p,TRISO}(T) &= \sum_i \phi_i C_{p,i}\,(T) \\ &\text{(b)} \quad & C_{p,homogenized}(T) &= \phi_{TRISO} C_{p,TRISO}(T) + (1-\phi_{TRISO}) C_{p,matrix}(T) \end{aligned} \tag{7-6}$$

The results of the transient test case for the three different homogenization schemes can be found in Figure 7-9. The behavior observed in the multiphysics model is exacerbated in the single-physics ramp transient case, where the decreased rate of heat diffusion out of the particle due to the low buffer thermal conductivity and high specific heat of the kernel dominates (short wavelength behavior) compared to the time evolution of the long-wavelength temperature solution. The results of both the steady-state multiphysics model and the transient single-physics model indicate that an improved TRISO treatment is required to close the gap between homogeneous and heterogeneous models for whole-core reactor analyses.

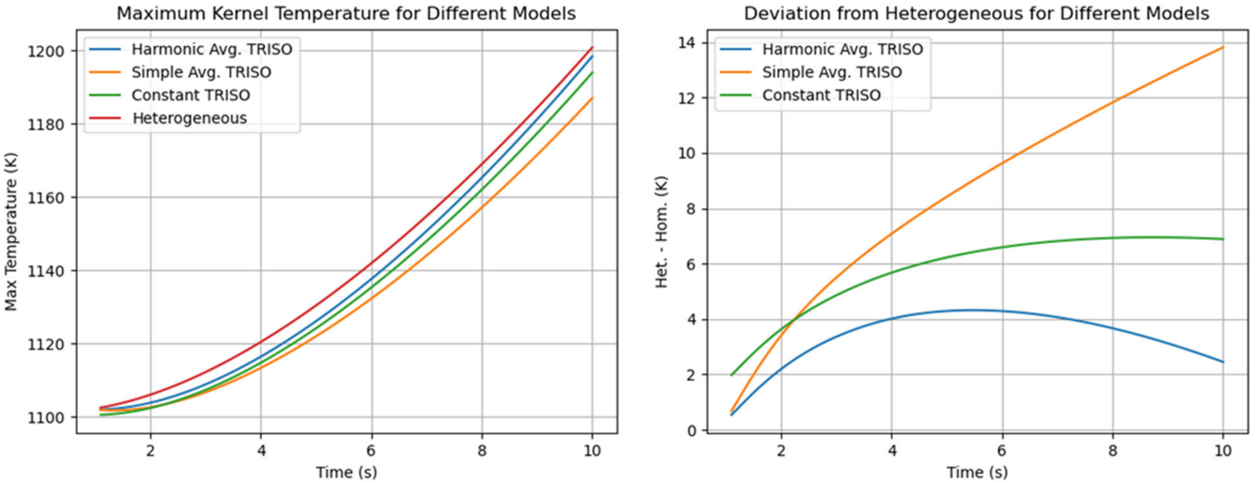

Figure 7-9 Comparison of different homogeneous TRISO models for a single-physics ramp transient. Left: temperature predictions. Right: deviation from the heterogenous model

Currently, two approaches have been investigated previously to add the effects of TRISO heterogeneity to engineering-scale heat conduction models. The first approach is the Homogeneous Layer Method (HLM), which decomposes the heterogeneous medium (fuel compact) into a series of concentric layers such that each layer is a separate material, where the thickness of each layer is chosen such that the mass fraction of the dispersed phase in the matrix phase is conserved. This process is repeated for an arbitrary number of layers (known as pseudo-particles) to increase the fidelity of the heterogeneous treatment. HLM proves to be disadvantageous when modelling fuel compacts as it requires many mesh divisions if a large number of pseudo-particles are required to capture clustering effects (as would be necessary for the 40% packing fraction in the GCMR).

The second approach used in the literature is Heat Source Decomposition (HSD) [26, 27]. HSD decomposes the heat source into a mean component and a fluctuation:

$$\dot{q} = \hat{q} + \sum_j \tilde{q}_j \qquad (7\text{-}7)$$

where $\hat{q}$ is the mean heat source (W/m^3) and $\tilde{q}_j$ is the fluctuation at TRISO particle position j (W/m^3). A constraint on the fluctuating heat source is that it must average to zero over the volume of the compact. Two different heat conduction equations are then solved for a macro-scale temperature T_{macro}, and fluctuating temperature $T_{fluct,i}$ based on these two different heat sources:

$$\begin{aligned} &\text{(a)} \qquad \rho C_{p,macro} \frac{\partial T_{macro}}{\partial t} = \nabla \cdot k_{macro} \vec{\nabla} T_{macro} + \hat{q} \\ &\text{(b)} \qquad \rho C_{p,micro,j} \frac{\partial T_{micro,j}}{\partial t} = \nabla \cdot k_{micro,j} \vec{\nabla} T_{micro,j} + \tilde{q}_j \end{aligned} \qquad (7\text{-}8)$$

where the subscript “macro” indicates the homogeneous material properties and temperatures, and the subscript “micro” indicates the material properties and temperature fluctuation of the TRISO particles at position j. The boundary and initial conditions for T_{macro} are identical to the boundary conditions used for homogeneous modelling, as T_{macro} captures the long-wavelength behavior of the temperature field. T_{micro} represents the short wavelength temperature perturbations caused by the heterogeneity in both the heat source and the thermal conductivity. The boundary condition for $T_{micro,j}$ is:

$$T_{micro,j}|_{\partial V_j} = -\frac{\int_{V_j} T_{micro,j} dV}{\int_{V_j} dV} \tag{7-9}$$

where V_j is the volume of TRISO particle j and ∂V_j is the outer boundary of said particle. Upon solving for the macroscopic and fluctuating temperatures, the full temperature field can be reconstructed as:

$$T = T_{macro} + \sum_j T_{micro,j} \tag{7-10}$$

HSD is exact so long as two conditions are satisfied: i) the macroscopic model resolves all heterogeneities in k_{macro} and $\rho C_{p,macro}$, and ii) $k_{micro,j}$ and $\rho C_{p,micro,j}$, are constant with respect to temperature (resulting in linear heat equations). If a homogenization scheme is used for either material property or material properties are nonlinear, HSD will become approximate. Heat conduction simulations performed at two different compact powers showed minimal differences in the resulting shape of the temperature field, indicating that the nonlinearity in k_{macro} and $k_{micro,j}$ is not severe enough to degrade the linearity of the heat equation and so the impact on the accuracy of steady-state simulations with HSD will be minimal. This is not the case for $C_{p,macro}$, and a special treatment is required to minimize the impact on the accuracy of transient calculations. In this work, the nonlinearity induced by the strong variation in the specific heat of the fuel is removed by decomposing $C_{p,macro}$ into the following:

$$\begin{aligned} &\text{(a)} \quad C_{p,macro}(T) = (1-\phi_{TRISO}) C_{p,matrix}(T) + \phi_{TRISO}\, \tilde{C}_{p,TRISO} \\ &\text{(b)} \quad \tilde{C}_{p,TRISO} = \frac{\int_{V_k} C_{p,TRISO}(\vec{r}, T_{macro}^{t-1}(\vec{r})) dV}{\int_{V_k} dV} \end{aligned} \tag{7-11}$$

where V_k is the volume assigned to the TRISO particle with a nearest point algorithm, and the temperature at the previous timestep / Picard iteration is used ($t-1$). This removes point-wise nonlinearity in the specific heat and treats it as a spatially-varying constant field on the current timestep.

HSD has been integrated into the homogeneous compact model with the MOOSE `MultiApp` system. A 1D r-spherical TRISO heat conduction sub-app is solved for each TRISO particle’s contribution to $T_{micro,j}$. The 1D r-spherical problem contains every TRISO layer, in addition to one additional layer which models the effects of the matrix. The radius of this pseudo-matrix layer is chosen such that it results in the same particle packing fraction as the bulk compact; it is necessary to ensure that the microscale calculation maintains the same asymptotic behavior. The average value of T_{macro} (evaluated at the previous timestep / Picard iteration) and $\hat{q}$ in the nearest neighborhood surrounding each particle is transferred to the sub-application. These are used to sample nonlinear material properties and compute $\tilde{q}$. The maximum kernel temperature fluctuation is transferred from each TRISO sub-apps and is linearly interpolated between TRISO particles to produce a scalar field of maximum temperature fluctuations for every element in the macroscale model. This temperature fluctuation is added to T_{macro} and transferred to the neutronics main application to apply temperature feedback. A diagram of this multi-scale multi-physics coupling scheme can be found in Figure 7-10.

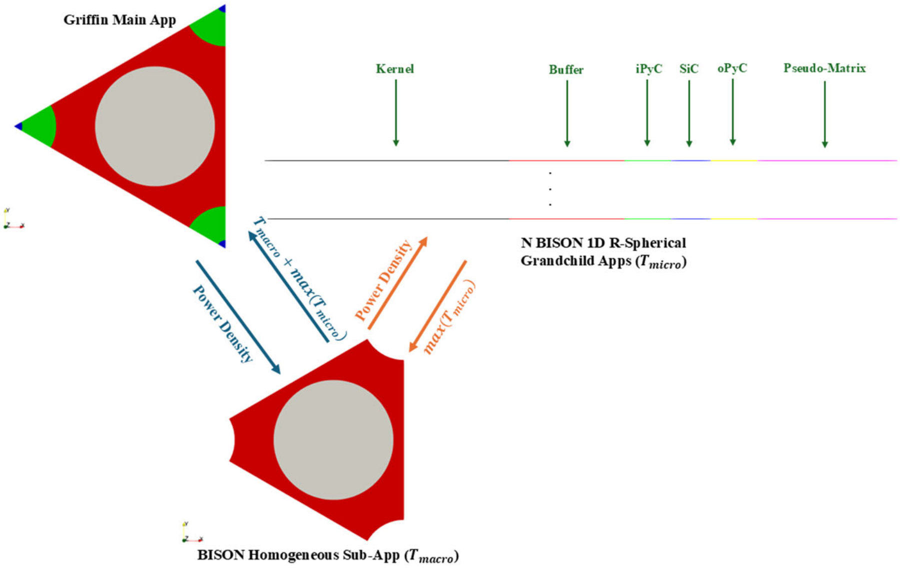

Figure 7-10 Coupling scheme between the different physics and length scales

As the harmonic homogenization approach yielded the closes value of maximum temperature and k_{eff}, it was down selected for a comparison against the heterogeneous result and to use as the macroscopic model for the HSD calculation. Table 7-3 summarizes the steady-state integral results for the multiphysics compact model. The addition of HSD resulted in modest improvements for both integral metrics over a purely homogeneous approach for both integral metrics. The single-physics transient case yielded a far better improvement vs the homogeneous model, as can be seen in Figure 7-11, where the difference between the HSD model and the heterogeneous model is within 2 K across the majority of the transient. These results motivate the application of HSD with a homogeneous treatment using a harmonic average to the whole-core GCMR model.

Table 7-3 Comparison of the maximum temperature and neutronics eigenvalue between HSD and non-HSD approaches for a total compact power of 24 W

Parameter (24 W)	**Heterogeneous**	**Harmonic Averaged TRISO**	**HSD (Harmonic Averaged TRISO)**
Max. T_{kernel} (K)	1099.0	1092.4	1,094.7
Δk_{eff} (het. - other) (pcm)	N/A	-50	-34

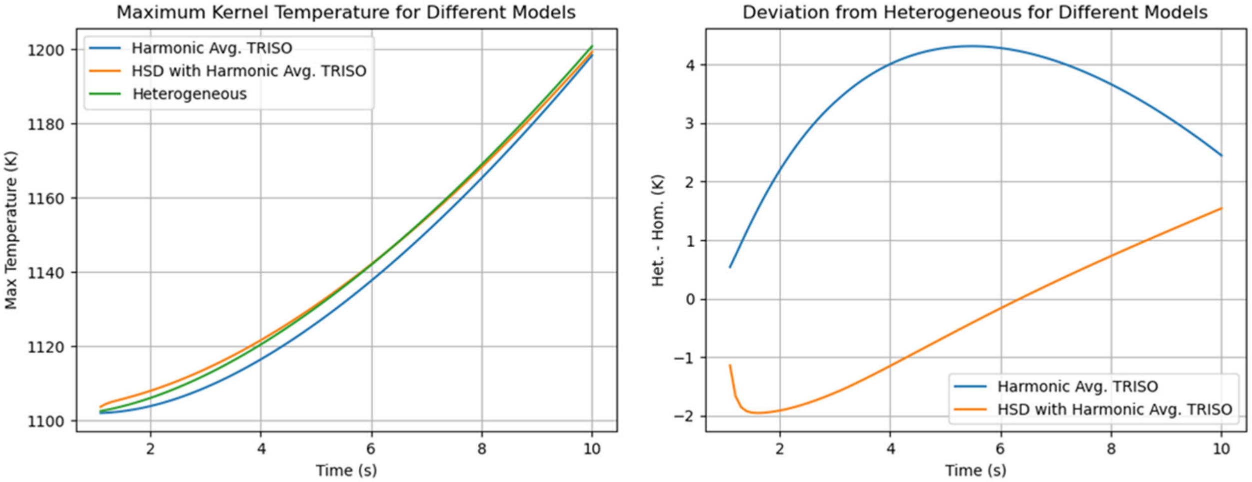

Figure 7-11 Comparison of homogeneous TRISO treatments to heterogeneous results, with and without HSD

7.3 Whole-Core GCMR TRISO Modelling

The whole-core GCMR multiphysics model contains 668 fuel pins, where each pin contains approximately 400,000 TRISO particles embedded in a compact. A naïve application of the HSD method discussed in Appendix A-2 would require well over 267,200,000 TRISO particle sub-apps. This would require a great deal of computing resources, which is not justified given the degree of improvement HSD yields over the modified macroscopic model. To minimize the memory and computing burden of this TRISO treatment, this work adopts the concept of virtual TRISO particles from HLM. 20 1D r-spherical sub-apps are created per fuel pin, where each set of sub-apps uses a different z-coordinate corresponding to an axial subdivision of the fuel. These 13,360 virtual particles are treated in the same manner as the TRISO sub-apps discussed in Appendix A-2, with a similar coupling scheme to Figure 7-10 where the only change is the addition of MOOSE THM sub-apps to the macroscale BISON temperature app. The use of virtual particles yields large memory/compute savings over a fully explicit simulation at the cost of no longer being able to take into consideration the effect of localized particle clustering within fuel compacts. We believe this trade-off is acceptable given the engineering length scales under consideration, and the inability for Griffin to fully simulate the effects of per-particle self-shielding. The remainder of the steady-state GCMR whole-core multiphysics model is identical to the model discussed in Section 4.2.1. Results for the steady-state model can be found in Figure 7-12, where the fluctuating temperature predicts a fuel temperature rise of 3.8 K over the macroscale model and a lower peak power density due to the increased temperature feedback.

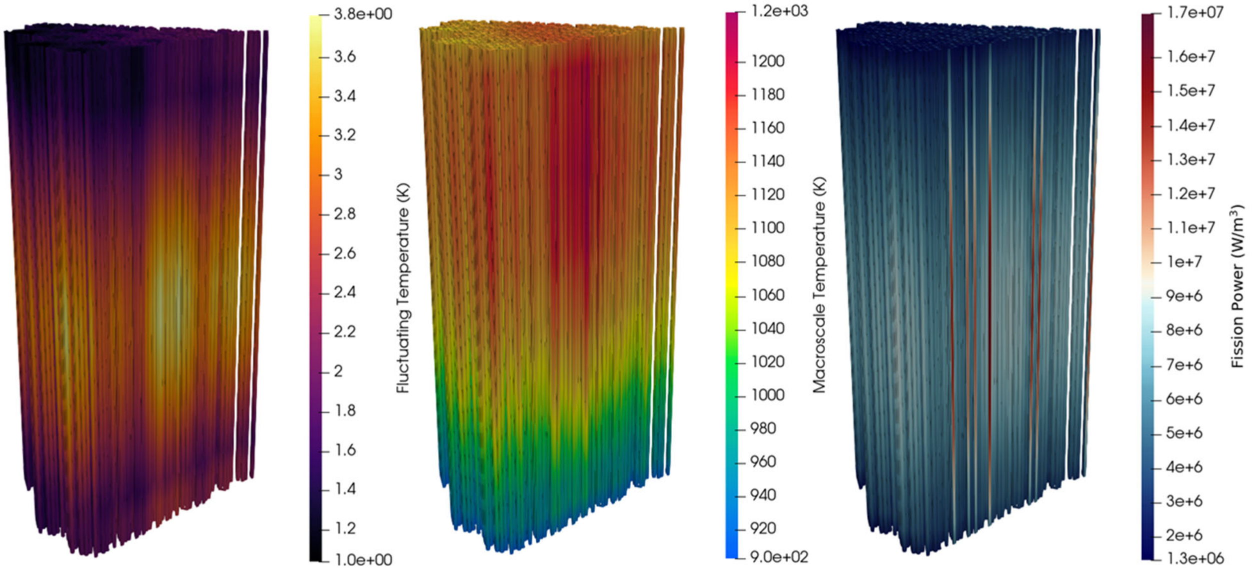

Figure 7-12 Steady-state multiphysics model with HSD incorporated. Left: T_{fluct} (K). Middle: T_{macro} (K). Right: power density (W/m^3)

In addition to applying a modified HSD treatment to the steady-state GCMR model, the impact of these higher fidelity approaches was investigated on transient responses for the limiting reactivity transients in the GCMR: inadvertent control drum rotations. At present, the long runtime of transient DFEM-SN transport calculations for drum rotations required the use of reduced order modelling to determine the impact of this new semi-explicit modelling approach on transient responses. It was determined that a Point Reactor Kinetics (PRK) model would suffice for these limiting cases, where the kinetics parameters discussed in Section 4.5.1 are used. In this transient model the BISON macroscale application acts as the main application, transferring the average fuel temperature to a PRK sub-app (to compute temperature feedback) and receives the normalized power to use when computing the updated power density. The transient cases under consideration are step reactivity insertions of 30 cents (199 pcm) and 50 cents (332 pcm) with temperature reactivity feedback. A temperature feedback coefficient of -4.58 pcm/K is used. The average fuel temperature (with HSD applied) is transferred to the PRK sub-app to compute temperature reactivity feedback. The full transient runs over 10 s; the Griffin and THM applications run with timesteps of 1 ms while the BISON applications (macroscale and fluctuating) run with timesteps of 10 ms. Initial conditions for the BISON applications are steady-state initial conditions from the steady-state model; the power density shape is also taken from the steady-state model. The transient results for power density (Figure 7-13), maximum fuel temperature (Figure 7-14), and temperature feedback reactivity (Figure 7-15) can be found below. These results are compared against the same transients using the previous BISON model.

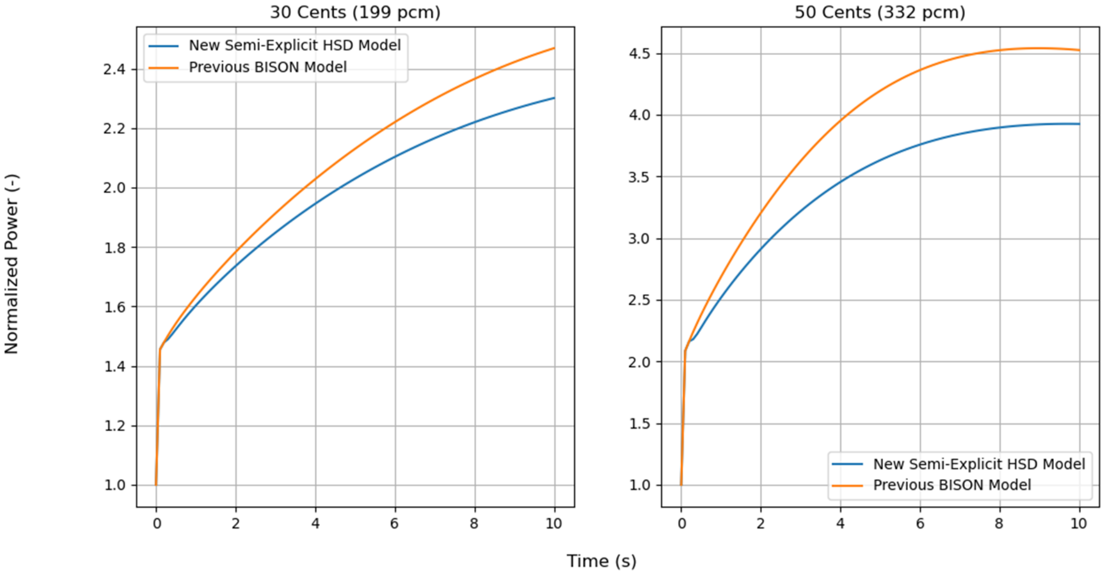

Figure 7-13 Normalized power for the simplified whole core transient model. Left: 30 cent insertion. Right: 50 cent insertion

When it comes to normalized power, the previous BISON model predicts a 4.1% (30 cent) and 13% (50 cent) higher reactor power by the end of the transient compared to the semi-explicit HSD model. This is largely due to the rapid increase in temperature in the fuel kernel and reduced heat transport out of the kernel, which drives reactivity down due to the negative temperature reactivity coefficient of the GCMR. This can be seen explicitly in Figure 7-14, where the maximum fuel temperature jumps rapidly within the first 30 ms of the transient, and then levels off as the rate of change of the temperature fluctuation begins to match the rate of change of the macroscale temperature. This behavior is mirrored in Figure 7-15, where reactivity drops quickly at the beginning of the transient from the sharp temperature increase.

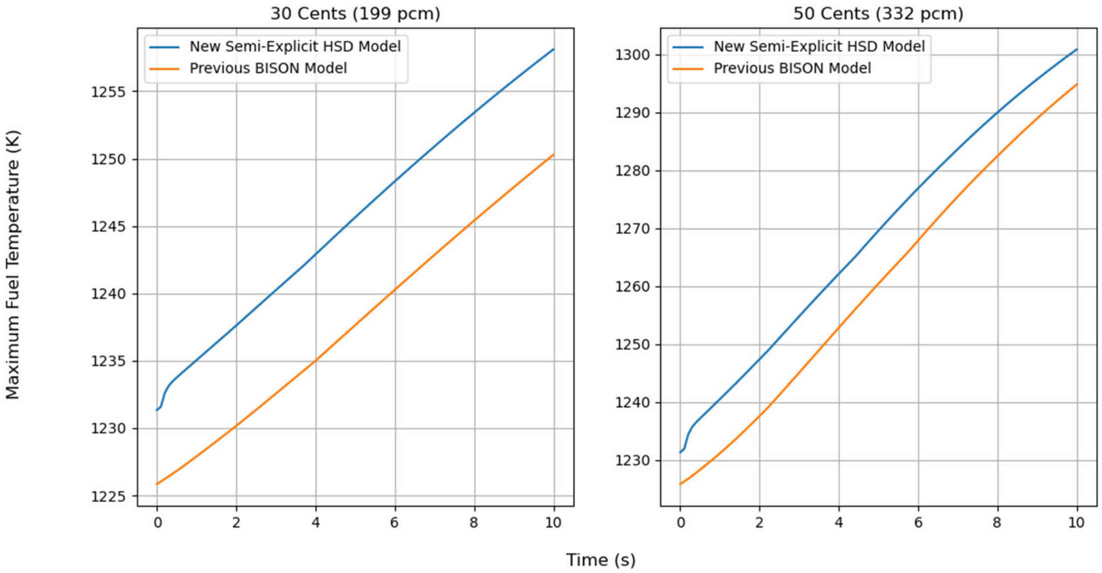

Figure 7-14 Maximum fuel temperature for the simplified whole core transient model. Left: 30 cent insertion. Right: 50 cent insertion

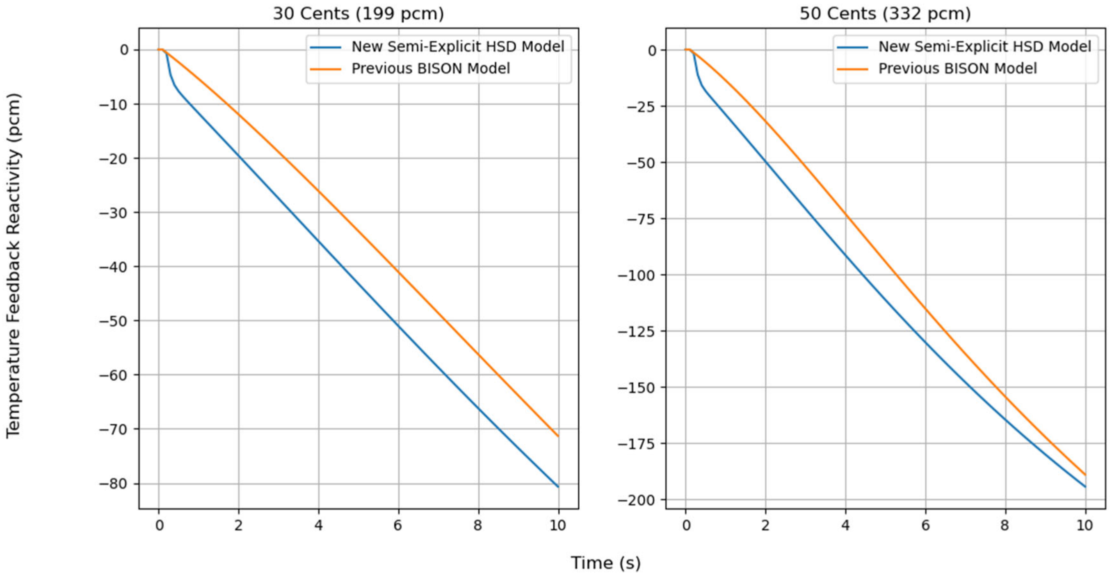

Figure 7-15 Temperature feedback reactivity for the simplified whole core transient model. Left: 30 cent insertion. Right: 50 cent insertion

www.anl.gov

ARGONNE NATIONAL LABORATORY

- U.S. Department of Energy research facility
- Operated by the UChicago Argonne, LLC
- Midwest's largest federally funded R&D facility
- Located in Lemont, IL, about 25 miles (40 km) southwest of Chicago, IL (USA)
- Conducts basic and applied research in dozens of fields
- Unique suite of leading-edge and rare scientific user facilities

CONTACT
Argonne National Laboratory
9700 South Cass Avenue
Lemont, IL 60439
630-252-2000

U.S. DEPARTMENT of ENERGY